Fault Tolerant Behavior of
Advanced Control Schemes of Induction Machine Drives

by

Saadia Gauhar

A Thesis Submitted in Partial Fulfillment
of the Requirements for the Degree of

Master of Applied Sciences in Electrical

in

The Faculty of Engineering and Applied Sciences

Electrical and Computer Engineering

University of Ontario Institute of Technology

January, 2016

ABSTRACT

Power electronics based variable-speed drives offer energy saving solutions, providing precise control and quick response time. They are required for sensitive process control in industrial applications and other emerging technologies such as electric vehicles.

This thesis examines two popular advanced control schemes of variable-speed induction machine drive applications. The two advanced control schemes, Indirect Field oriented control (IFOC) and Direct torque control (DTC), are compared by examining their implementation complexity, parameter sensitivity, dynamic responses, steady state performance and, most importantly, under power line fault scenarios. MATLAB-Simulink package is used to develop system models for both control schemes. System studies are done under normal and abnormal operating conditions. In the end, conclusions are drawn based on their behavior and comparison of performance characteristics under dynamic and AC fault (single-line to ground, phase to phase and triple-line to ground) conditions, highlighting the fault tolerant characteristics of the two drive schemes.

Keywords: *Induction machine drives, variable speed drives, field oriented control, vector control, FOC, direct torque control, DTC, fault tolerant behavior of ac motors, fault analysis, fault analysis of induction machines, power line faults in AC drives, power converters, voltage source inverter, VSI, hysteresis current control, space vector modulation.*

ACKNOWLEDGMENTS

I would like to express my sincere gratitude to my advisor Dr. Vijay Sood for the continuous support of my master's study and related research, for his patience, motivation, and immense knowledge. His guidance helped me in all the time of research and writing of this thesis. I could not have imagined having a better advisor and mentor for my M.A.Sc.

I would like to take the opportunity to thank Joel Stewart for all his support and efforts that proofed to be very helpful.

I would also like to thank my family: my parents, my brother and sister for supporting me spiritually throughout writing this thesis and my life in general. Last but not the least; I would like to thank my colleague and friend Saeeda Sana for all her help and support.

Table of Contents

NOMENCLATURE

N_s	Synchronous speed, in RPM
f	Frequency, in Hertz
P	Number of machine poles
ω_s	Synchronous speed, in Rads/s
S	Slip, in per unit
ω_{sl}	Angular slip speed, in Rads/s
ω_r	Rotor speed, in Rads/s
θ_r	Rotor position angle, in Radians
θe	Synchronous rotating frame angle, in Radians
$\overrightarrow{\lambda_r}$	Rotor flux linkage vector
$\overrightarrow{\lambda_s}$	Stator flux linkage vector
L_r	Induction machine rotor self-inductance, in Henries
L_s	Induction machine stator self-inductance, in Henries
L_m	Induction machine magnetizing inductance, in Henries
σ	Total leakage factor
$\overrightarrow{\iota_s}$	Stator current vector
T_e	Electromagnetic torque, in N.m
ϕag	air-gap flux
I_r	RMS rotor current (referred to stator), in Amps
δ	Torque angle, in Radians
k	Constant
V_m	Peak phase voltage, in Volts
R_r	Induction machine referred rotor resistance, in Ohms
L_{lr}	Rotor leakage inductance, in Henries
V_s	Voltage source, in Volts
R_s	Stator resistance, in Ohms
I_s	RMS stator current, in Amps
cos ϕ	Input power factor
P_{FW}	Friction and windage loss of the machine, in Watts
ω_e	Stator or line frequency, in Rads/s
I_m	RMS magnetizing current, in Amps
L_{ls}	Stator leakage inductance, in Henries
f_{sl}	Slip frequency, in Hertz
f_s	Frequency of the stator variables, in Hertz
v_{ds}	Stator direct axis voltage, in Volts

v_{qs}	Stator direct axis voltage, in Volts
i_{qs}	Rotor quadrature axis current, in Amps
i_{ds}	Stator direct axis current, in Amps
λ_{ds}	Stator direct axis flux linkage, in Wb
λ_{qs}	Stator quadrature axis flux linkage, in Wb
p	Derivative operator (d/dt)
λ_{dr}	Rotor direct axis flux linkage, in Wb
λ_{qr}	Rotor quadrature axis flux linkage, in Wb
i_{dr}	Rotor direct axis current, in Amps
i_{qs}	Stator quadrature axis current, in Amps
θ_c	Lag angle between q^s-axis and phase a windings, in Radians
ω_c	The speed of arbitrary reference frame in induction motor, in Rads/s
θ_s	Stator-current phasor angle, in Radians
v_d	DC voltage, in Volts
V_{LL}	Line to line RMS voltage, in Volts
I_d	DC current, in Amps
m_a	Amplitude modulation ratio
$V_{control}$	Peak amplitude of the control signal, in Volts
$V_{carrier}$	Peak amplitude of the carrier signal, in Volts
T_L	Load torque, in N.m
λ_{ag}	Air gap flux linkage, in Wb
J	Machine inertia, in kg/m^2
λ_r	Rotor flux linkage, in Wb
θ_{sl}	Slip angle, in Radians
γ	Angle between stator and rotor fluxes (torque angle), in Degrees

LIST OF FIGURES

LIST OF TABLES

1 General Background and Research Goals

1.1 Introduction

AC motors as adjustable speed drives are widely used in industries. Among all types of AC motors, Permanent Magnet Synchronous and Induction machines have become very popular. Induction machines are cost effective and rugged; they are available in a wide range of horse power ratings. Three phase induction machines are largely used in variable speed drives; these drives regulate speed, rotational force, and output torque. Applications of variable speed drives include; fans, pumps, electric vehicles, elevators, chillers, heaters, ventilators, HVAC, wind power generation, etc. [1]

Formerly, DC machines were preferred for use as variable speed drives, but they suffered from many disadvantages such as higher costs, higher rotor inertia, and maintenance issues. The commutators and brushes of the DC machine limit the machine speed and peak current, causing EMI problems. Due to this, DC machines were not able to operate in dirty and explosive environments. However, DC machine drives and control systems are much simpler, and the machine torque is very responsive. AC machines do not suffer from such drawbacks, and in the last few decades, AC machines are replacing DC machines in the variable speed drives industry. Power electronics has played a big role in this revolutionary development; modern semiconductors such as Insulated Gate Bipolar Transistor (IGBT) have facilitated the use of AC machines in variable speed drive industry. [1]

1.2 Literature Review

Most cost effective speed control of Induction machine is realized by frequency converters. Various topologies of frequency converters are covered in literature, however, the most readily applied topology consists of a diode rectifier, a DC link and a PWM voltage source inverter (VSI) as shown in Figure 1.1.

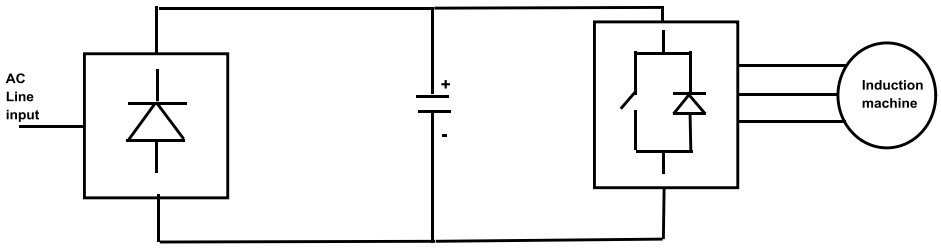

Figure 1.1: PWM Voltage Source Inverter with diode Rectifier [2].

Characteristics of high performance frequency controlled PWM inverter drive are as follows:

- Bipolar voltage PWM.
- Constant switching frequency.
- Fast flux and torque response.
- Low flux and torque ripple.
- Maximum torque output in vast range of speed operating regions.
- Four quadrant operation.

The variable frequency induction machine control schemes are divided into scalar and vector controls, as shown in Figure 1.2; [3]

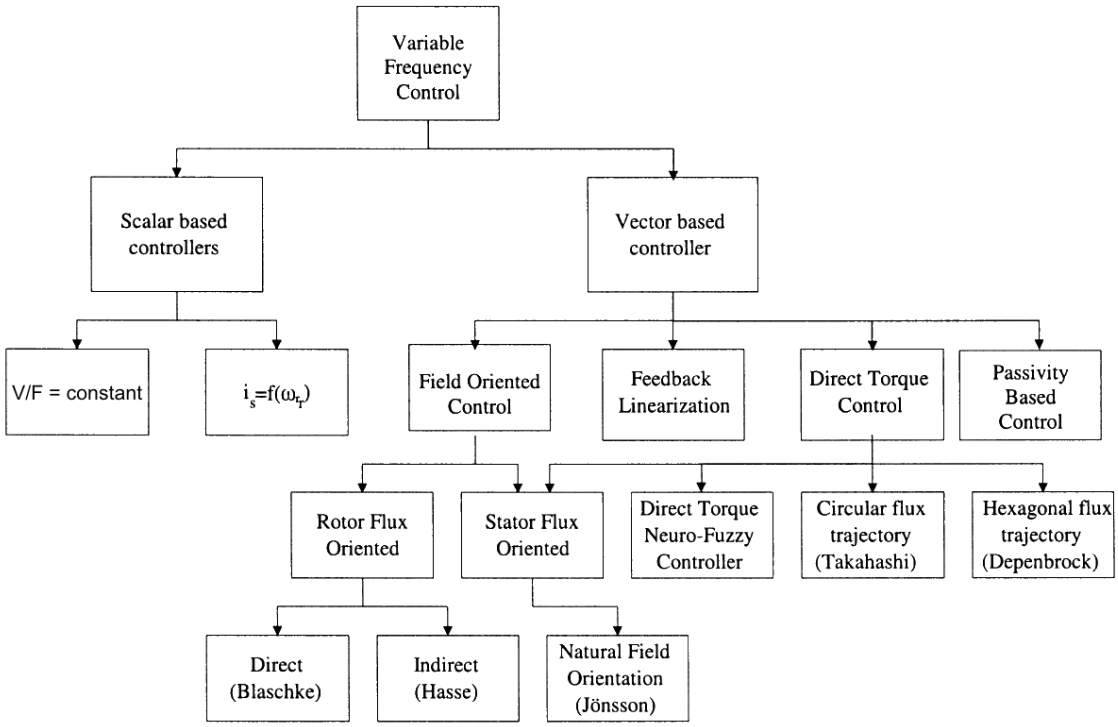

Figure 1.2: Classification of Induction Machine control methods [3].

Scalar based controllers, are quite simple to implement, and are very cost effective. Scalar controllers have produced acceptable steady state performance, but lacked in dynamic state response [4], because of deviations in the air-gap flux linkages in both magnitude and phase. The magnitude and frequency of the stator and rotor phase currents are used for controlling these variations in the air-gap flux linkages [4]. The most popular scalar control strategy is the constant Voltage per Hertz (V/F) method. V/F control strategy is quite simple to implement, as both the torque and the flux are direct functions of voltage and frequency [1], therefore, there is an inherent coupling effect. Due to this coupling effect, V/F control strategy has a slow and sluggish response time, also due to the presence of higher-order harmonics the system is exposed to instability

[5]. Other drawbacks of V/F control strategy are; high transient currents due to changes in torque, which could result in nuisance tripping. To compensate for the tripping, the machine acceleration and deceleration rates need to be reduced; this results in a sluggish response, and deteriorating the torque capabilities of the machine. Furthermore, the time associated with the transistor switching, the machine maybe exposed to instability problems leading to poor performance. Therefore, V/F control based variable speed drives, are only limited to applications such as pump type loads [6].

However, vector based controllers, invented in the early 1970s, decoupled these effects, and demonstrated that AC machines can be controlled in a similar fashion as separately excited DC machines. This invention, lead to a renaissance in the high performance control of AC machines drives. Vector control strategies are complex, and they demand use of a microprocessor or DSP [1]. It was not until the early 1980s, when vector based controllers were commercialised for induction machine drives. At that time, the cost of these variable speed drives was high, due to complexity and higher processing power requirements as compared to DC machine drives [4].

One of the first vector control strategies for induction machines was Field Oriented Control (FOC) which was unveiled by K. Hasse as Indirect Field Oriented Control (IFOC) in [7]. Another similar Field Oriented Control method was presented by F. Blaschke as Direct Field Oriented Control (DFOC) in [8]. Both the strategies were published in the early 1970s; these strategies enabled induction machines for high performance over the years and have now become industry standard. In the Field Oriented Control the machine's equations are transformed in a coordinate system that

rotates in accordance with the machine's rotor flux vector. This method produces new field coordinates, under which there is a linear relationship between the control variables and the machine's torque. This strategy guarantees fully decoupled torque and flux components, by decomposing the currents into two components; torque producing and flux producing components.

In the Direct Field Oriented Control (DFOC) method, proposed by F. Blashcke, a flux estimator/calculator or sensor is used to find out the instantaneous value of the flux by direct measurement. In the Indirect Field Oriented Control (IFOC) method proposed by K. Hasse, three orientations; stator, rotor or air gap flux are possible as it is based on inverse flux model dynamics, his method is more commonly used as it is simpler to implement [9]. However, other coordinate transformations could also be used to attain decoupling and linearization of the induction machine equations. This idea resulted in a method known as modern non-linear control [10], [11], [12]. Other methods known as Feedback linearization control decoupling have been introduced which talks about nonlinear transformation of the induction machine state variables, enabling a new coordinate system where speed and flux magnitudes are decoupled by feedback system [10], [11], [13], [14], [15], [16]. An identical work has been done by Z. Krzeminski, who derived a multi-scalar model of induction machine [17]. A method that is based on variation theory and energy shaping has also been considered recently, known as Passivity based control (PBC). In this method the induction machine is described in terms of Euler language equations expressed in generalized coordinates [18]. This vector control method suffers from one big disadvantage; i.e. parameter variations such as

rotor time constant and inaccurate estimation of flux at fairly low speeds. This leads to a decline in machine performance, and even a conventionally designed PI controller is not able to provide a decent performance under these conditions [9].

In the 1980s a new vector based control strategy was proposed by I. Takahashi and T. Noguchi, called the Direct Torque Control (DTC) [19] and by M. Depenbrock, called the Direct Self Control (DSC) [20], [21], [22]. These methods have developed from the idea of a coordinate transformation and analogy with DC machine control. Hysteresis controllers, also known as bang-bang controllers, respond very well to on-off switching of the inverter semiconductor power devices. This control method is the direct control of the torque and stator flux of an AC drive by inverter voltage space vector selection through a look-up table [1]. This control strategy has been under on-going research since 1980s, and has been continuously developed further by many researchers [23], [24], [25], [26]. Direct torque control (DTC) and Direct self-control (DSC) have good dynamic control of the torque without any transducers or sensors on the machine shaft. Therefore these methods are considered as "sensorless drive control". DSC control strategy is more suitable for high power applications, where a lower switching frequency can justify higher current distortions. On the other hand, DTC is preferred for medium to low power applications [26]. Disadvantages of DTC are as follows; [26]

- Control of torque and flux is challenging at lower machine speeds.
- High current and torque ripples.
- Irregular switching frequency behaviour.
- At low speeds, there are noise issues.

- Lack of direct current control.

In the past decade researchers have tried to solve the issues of Direct Torque Control (DTC) scheme as seen in [27], [28], [29], [30], [31]. J.N. Nash published a paper on DTC where he implemented special functions such as flying start, flux braking, flux optimization and power loss ride-through. The control scheme he proposed was based on sensorless variable frequency drive [32]. Over the years, another DTC control technique has become very popular, known as direct torque control Space Vector Modulation (DTC-SVM) scheme. Research published by T.G. Habetler, where he describes controlling the torque and flux using calculated voltage space vectors. He uses space vector PWM technique to calculate the inverter duty cycle. His scheme improves transient performance of the induction machine [33]. Over the years T.G. Habetler and his fellow researchers have published numerous other papers on improving DTC control scheme [34], [35], [36].

Some criteria to evaluate the performance of DFOC and DTC are proposed in [26]. In this paper, the authors have compared the two schemes in both steady-state and transient operating conditions. This paper has concluded that DTC scheme is simpler to implement and maybe more suitable for high dynamic applications. Few other papers have been published recently analyzing and outlining the comparison between the two vector control techniques [37], [38], [39], [40] and [41]. These studies have outlined the characteristics of the control algorithms, dynamic electromechanical responses, and the sensitivity analysis of the machine parameters. However, there is a lack of research work that compares FOC and DTC for induction machine operation during power quality

issues such as power line faults. Power line faults can cause performance degradation. It is necessary to study the behaviour of FOC and DTC control drives for induction machine to help avoid unplanned standstills, and design a system such that the induction machine operation is within reasonable limits,especially during emergency operations in case of power line faults. These are done to avoid high costs that may be incurred due to power failures, and minimize repair times and effort. Breakdown or standstill of even few induction machines in a system can cause a complete system failure (malfunction). Diagnosis and studies on induction machine failures during power line faults with constant speed and scalar control is presented in [42]. Classification of faults in voltage source inverter with a diode rectifier for induction machine drive can have following occurrences of fault types [43] [44];

- AC line faults
- DC bus faults
- Power switch fault short and open circuits
- Fault in controls equipment.

Matlab-Simulink package has several great tools for analysis of transient and steady-state responses. Moreover, the control and power electronics tool boxes are state of the art, and are quite advanced for modelling the voltage based inverter, induction machine and employing control algorithms to simulate any type of load and faults. Decoupling control has been possible through mathematical coordinate transformations, which converts the three-phase AC to two-phase orthogonal DC components. The abc to d-q transformation, called the Clarke transformation, has been

explained and modeled in Matlab-Simulink [45]. Reference [41] also uses Matlab-Simulink for the comparison of the two vector control strategies. This thesis will focus on commonly occurring power quality issues that have adverse effects on induction machine drives, which employs DTC and FOC control schemes for medium voltage applications [66].

1.3 Research Scope and Objectives

There are many types of induction machine control schemes that have been proposed and are detailed in the literature review in section 1.2. Each one of them has their own advantages and drawbacks, depending on the type of application;

The most popular drive control schemes are as follows;

- Scalar control – Constant Volts per Hertz ratio
- Vector Control – Field Oriented Control (direct and indirect)
- Direct Torque Control

Variable speed drives (VSD) offer energy saving and fast and precise responses which are needed in many industrial process control applications i.e. smoother operation, acceleration/deceleration controllability, compensation for changing process variables, different operating speeds for each process type, slow operations during initial setups, rate of production, precise positioning, control of torque and tension, allow catching of spinning load after an outage.

Power electronic converters have played an important role in the development of variable speed drives of induction machines. Power semiconductor switches such as IGBTs have allowed precision control of voltage, current, power and frequency in a very

economical way and this has led to the development of advance control schemes for induction machines. For VSD applications, advanced control schemes of induction machines have brought about a renaissance in the industry, and have almost replaced DC machines drives. Indirect field oriented control and direct torque control schemes have become industrial standards for medium to high voltage variable speed drive systems, owing to their superior dynamic performance and cost effectiveness. Both control schemes have their own advantages and disadvantages. Some research papers have been published to compare the two for variable speed drive applications.

The objective of this thesis is a thorough comparative study of both control schemes; focusing on implementation complexity, basic control characteristics, static and dynamic performance and parameter sensitivity analysis and power quality issues. Matlab Simulink power system block is a very powerful tool and will be used in order to develop system models for both advanced control drives; Matlab provides tools to analyze dynamic transient responses in time and frequency domains. The results, analysis and study of these methods will enhance the effective control of both the motor torque and flux regardless of load torque parameter variations or any other extraneous disturbances due to power quality issues.

1.4 Thesis Outline

This thesis is laid out as follows;

- Chapter 1 gives an introduction and general overview on the subject of the thesis. The scope and objectives of the thesis is also outlined here.

- Chapter 2 gives induction machine equivalent circuits and discusses operating principles in steady state. Furthermore, this chapter also develops dynamic models of induction machine in d-q stationary reference frame and synchronous rotating frame that are essential for the development of advanced control schemes of induction motors in later chapters.
- Chapter 3 discusses important power electronic voltage source converters and also presents with various control strategies such as space vector PWM, which will be later used in building the system models for theses power devices.
- Chapter 4 discusses advanced control schemes for induction machines. This chapter focuses on two important control schemes; direct torque control and field oriented control, later in this chapter the proposed system models developed in Matlab Simulink are presented.
- Chapter 5 is divided into two parts. In the first part, steady state and dynamic operating conditions are established and operational performance in both states are studied and compared. In the second part, the proposed models are introduced to various types of symmetrical and asymmetrical faults at the AC side (grid), and the system responses are studied and compared.
- Chapter 6 presents discussions and concluding remarks, and later with recommendations for future work is suggested.

2 Induction Machine Operating Characteristics

2.1 Introduction

To design a control drive system for an induction machine, in-depth knowledge about machine parameters and the dynamic model is compulsory. Generally, industrial drives are classified into constant speed and variable speed drives.

Main characteristics advantages of induction machines are [1]; economical, rugged and robust, can operate in any environmental condition, reliable, ranges of power from fractional horse power (FHP) to multi megawatt capacity and maintenance free. Single phase induction machine do not have self-starting torque. Whereas, three phase induction machine has self-starting torque and are often used in variable speed drives applications. The three phase machine have either wye or delta windings, that are distributed sinusoidally and embedded in slots.

This chapter will focus mainly on the basic static and dynamic performance characteristics of induction machines, with variable speed drive applications.

2.2 Steady State Performance

Equations that have been developed in the previous section will be helpful to analyze the steady state performance of the induction machine. Figure 2.5, shows a torque vs. slip characteristics for constant input voltage. The following characteristics can be seen from Figure 2.5 [4];

- At low slip, the torque is linear and proportional to the slip.

- Breakdown torque is reached beyond the maximum torque region; here the torque becomes inversely proportional to the slip.
- At standstill (i.e. slip = 1), at this point the torque produced is called standstill torque. For load acceleration, the standstill torque has to be larger than the load torque.
- Positive slope region is where the stable operating region lies, here if the torque is operating at unity with a low slip, and the load torque is increased, the rotor slows down, therefore establishing a larger slip, and in turn the electromagnetic torque of the machine is also increased in order to meet the load torque requirement.
- On the other hand, at the same torque and disturbance introduced in the load torque, will increase the slip, and thus resulting in less torque production, which will diverge the electromagnetic torque from reaching the load torque requirement, and finally giving up i.e. operation in the unstable region.

Thus it is recommended to operate the motor in stable region, near low slip to attain higher efficiencies. As the rotor copper losses are directly proportional to slip and slip power, thus at low slip these losses are minimal.

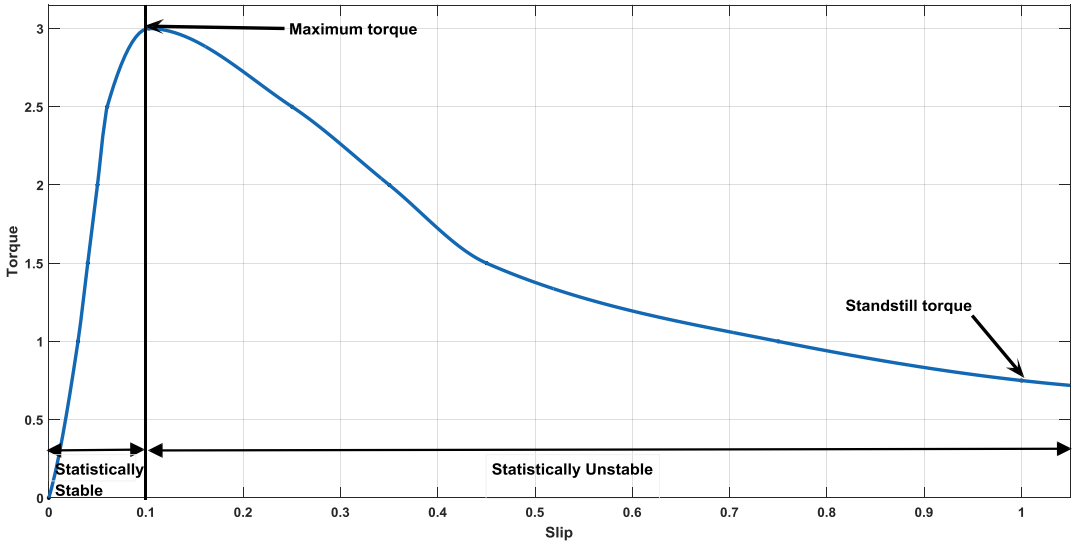

Figure 2.5: Induction machine torque-slip characteristics.

Now considering Figure 2.6, generation and breaking characteristics of induction machine for a wide range of slip with rated stator voltage and frequency, the following characteristics can be seen [4];

- For slip greater than one (S > 1), this operating region is reached when the rotor is spinning at the opposite direction to the phase sequence supply voltage and frequency supplied to the stator, creating a stator flux linkage counter to the rotor speed direction, which results in braking action of the motor. Therefore the rotor speed is negative to the synchronous speed, creating slip larger than 1, bringing the rotor speed to standstill.
- Rotor speed greater than the synchronous speed, at the point the slip is negative, which brings the motor in generation mode from the motoring mode, the torque also changes from positive to negative. The negative

torque-slip characteristics is same as in Figure 2.5, other than that the breakdown torque is of higher value. Due to the fact that mutual flux linkages are strengthened by the generation mode of the induction motor.

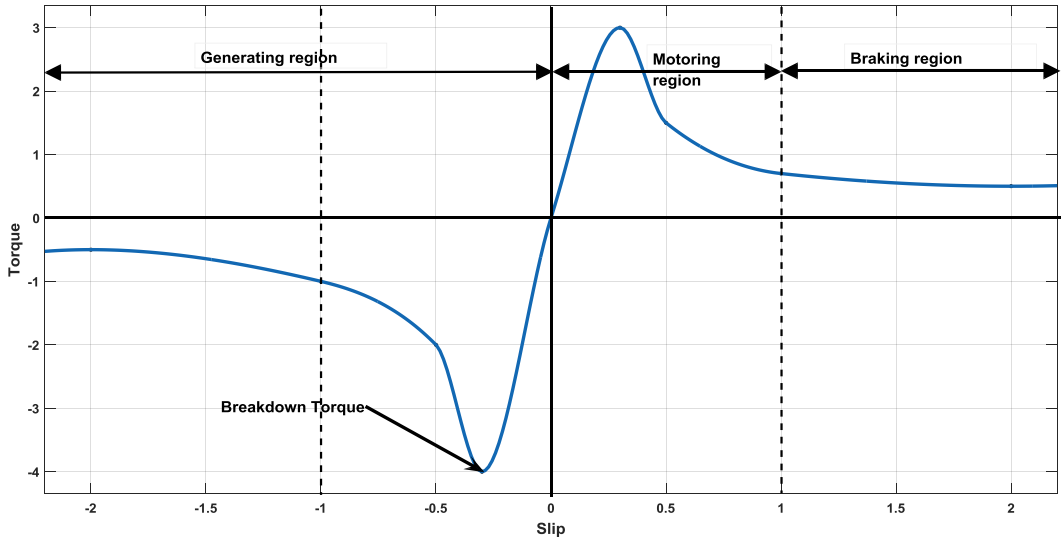

Figure 2.7: Motoring, generation and braking characteristics of induction machine.

Looking at the performance characteristics of induction machine in Figure 2.7; it is clearly seen that at standstill; the stator current on rated voltage is 5.35pu, and the efficiency is 1 - S, although there is torque generated at standstill, but the output power is zero, due to zero rotor speed. For VSD application; the slip must be between 0 to 0.13pu, which is the positive slope or the stable region of the torque-slip characteristics as seen in Figure 2.5. Here in this region, the machine efficiency is higher due to small rotor copper losses.

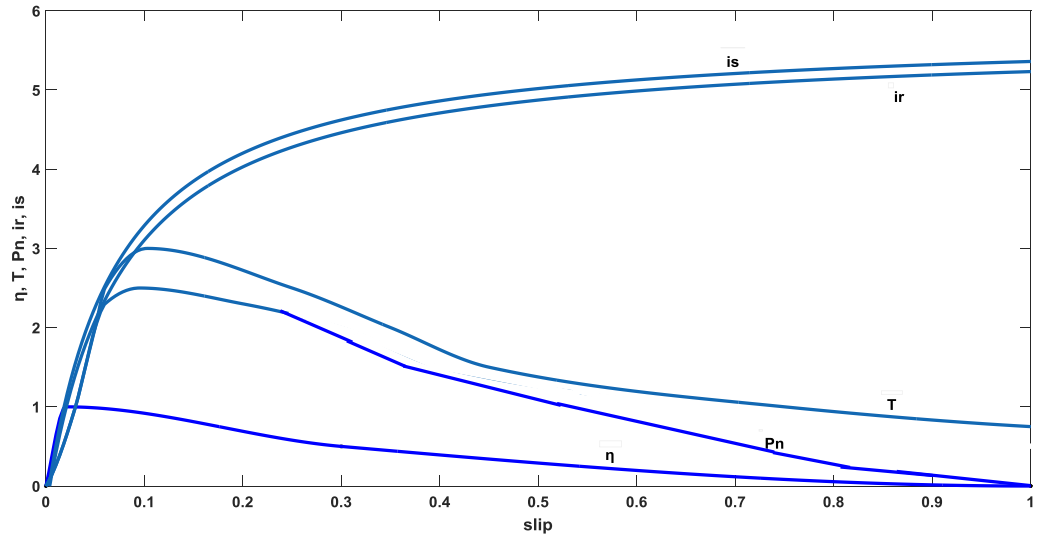

Figure 2.8: Performance characteristics of induction machine [4].

The machine starting torque at S = 1 from the torque expression equation 2.14 is written as [1];

$$T_{es} = 3\left(\frac{P}{2}\right)\frac{R_r}{\omega_e}\frac{V_s^2}{(R_s + R_r)^2\omega_e^2(L_{ls} + L_{lr})^2} \tag{2.1}$$

2.3 Characteristics of different types of Loads

There are three main types of load that can be defined by their torque and speed characteristics;

1. Constant torque: Most of the industrial machines that are required for work such as shaping, cutting, grinding or shearing, require constant torque irrespective of the speed. Also, cranes during the hoisting and conveyors handling constant weight of material per unit time also exhibit this type of characteristics.

2. Torque proportional to speed squared($T = k\omega_s^2$): Fans, rotary pumps, compressors and propellers also exhibit this type of load characteristics.
3. Torque inversely proportional to speed($T = {}^{k}/_{\omega_s}$): Certain types of lathes, boring machines, milling machines, steel mill coiler and electric traction load exhibit hyperbolic speed-torque characteristics.

2.4 Dynamic modelling of induction machines

The steady state performance of the induction machine was described in previous sections. For variable speed drive application, induction machine must have a feedback loop, and thus its transient response is of utmost importance, and must be taken into consideration. Hence, it is necessary to evaluate the dynamics of converter fed VSD for induction machine and its interactions in order to determine deviations of currents and torque in the power converters and the machine. Dynamic modelling takes into account the instantaneous effects of varying voltages, currents, stator frequency and torque disturbances. Furthermore, in order to develop high performance vector control drives, dynamic d-q models of induction machines are imperative. Consequently, dynamic machine models in synchronous rotating and stationary reference frame will be presented in this section.

2.4.1 Three phase to two phase transformation in stationary reference frame

The equivalence between two phase and three phase machine is established based on equality of mmf and equal current magnitudes. The q^s-axis is assumed to be

lagging the a-axis by θ_c. Figure 2.8, shows the phasor diagram of the variables in three phase and two phase axes. The relationship between d^s-q^s-0^s and a-b-c currents is represented as [4];

$$\begin{bmatrix} {i_{qs}}^s \\ {i_{ds}}^s \\ {i_0}^s \end{bmatrix} = \frac{2}{3}\begin{bmatrix} \cos\theta_c & \cos\left(\theta_c - \frac{2\pi}{3}\right) & \cos\left(\theta_c + \frac{2\pi}{3}\right) \\ \sin\theta_c & \sin\left(\theta_c - \frac{2\pi}{3}\right) & \sin\left(\theta_c + \frac{2\pi}{3}\right) \\ \frac{1}{2} & \frac{1}{2} & \frac{1}{2} \end{bmatrix} \cdot \begin{bmatrix} i_{as} \\ i_{bs} \\ i_{cs} \end{bmatrix} \tag{2.2}$$

Where, subscript "s" denotes stationary reference frame. Where ${i_0}^s$ represents the imbalance in a-b-c phase currents and is the zero sequence component of the current. ${i_0}^s$ does not produce a resultant magnetic field. The transformation from two-phase currents to three-phase currents can be expressed as [4];

$$\begin{bmatrix} i_a \\ i_b \\ i_c \end{bmatrix} = \begin{bmatrix} \cos\theta_c & \sin\theta_c & 1 \\ \cos\left(\theta_c - \frac{2\pi}{3}\right) & \sin\left(\theta_c - \frac{2\pi}{3}\right) & 1 \\ \cos\left(\theta_c + \frac{2\pi}{3}\right) & \sin\left(\theta_c + \frac{2\pi}{3}\right) & 1 \end{bmatrix} \cdot \begin{bmatrix} {i_{qs}}^s \\ {i_{ds}}^s \\ {i_0}^s \end{bmatrix} \tag{2.3}$$

Transformations indicated in equations 2.21 and 2.22 are also applicable to voltages and flux linkages. When there is an inherent relationship (such as equal phase displacement and magnitude) between d^s-q^s variables and a-b-c variables, in such a situation there are only two independent variables in a-b-c, and the third one can be found as the negative sum of the other two. On the other hand, when there is no inherent relationship between the phase variables, then it is important to have a zero sequence component in order to obtain a-b-c variable from d^s-q^s-0^s variables.

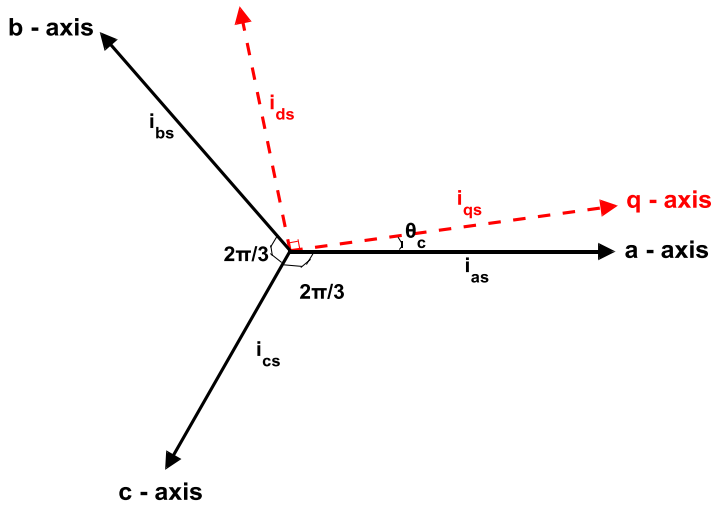

Figure 2.8: Stationary frame abc to $d^s q^s$ axes transformation.

Usually q^s-axis is aligned with phase a windings, which means that the d^s-q^s frame is fixed to the stator. This model is called stator reference frame model, where $\theta_c = 0$, thus the transformation from a-b-c to d^s-q^s is given by [4];

$$\begin{bmatrix} {i_{qs}}^s \\ {i_{ds}}^s \\ {i_0}^s \end{bmatrix} = \frac{2}{3} \begin{bmatrix} 1 & -\frac{1}{2} & -\frac{1}{2} \\ 0 & -\frac{\sqrt{3}}{2} & \frac{\sqrt{3}}{2} \\ \frac{1}{2} & \frac{1}{2} & \frac{1}{2} \end{bmatrix} \cdot \begin{bmatrix} i_{as} \\ i_{bs} \\ i_{cs} \end{bmatrix} \tag{2.4}$$

The sum of three phase currents in a balanced system is given by;

$$i_{as} + i_{bs} + i_{cs} = 0 \tag{2.5}$$

Thus the zero-sequence current value becomes zero;

$$i_0 = \frac{1}{3}(i_{as} + i_{bs} + i_{cs}) = 0 \tag{2.6}$$

The transformation derived in equation 2.24 is also applicable voltages and flux linkages.

Taking rotor frame as reference now, the angular position of the rotor reference frame is, $\theta_c = \theta_r$, thus the transformation from a-b-c to d^s-q^s is given by [4];

$$\begin{bmatrix} {i_{qs}}^s \\ {i_{ds}}^s \\ {i_0}^s \end{bmatrix} = \frac{2}{3}\begin{bmatrix} \cos\theta_r & \cos\left(\theta_r - \frac{2\pi}{3}\right) & \cos\left(\theta_r + \frac{2\pi}{3}\right) \\ \sin\theta_r & \sin\left(\theta_r - \frac{2\pi}{3}\right) & \sin\left(\theta_r + \frac{2\pi}{3}\right) \\ \frac{1}{2} & \frac{1}{2} & \frac{1}{2} \end{bmatrix} \cdot \begin{bmatrix} i_{as} \\ i_{bs} \\ i_{cs} \end{bmatrix} \tag{2.7}$$

Similarly, transformation derived in equation 2.26 is applicable to voltages and flux linkages.

2.4.2 Synchronous rotating reference frame

Figure 2.9 shows synchronously rotating d^e-q^e axes, rotating at synchronous speed of ω_e with respect to d^s-q^s axes and with an angle θ_e;

$$\theta_c = \theta_e = \omega_e t \tag{2.8}$$

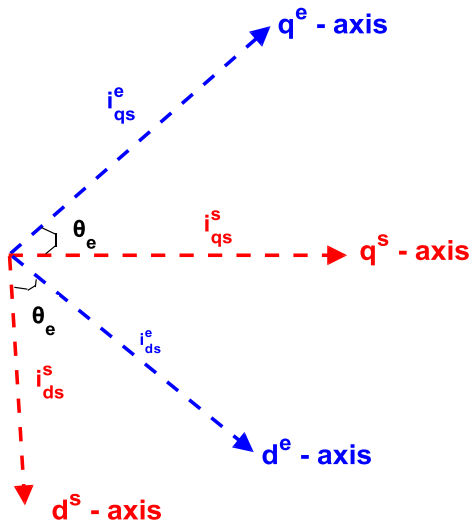

Figure 2.9: Stationary frame d^s-q^s axes to synchronous rotating frame d^e-q^e axes.

Thus the relationship between rotating frame parameters and stationary frame are [1];

$$\left.\begin{aligned} i_{qs}^{s} &= i_{qs}^{e}\cos\theta_e + i_{ds}^{e}\sin\theta_e \\ i_{ds}^{s} &= -i_{qs}^{e}\sin\theta_e + i_{ds}^{e}\cos\theta_e \end{aligned}\right\} \tag{2.9}$$

Now substituting equation 2.28 into 2.22, the transformation between three phase stationary frame to two phase synchronous frame is obtained as [4];

$$\begin{bmatrix} i_{qs}^{e} \\ i_{ds}^{e} \\ i_0 \end{bmatrix} = \frac{2}{3}\begin{bmatrix} \cos\theta_e & \cos\left(\theta_e - \frac{2\pi}{3}\right) & \cos\left(\theta_e + \frac{2\pi}{3}\right) \\ \sin\theta_e & \sin\left(\theta_e - \frac{2\pi}{3}\right) & \sin\left(\theta_e + \frac{2\pi}{3}\right) \\ \frac{1}{2} & \frac{1}{2} & \frac{1}{2} \end{bmatrix} \cdot \begin{bmatrix} i_{as} \\ i_{bs} \\ i_{cs} \end{bmatrix} \tag{2.10}$$

The transformation equation 2.29 is also applicable to voltages and flux linkages. It is seen that the synchronous reference frame transforms the sinusoidal inputs to DC quantities. This is an important derivation, since advanced control schemes for induction machines use this model to estimate control inputs, by decoupling the torque and flux channels.

The induction machine model in synchronous reference frames is expressed as [4];

$$\begin{bmatrix} v_{qs}^{e} \\ v_{ds}^{e} \\ v_{qr}^{e} \\ v_{dr}^{e} \end{bmatrix} = \begin{bmatrix} R_s + L_s p & \omega_s L_s & L_m p & \omega_s L_m \\ -\omega_s L_s & R_s + L_s p & -\omega_s L_m & L_m p \\ L_m p & (\omega_s - \omega_r) L_m & R_r + L_r p & (\omega_s - \omega_r) L_r \\ -(\omega_s - \omega_r) L_m & L_m p & -(\omega_s - \omega_r) L_r & R_r + L_r p \end{bmatrix} \begin{bmatrix} i_{qs}^{e} \\ i_{ds}^{e} \\ i_{qr}^{e} \\ i_{dr}^{e} \end{bmatrix} \tag{2.11}$$

Superscript “e” denotes electrical synchronous reference frame.

The electromagnetic torque is represented as [4];

$$T_e = \frac{3}{2}\frac{P}{2} L_m \left(i_{qs}^{e} i_{dr}^{e} - i_{ds}^{e} i_{qr}^{e} \right) \tag{2.12}$$

3 Voltage Source Converters

3.1 Voltage Source Rectifier

A three phase rectifier has lower ripple content in the waveforms and a higher power handling capability. A full bridge, three phase rectifier is shown in Figure 3.1;

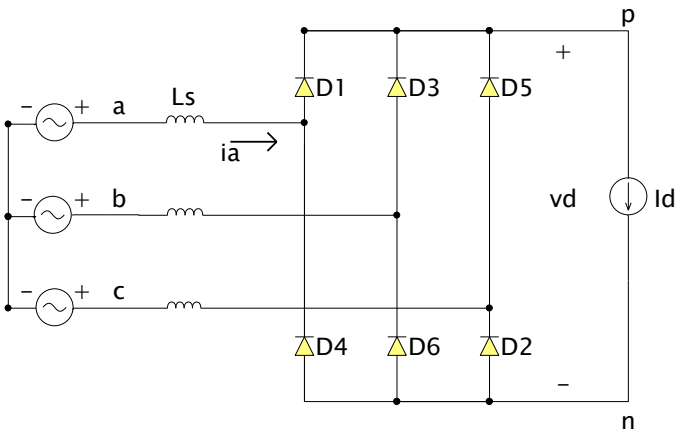

Figure 3.1: Full-bridge three phase rectifier [2].

The DC side in the Figure 3.1 is shown by a current source I_d, the current commutation is not instantaneous due to finite L_s at the grid side. The voltage drop during the commutation interval is shown in Figure 3.2. This voltage drop occurs at every 60^0 interval; therefore the average DC voltage is [2];

$$V_d = 1.35V_{LL} - \frac{3}{\pi}\omega L_s I_d \tag{3.1}$$

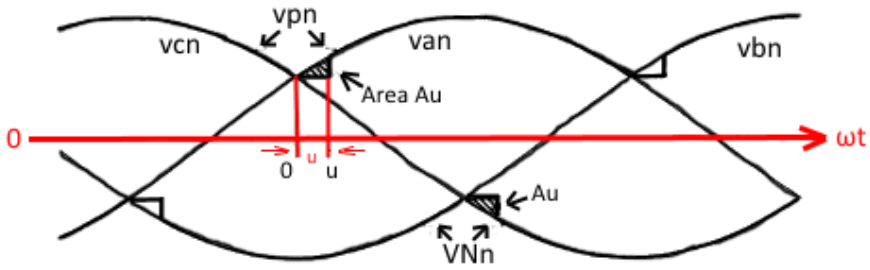

Figure 3.2: Current commutation of the rectifier [2].

3.2 Voltage Source Inverter

Power conversion from DC to AC is performed in switched mode, with the help of power semiconductors, which are controlled in an on-off fashion. The output AC voltage from the inverter has adjustable magnitude and frequency, as desired. Advances in power electronics and particularly the introduction of IGBTs have enabled the full control of switched mode inverters. Due to its many advantages, the IGBTs are ideal switching devices to be used in the VSI for driving induction motors.

A three phase bridge inverter (Figure 3.3) consists of three half bridges, that are shifted by 120^0, to generate the three phase AC voltage waveform. The input to the inverter is DC voltage from a rectifier which has been discussed previously. The power flow in each of the motor phases is controlled with the duty cycle of the respective switches. Pulse width modulation technique (PWM) is used to obtain desired duty cycle for each switch. There are several different types of modulation techniques that have been proposed and are still under research [46] [47] [48] [49] [50] [51] [52] [53] [54].

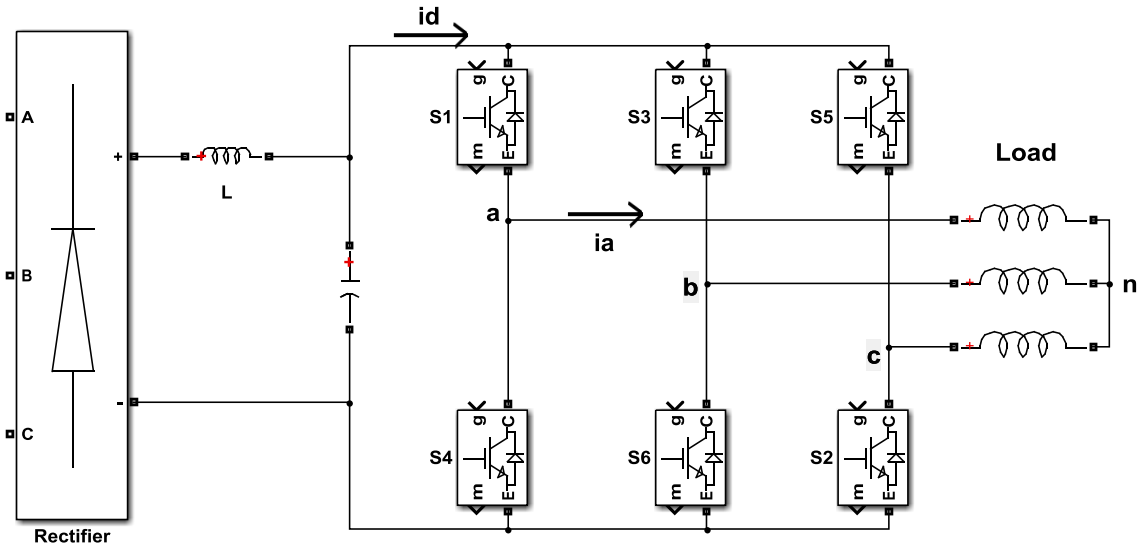

Figure 3.3: Three-phase bridge inverter with a diode rectifier [1].

3.3 Pulse Width Modulation (PWM)

PWM is a technique that generates low frequency signals to control the power switches from high frequency pulses. The low frequency is the average voltage over a switching period. The power switches, that are fed with the PWM pulse signal switches the output voltage of an inverter leg in between the upper and lower DC rail voltages. PWM is obtained by comparing two signals; a carrier and the modulating signal. The main classification of PWM methods are as follows [65];

- Sinusoidal PWM (SPWM)
- Selected harmonic elimination PWM
- Random PWM
- Hysteresis band current control PWM

- Space vector PWM

3.3.1 Hysteresis-Band Current Control PWM

Hysteresis band PWM is an instantaneous feedback current control technique where the actual current continuously tracks the command current within a hysteresis band. This type of modulation, introduces an envelope with upper and lower band limits, around the reference sinusoidal wave; the actual current ripple is confined within this hysteresis band, such that the actual current follows the reference sinusoidal waveform as show in Figure 3.4 [65]. The hysteresis modulation technique is a feedback current control method, where the motor line currents are compared with the reference sinusoidal current which is generated with a desired magnitude and frequency. If the current crosses the upper band limit of the hysteresis band, the upper power switch of the inverter leg is turned OFF, while the lower power switch is turned ON, therefore the current starts to decline. Hence, the output voltage transitions from $+0.5V_d$ to $–0.5V_d$. When the current reaches the lower band limit of the hysteresis band, the bottom power switch of the inverter leg is turned OFF, while the upper power switch is turned ON, subsequently the current stays within the defined hysteresis band limits, and forced to track the reference value back and forth or in a bang-bang switching manner. A dead time is provided at each transition to avoid short circuiting.

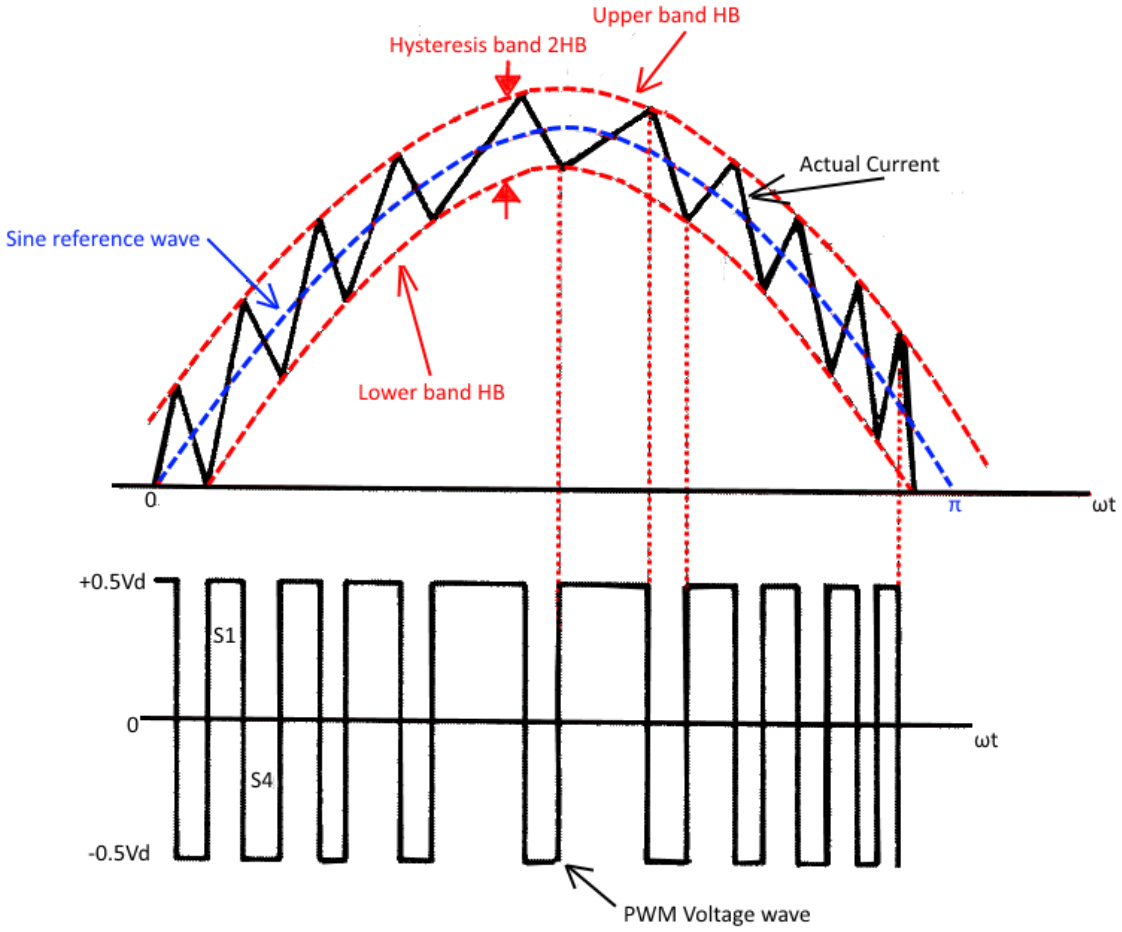

Figure 3.4: Principle of hysteresis band current control PWM [1].

The positive and negative slopes of the current are defined as [1];

$$\frac{di}{dt} = \frac{0.5V_d - V_{cm} \sin \omega_e t}{L} \tag{3.2}$$

$$\frac{di}{dt} = \frac{-(0.5V_d + V_{cm} \sin \omega_e t)}{L} \tag{3.3}$$

Where $0.5V_d$ is the applied voltage and $V_{cm} \sin \omega_e t$ is the instantaneous value of the opposing load counter EMF, and L is the load inductance.

The switching frequency and the peak to peak current ripple are dependent on the width of the hysteresis band. For instance, a smaller envelope will increase the switching frequency and lower the current ripple. It is desirable to have an optimum width of the band such that there is good balance between the switching losses and harmonic ripples. Figure 3.5, shows the control block diagram for the hysteresis band PWM, the bandwidth HB is [1];

$$HB = V_{comp} \frac{R_2}{R_1 + R_2} \tag{3.4}$$

The conditions for switching the devices are [1];

Upper switch ON: $\left(i_{ref}^{*} - i\right) > HB$

Lower switch ON: $\left(i_{ref}^{*} - i\right) < -HB$

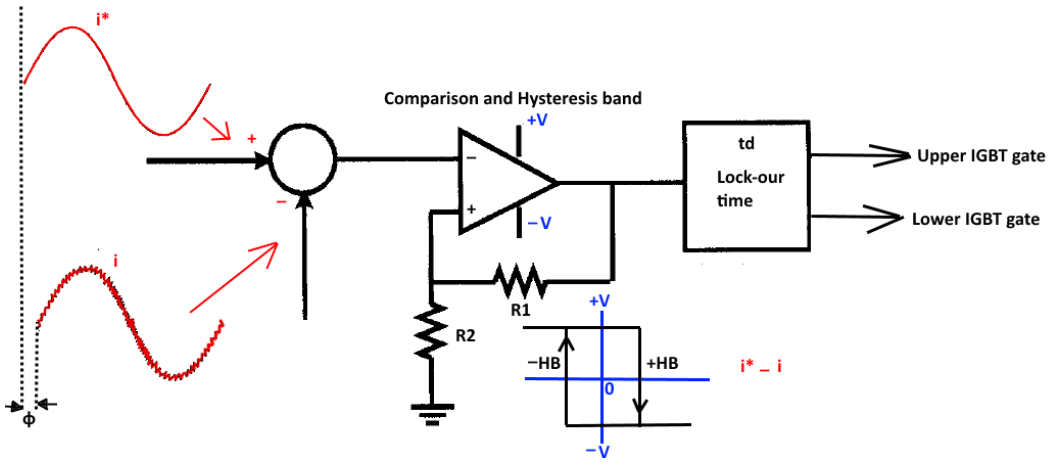

Figure 3.5: Hysteresis band current controller block diagram [1].

The main advantages of hysteresis current controller are that it is very easy to implement, it gives fast transient response, direct limiting of device peak current, and insensitivity to the DC link voltage ripple, permitting a lower value of the filter capacitor.

4 Advanced Control Schemes

4.1 Introduction

Scalar control of induction machines also known as Volts per Hertz control have been widely used in industrial applications, as it is easy to implement, and economically feasible. For an open loop scalar control technique feedback signals are not required, a more advanced scalar control is closed loop method which offers a more precise solution to controlling the speed and torque of the machine.

This technique is based on varying two parameters of the machine simultaneously. Following are the requirements of such a system;

- Varying the frequency of the VSI according to the desired output speed of the machine.
- Adjusting the output voltage of the VSI to maintain a constant air gap flux to ensure machine is in constant torque region.
- Supplying rated current on a continuous basis at any given frequency.

The system employs a three phase VSI, which has DC input from an uncontrolled rectifier. The PWM VSI is based on IGBTs providing three phase voltages and currents to the motor, with fully controllable magnitude and frequency. Figure 4.1, shows the system configuration in a block diagram, any PWM modulation technique could be employed for providing gate signals to the IGBTs in the VSI.

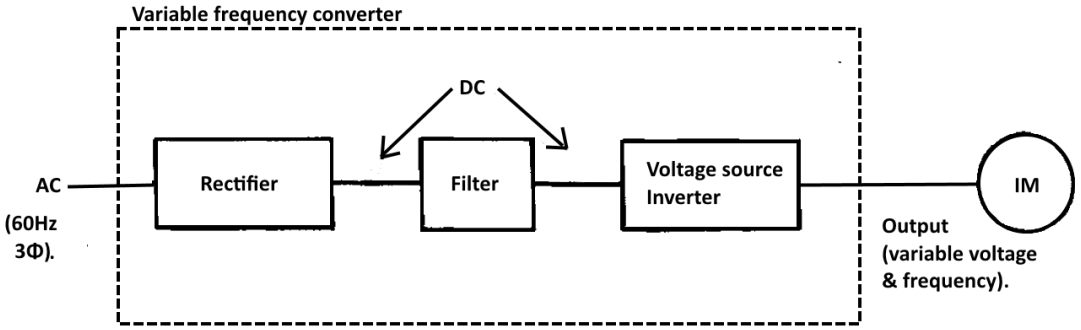

Figure 4.1: Variable frequency converter block diagram [2].

The input speed reference signal ω_{ref} is the main control variable; the frequency f of the inverter voltage is controlled by this parameter. The phase voltage command is setup from the speed command signal by gain factor G (V/F ratio), ensuring that the stator flux λ_s remains constant, which corresponds to air gap flux λ_{ag}, neglecting any changes in the stator resistance and leakage inductance of the machine; The stator voltage is needed to be proportional to the output frequency of the inverter;

$$\lambda_s = \frac{V_s}{2\pi f} \tag{4.1}$$

If the frequency is reduced at the rated stator voltage, the flux will start to saturate, resulting in excessive stator current and distortion of the flux waveforms [1]. In order to avoid this, when the machine is setup to run below the rated frequency region, the stator voltage must also be reduced in the same proportion, to maintain the flux to its rated value. When the machine is operating in the region of rated frequency, the maximum torque is maintained. However, in the region of low frequency the stator

resistance voltage tends to drop, which must be compensated by a voltage boost to ensure maximum torque is maintained. Therefore, a voltage boost is required at lower speeds so that the rated flux and corresponding torque is available at very low speeds.

As the frequency starts to rise beyond the rated frequency, the stator voltage saturates, decreasing the flux; this is known as the flux weakening region, and here the developed torque starts to decline. This flux weakening region allows the induction machine to operate beyond the rated speed range.

Scalar control techniques used for voltage source converter drives have provided good steady state responses, but poor dynamic response. This is due to the deviation in the air-gap flux linkages, which occurs not only in magnitude but also in phase. Stator and rotor phase currents and instantaneous phases, control the variations in the flux linkages, previous techniques made use of the stator current and magnitude and frequency, but not their phases. Therefore, there is deviation of magnitude and phase of the air gap flux linkages. These divergences in the air-gap flux linkages affect electromagnetic torque, which also reflects as speed oscillations. Scalar control technique is not suitable for high performance applications, such as centrifuges, servos, robotic actuators, process drives, and mills, where fast positioning, high precision and speed control are required. Furthermore, the deviations in air gap flux linkages lead to large stator currents, which require high rating of peak currents for power converter in the drive system to meet the dynamics [4].

4.2 Field Oriented Control (FOC)

Like DC motor drives, independent control of torque and flux is achievable in AC machine drives. Control of the phase, frequency and magnitude of the currents and consequently the control of flux phasor is achievable by inverter control. This is achieved in field co-ordinates, and hence the name field oriented control or vector control. Field oriented control has made AC drives more superior to DC drives due to their dynamic performance and independent control of flux and torque.

4.2.1 Principle of Field Oriented Control

The principal control of separately excited DC machine is emulated in field oriented control. The stator currents are decomposed into flux producing components and torque producing components, giving independent control. Using rotor flux orientation, the three stator currents are transformed into d and q axes currents in synchronous reference frame by using the transformations in chapter 2. The rotor flux orientation aligns the d-axis of the synchronous reference frame with the rotor flux vector $\overrightarrow{\lambda_r}$. Therefore, the resulting d and q axes rotor flux components and the torque can be expressed as; [55]

$$\lambda_{qr} = 0 \; and \; \lambda_{dr} = \lambda_r \tag{4.2}$$

$$T_e = K_T \lambda_{dr} i_{qs} = K_T \lambda_r i_{qs} \tag{4.3}$$

The torque equation 4.3, expresses that with the rotor field orientation, the torque equations for the induction machine is similar to the torque expression of a separately excited DC machine.

From Figure 4.2, the stator current vector $\overrightarrow{\imath_s}$ is decomposed into two components; the d-axis current $\overrightarrow{\imath_{ds}}$ and q-axis current $\overrightarrow{\imath_{qs}}$. The d-axis current $\overrightarrow{\imath_{ds}}$ is the flux producing current while the q-axis current $\overrightarrow{\imath_{qs}}$ is the torque producing current. Hence, the flux and torque producing components of the current are DC quantities; therefore these components are ideal for use as control variables. When i_{qs} is controlled it affects the actual current i_{qs} only, and does not affect the flux λ_r, and in the same way when i_{ds} is controlled, it affects the flux λ_r only, and does not affect the i_{qs} component of the current. Thus, the developed torque can be directly controlled through q-axis stator current i_{qs}, if λ_r is kept constant [55] [4].

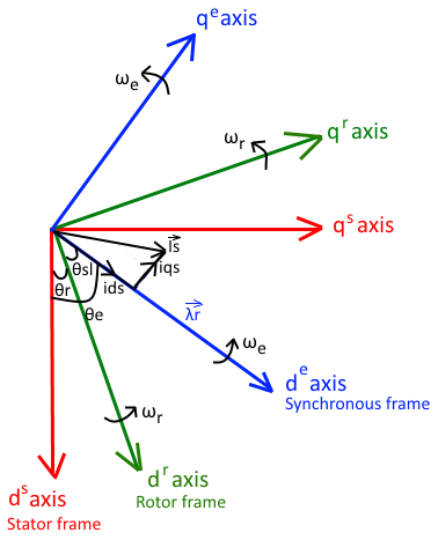

Figure 4.2: Rotor flux field orientation (d-axis aligned with $\overrightarrow{\lambda_r}$) [55].

Accurate determination of the rotor flux angle θ_e for rotor flux oriented control is essential; various methods could be used to calculate the angle. Such as, it can be found from measured stator voltages and currents, or it can be calculated from the following equations [4];

$$\theta_e = \theta_r + \theta_{sl} \tag{4.4}$$

$$\theta_e = \int (\omega_r + \omega_{sl})dt = \int \omega_e dt \tag{4.5}$$

Field oriented control technique is classified according to how the rotor flux angle is acquired. The two types of control schemes are;

- Direct field oriented control where the rotor flux angle is calculated by using flux sensing windings, or by using measured terminal voltages and currents.
- Indirect field oriented control where the rotor flux angle is found by using rotor position measurement and partial estimation by machine parameters.

4.2.2 Indirect field oriented control (IFOC)

This technique generates θ_e, in a feedforward manner; IFOC is very common in the industry as compared to DFOC.

Using the dynamic equation of the induction machines in the synchronous rotating reference frame presented in chapter 2, the rotor circuit equations can be written as [4];

$$R_r i_{qr} + \frac{d\lambda_{qr}}{dt} + \omega_{sl}\lambda_{dr} = 0 \tag{4.6}$$

$$R_r i_{dr} + \frac{d\lambda_{dr}}{dt} - \omega_{sl}\lambda_{qr} = 0 \tag{4.7}$$

The rotor flux linkage expressions are [1];

$$\lambda_{qr} = L_m i_{qs} + L_r i_{qr} \tag{4.8}$$

$$\lambda_{dr} = L_m i_{ds} + L_r i_{dr} \tag{4.9}$$

The total rotor flux λ_r is aligned to d-axis, thus yielding [4] [1];

$$\lambda_r = \lambda_{dr} \tag{4.10}$$

$$\lambda_{qr} = 0 \tag{4.11}$$

$$\frac{d\lambda_{qr}}{dt} = 0 \tag{4.12}$$

$$\frac{L_r}{R_r}\frac{d\lambda_r}{dt} + \lambda_r = L_m i_{ds} \tag{4.13}$$

Therefore the following equations could be written [4] [1];

$$i_{qr} = -\frac{L_m}{L_r} i_{qs} \tag{4.14}$$

$$i_{dr} = \frac{\lambda_r}{L_r} - \frac{L_m}{L_r} i_{ds} \tag{4.15}$$

$$\omega_{sl} = \frac{L_m R_r}{\lambda_r L_r} i_{qs} \tag{4.16}$$

The electromagnetic torque is derived as [4];

$$T_e = \frac{3}{2}\frac{P}{2}\frac{L_m}{L_r}\left(\lambda_r i_{qs}\right) \tag{4.17}$$

Here L_r/R_r (τ_r) is the induction machine rotor time constant on the order of a second. If the rotor flux linkage is kept constant, then from equation 4.24; torque is proportional to the q-axis stator current component i_{qs}. The rotor flux angle θ_e is calculated from the measured rotor speed and calculated slip angle based on motor parameters, thus the expression for calculating the rotor flux angle is [55];

$$\theta_e = \int (\omega_r + \omega_{sl}) dt = \theta_r + \theta_{sl} \tag{4.18}$$

4.2.3 Simulink modelling

The indirect field oriented control strategy is implemented with the help of equations 4.21, 4.23, 4.24 and 4.25. The power circuit implementing IFOC consists of front end diode rectifier and a voltage source PWM inverter with a dynamic braking chopper. The braking chopper is used for regenerative braking, allowing motor to decelerate when the speed is set to reduce during dynamic simulations, see Appendix A for details about braking chopper module. A hysteresis band current controller PWM technique is implemented to send gate pulses to the VSC, the complete system is shown in Figure 4.3.

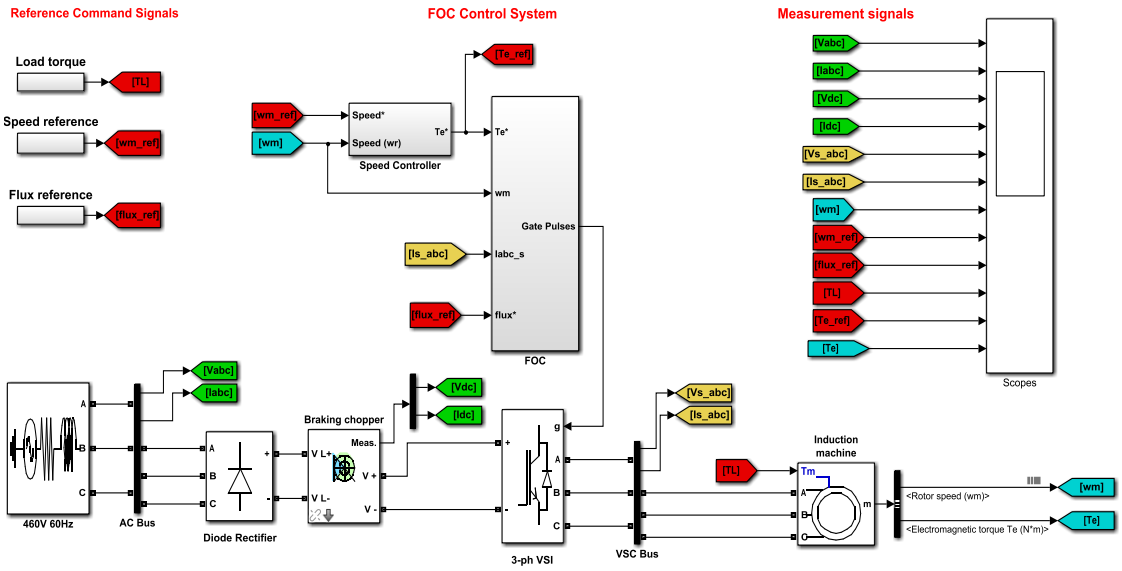

Figure 4.3: Complete Indirect Field Oriented Control Scheme model (in Simulink).

A speed controller is used to generate the torque command as a function of the speed error signal, through a PI controller and a torque limiter. The torque producing quadrature current component i_{qs}* which is in synchronous rotating frame is generated

from equation 4.24. The user flux command is used in equation 4.20, for determining the direct current component i_{ds}* which is in synchronous rotating frame.

The machine stator currents (i_{abc}) are transformed to synchronous rotating d-q current components, which are then used to generate slip speed ω_{sl}* using equation 4.23. Now this reference slip speed ω_{sl}* is added with measured rotor speed ω_r and the result is integrated to produce rotor flux angle θ_e from equation 4.25.

Reference quadrature and direct current components (i_{qs}* and i_{ds}*) obtained from reference torque and flux are in synchronous rotating frames, they are transformed to stationary three phase current references (i_{as}*, i_{bs}* and i_{cs}*) with the help of angle θ_e. Transformation equations for converting d-q synchronous frame to stationary frame are given in chapter 2.

The three phase reference currents are compared with three phase machine currents in hysteresis current controllers to generate gate signals for VSI switch modules. All the designed Simulink models for IFOC are shown in Appendix A, Section 8.1.

4.3 Direct Torque Control (DTC)

Direct torque control scheme directly links the stator voltage to the torque and flux of the machine, unlike field oriented control which heavily relies on stator current to control the torque and flux of the machine, DTC precisely controls the torque and flux of the induction machine by VSI voltage space vector selection through a look up table [1]. DTC makes use of the power electronic switches in the VSC for decoupling the non-linear

system of the induction motor. It eliminates the need to use intermediate current control loops, thus the design of the variable speed drive using this scheme is less complex and simpler to implement. DTC technique provides fast torque response, low inverter switching frequency and low harmonic losses [56]. DTC is basically sensorless, the actual rotor speed is not required in the torque mode of operation, due to absence of coordinate transformation. Variations in the rotor parameters do not affect this control scheme, but variations in the stator resistance (due to thermal reasons) can cause few problems with this technique [57].

4.3.1 Principle of Direct Torque Control

DTC is mainly based on hysteresis control of the torque and flux together with optimal VSI switching logic based on space vector, which is described in Chapter 3. DTC also requires an accurate machine model, for the estimation of stator flux, machine's torque, and for accurate measurements of the input stator voltages and currents [57]. Neglecting stator voltage drop due to stator resistance, it can be said that stator flux can be directly controlled by the stator applied voltage [55];

$$\frac{\overrightarrow{d\lambda_s}}{dt} = \overrightarrow{v_s} - R_s\overrightarrow{\iota_s} \tag{4.19}$$

This equation shows that the stator flux vector reacts instantly to changes in stator voltage vector. Thus it is clear that the VSI output voltage space vector can directly control the stator flux, by selecting the appropriate VSI output voltage, stator flux can be set as needed.

The electromagnetic torque developed by the machine can be expressed as [55];

$$T_e = \frac{3P}{2}\frac{L_m}{\sigma L_s L_r}\lambda_s \lambda_r \sin\gamma \tag{4.20}$$

When the VSI voltage vectors are applied, the stator flux vector $\overrightarrow{\lambda_s}$ is displaced from the rotor flux vector $\overrightarrow{\lambda_r}$, thus increasing or decreasing the electromagnetic torque, as the torque angle γ is changed. Therefore it can be determined that the machine's torque is instantly changed by displacing the stator flux linkage space vector as required by the torque demand [57]. This scheme requires set values of torque and flux as inputs, to establish a closed loop control, current controllers are not required, but two and three level hysteresis controllers are used to obtain required flux and torque responses, through hysteresis bandwidth. An appropriate VSI voltage vector is selected according to the position of the stator flux linkage vector, for a two level VSI voltage space vectors; there are six sectors in a two dimensional complex plane, corresponding to six active voltage vectors that are spaced 60^0 from each other. The rotor flux linkage space vector is large when compared to stator flux linkage vector, thus it changes slowly, and is assumed to be constant.

4.3.2 Control Strategy

The flux and torque commands (λ_s* and T_e*) are compared with the calculated flux and torque values which are generated from the flux/torque calculator block which calculates these values from the machine terminal voltages and currents, and their errors are then sent to the hysteresis band controller. In order to develop the

flux/torque calculator block, the stator flux vector $\overrightarrow{\lambda_s}$ in the stationary frame is expressed as [55];

$$\overrightarrow{\lambda_s} = \lambda_{ds} + j\lambda_{qs} = \int (v_{ds} - R_s i_{ds})dt + j\left(v_{qs} - R_s i_{qs}\right)dt \tag{4.21}$$

Therefore the magnitude and angle of the stator flux vector are [55];

$$\lambda_s = \sqrt{\left(\lambda_{ds}^2 + \lambda_{qs}^2\right)} \tag{4.22}$$

$$\theta_s = \tan^{-1}\left(\frac{\lambda_{qs}}{\lambda_{ds}}\right) \tag{4.23}$$

And the developed electromagnetic torque can be calculated as [55];

$$T_e = \frac{3P}{2}\left(i_{qs}\lambda_{ds} - i_{ds}\lambda_{qs}\right) \tag{4.24}$$

The above equations 4.28, 4.29, 4.30 and 4.31, shows that the stator flux and machine torque physical values can be calculated using measured stator voltages and currents, and motor parameter stator resistance R_s. This clearly indicates that DTC does not suffer from motor parameter sensitivity, except from stator resistance temperature fluctuations, when compared with field oriented control that depends upon almost all motor parameters.

The hysteresis band controller for the flux has two levels of output [1];

$$H_\lambda = 1 \; for \; E_\lambda > HB_\lambda \tag{4.25}$$

$$H_\lambda = -1 \; for \; E_\lambda < HB_\lambda \tag{4.26}$$

Where $2HB_\lambda$ = bandwidth of the flux hysteresis controller.

The stator flux λ_s is restricted to stay within the bandwidth of the hysteresis controller tracking the reference flux λ_s^* in a zig zag path as shown in Figure 4.4(a).

The torque error is processed through a three level hysteresis controller that has three levels of output [1];

$$H_{Te} = 1 \; for \; E_{Te} > +HB_{Te} \tag{4.27}$$

$$H_{Te} = -1 \; for \; E_{Te} < -HB_{Te} \tag{4.28}$$

$$H_{Te} = 0 \; for \; -HB_{Te} < E_{Te} < +HB_{Te} \tag{4.29}$$

The output from the hysteresis band controller establishes the selection of the voltage space vector. Sector selection block generates a sector number in which the stator flux vector is positioned. The sector generator block has one output, which is defined by six sectors that are 60^0 ($\pi/3$ radians) apart as shown in Figure 4.4. Outputs from the hysteresis band controllers and the sector generator selects the appropriate voltage vector from the vector lookup table as shown in Table 4.1, that determines the gate signals sent to the VSI. Table 4.1 applies the selected voltage vector as a gate signal

to the VSI which fundamentally affects both the machine torque and the stator flux simultaneoulsy. By neglecting stator resistance, following equations can be deduced [1];

$$\overrightarrow{V_s} = \frac{d\lambda_s}{dt} \tag{4.37}$$

$$\vec{\Delta}\lambda_s = \overrightarrow{V_s}.\Delta t \tag{4.30}$$

From equation 4.37, by applying stator voltage vector, incremental change in λ_s is achieved for a time of Δt, as shown in Figure 4.4. An example of the flux trajectory from segments AB, BC, CD and DE and their respective voltage vectors are also shown in Figure 4.4(a). The DTC block diagram is shown in Figure 4.5.

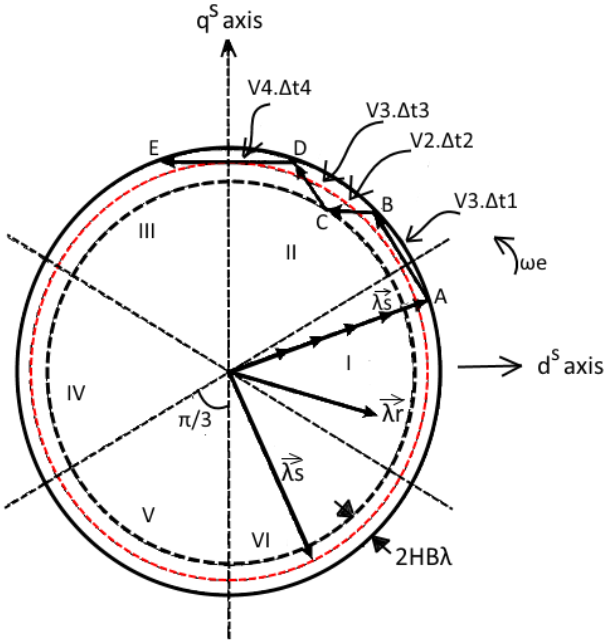

(a) Trajectory of stator flux vector

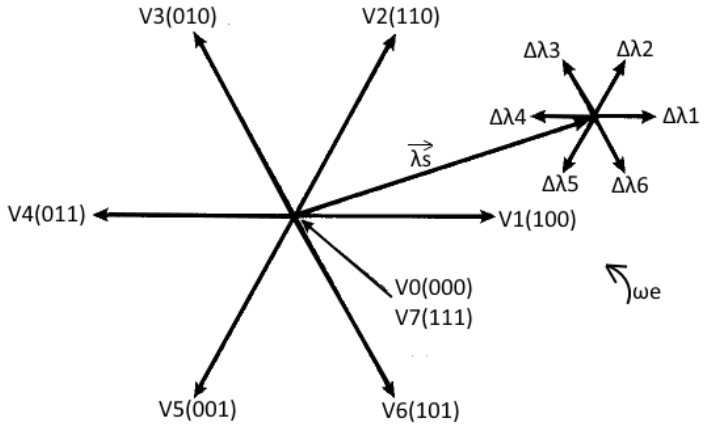

(b) Inverter voltage vectors.

Figure 4.4 (a) & (b): Concept of DTC control strategy [1].

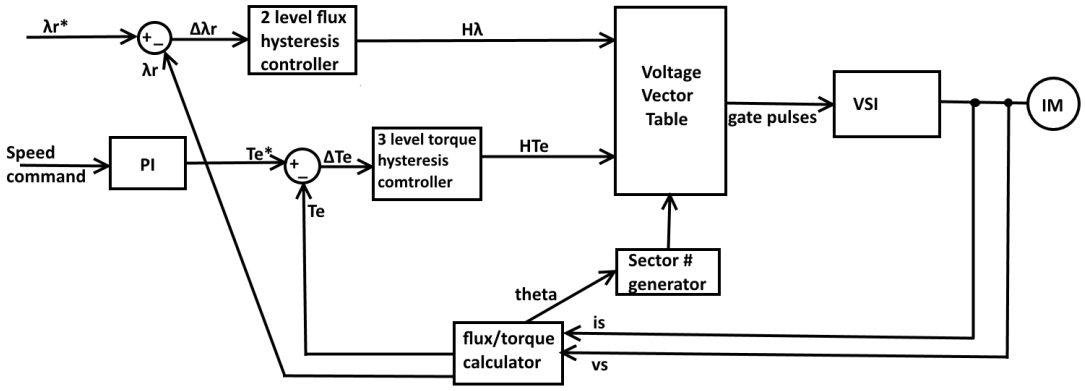

Figure 4.5: Direct Torque Control Scheme block diagram.

As seen from Table 4.2, the table is derieved from Figure 4.4, showing the magnitude and direction of the torque and flux change according to the applied voltage vector for the position of λ_s. The flux can be increased by the voltage vectors V_1, V_2, and V_6, and it can be decreased by voltage vectors V_3, V_4, and V_5. On the other hand, torque is increased by the voltage vectors V_2, V_3, and V_4,and can be decreased by voltage vectors V_1, V_5 and V_6. As for the zero voltage vectors V_0 and V_7, the machine terminals are short-circuited, keeping the flux and torque unchanged [19].

Table 4.1: Switching logic of VSI voltage vectors [19]

H_λ	H_{Te}	Sector I	Sector II	Sector III	Sector IV	Sector V	Sector VI
1	1	$\overrightarrow{V_2}$	$\overrightarrow{V_3}$	$\overrightarrow{V_4}$	$\overrightarrow{V_5}$	$\overrightarrow{V_6}$	$\overrightarrow{V_1}$
	0	$\overrightarrow{V_0}$	$\overrightarrow{V_7}$	$\overrightarrow{V_0}$	$\overrightarrow{V_7}$	$\overrightarrow{V_0}$	$\overrightarrow{V_7}$
	-1	$\overrightarrow{V_6}$	$\overrightarrow{V_1}$	$\overrightarrow{V_2}$	$\overrightarrow{V_3}$	$\overrightarrow{V_4}$	$\overrightarrow{V_5}$
-1	1	$\overrightarrow{V_3}$	$\overrightarrow{V_4}$	$\overrightarrow{V_5}$	$\overrightarrow{V_6}$	$\overrightarrow{V_1}$	$\overrightarrow{V_2}$
	0	$\overrightarrow{V_7}$	$\overrightarrow{V_0}$	$\overrightarrow{V_7}$	$\overrightarrow{V_0}$	$\overrightarrow{V_7}$	$\overrightarrow{V_0}$
	-1	$\overrightarrow{V_5}$	$\overrightarrow{V_6}$	$\overrightarrow{V_1}$	$\overrightarrow{V_2}$	$\overrightarrow{V_3}$	$\overrightarrow{V_4}$

Active voltage vectors: $\overrightarrow{V_1} = 100, \overrightarrow{V_2} = 110, \overrightarrow{V_3} = 010, \overrightarrow{V_4} = 011, \overrightarrow{V_5} = 001, \overrightarrow{V_6} = 101.$

Zero voltage vectors: $\overrightarrow{V_0} = 111, \overrightarrow{V_7} = 000.$

Table 4.2: Flux and Torque variations due to applied voltage vector (arrow indicated magnitude and direction) [19]

Voltage vectors	$\overrightarrow{V_1}$	$\overrightarrow{V_2}$	$\overrightarrow{V_3}$	$\overrightarrow{V_4}$	$\overrightarrow{V_5}$	$\overrightarrow{V_6}$	$\overrightarrow{V_0}$ $\overrightarrow{V_7}$
λ_s	↑	↑	↓	↓	↓	↑	0
T_e	↓	↑	↑	↑	↓	↓	↓

4.3.3 Simulink modelling

The Simulink model for a complete direct torque control induction machine system is shown in Figure 4.6.

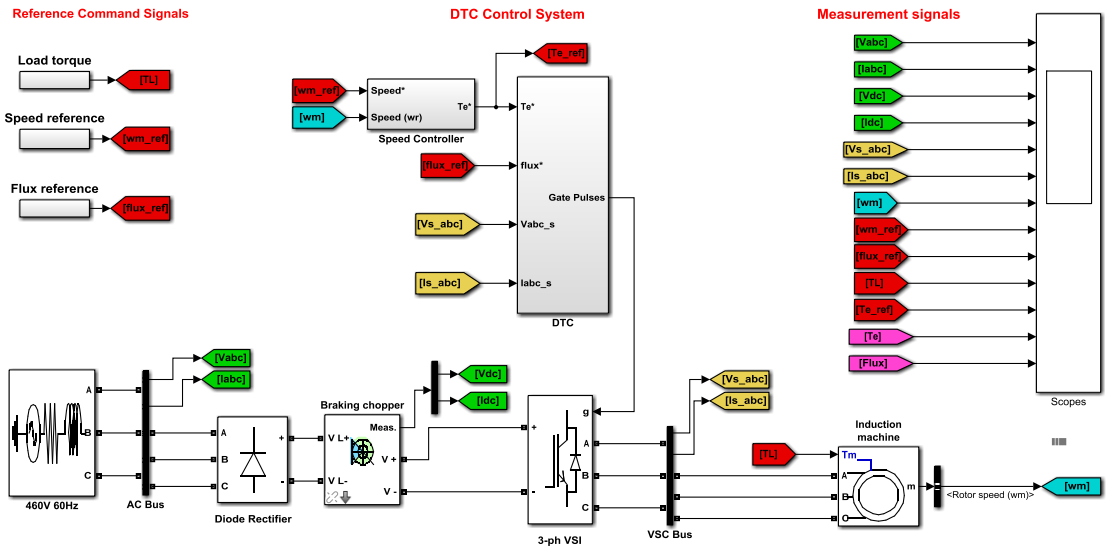

Figure 4.6: Complete Direct Torque Control system model (in Simulink).

The speed controller block is used in the same way as in IFOC drive model to generate reference electromagnetic torque. The DTC block is the actual controller that generates six gate pulses for VSI. The inputs to the subsystem are the machine torque reference and flux reference commands, together with measured VSI voltages and currents (V_{abc} and I_{abc}).

The measured voltages and currents from the VSI output are converted to d-q axis (v_{qd} and i_{qd}), using equations 4.31 to 4.33, the values of machine torque T_e, machine stator flux λ_s and flux angle θ_s are calculated. The torque error is passed through a three level hysteresis controller that is based on equations 4.34 to 4.36. Whereas, the flux

error is passed through a two level hysteresis comparator that is based on equations 4.32 and 4.33. The output from the comparators together with the sector number, which is generated from the flux sector selector subsystem block, are used to select voltage space vectors from a look up table (based on Table 4.1), which generates gate signal pulses for the VSI. All the designed Simulink models for DTC are shown in Appendix A, Section 8.1.

5 Case Studies

5.1 Introduction

Simulink models of DTC and IFOC control schemes are simulated to compare the performances of the two advanced control techniques of induction machine drives in normal and abnormal operating conditions. Under normal operating conditions, analysis is performed to compare the start-up behavior of the machine drives. Under dynamic/transient conditions, analysis is performed with steps changes in load torque, speed, and flux for comparison of the machine drives. Furthermore, under abnormal operating conditions such as fluctuations in voltages, frequency and harmonics of the three phase AC voltages, and their effects on the machine drives are observed and discussed. System parameters are kept identical for both the control schemes to be able to make a fair comparison. System parameters, are shown in Table 9.2 in Appendix B;

5.2 Normal operating conditions

In this section machine, the drives will be operated under normal operating conditions, and a comparison will be done for machine start-up, steady state, and dynamic state behaviors.

5.2.1 Steady-state operation comparison

Steady state comparison is best to make analysis and observation of machine start up conditions. It is one of the most crucial analysis condition needed to make a fair

comparison of both the advanced control schemes. The drive controller for both the schemes is setup with full load torque of 11 N.m (1pu) with speed command set to 200 RPM (0.22pu) and stator flux setup to its nominal value 0.8Wb. Following analysis is done on rotor speed, electromagnetic torque, stator and rotor fluxes and stator currents;

- **Rotor speed comparison:** As seen in Figure 5.1, FOC takes about 0.36 seconds to reach the speed command of 0.22pu, whereas DTC takes about 0.38 seconds. Therefore, FOC clearly shows a better speed response than DTC.

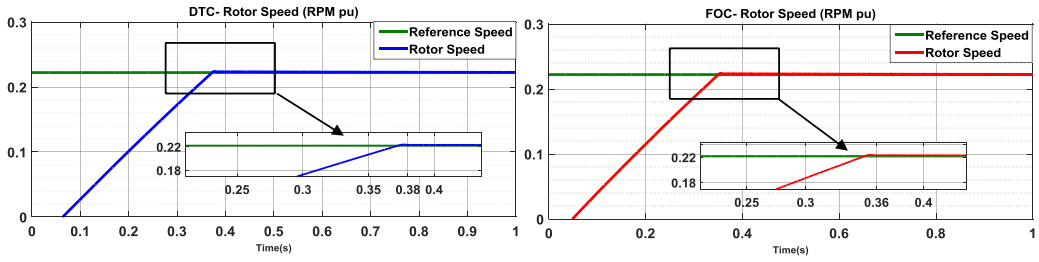

Figure 5.1: DTC & FOC Rotor speed (steady-state analysis).

- **Electromagnetic torque comparison:** As seen in Figure 5.2, DTC takes about 0.02 seconds to reach the reference torque command, whereas FOC takes about 0.028 seconds. DTC tracks the demand torque faster than FOC, this is because FOC scheme uses currents as controlled variables and currents are maintained within limits, in DTC scheme currents are not limited, thus allowing DTC to draw higher currents at start-up to reach the demanded torque faster. It is also

observed that DTC scheme has higher torque ripples than FOC; this is because of variable switching frequency due to hysteresis controllers.

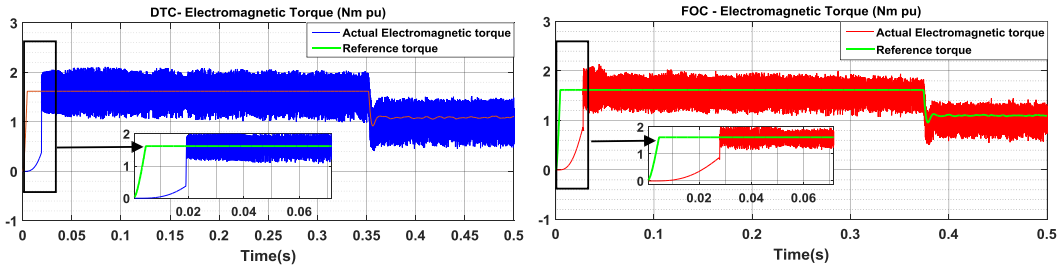

Figure 5.2: DTC & FOC Electromagnetic Torque (steady-state analysis)

- **Flux comparison:** In DTC drive scheme, the stator flux is directly controlled through two level flux hysteresis controller and stator voltage vectors, thus the stator flux reaches its nominal value promptly as seen in Figure 5.3. On the other hand, FOC doesn't have direct flux control, the rotor flux is controlled through the direct current component i_d, and therefore the rotor flux response is slower in this respect as seen in Figure 5.3. The rotor flux in FOC scheme is dependent upon the rotor time constant (τ_r) i.e. 0.14 seconds in this case and this is the time rotor flux takes to settle down. The rotor flux tracks the stator flux in DTC scheme with a time constant equal to $\sigma\ \tau_r$ i.e. 0.04 seconds in this case.

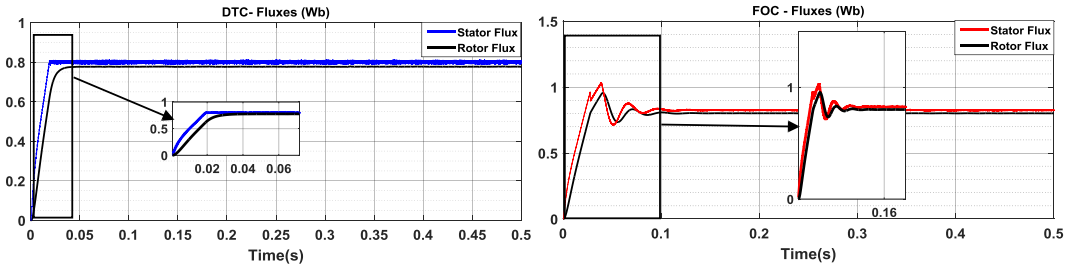

Figure 5.3: DTC & FOC Fluxes (steady-state analysis).

- **Stator current comparison:** As seen in Figure 5.4, DTC startup current drawn is 3.8pu, and FOC startup current draw is 2.1pu. FOC scheme has current regulators that directly controls and limits the machine stator currents, thus maintaining machine currents at all times. On the other hand, DTC scheme does not employ any direct current controller; therefore the machine draws significantly higher currents at startup. This could be a problem for DTC scheme if an application requires regular start and stop modes, and then special measures need to be taken in such operating conditions.

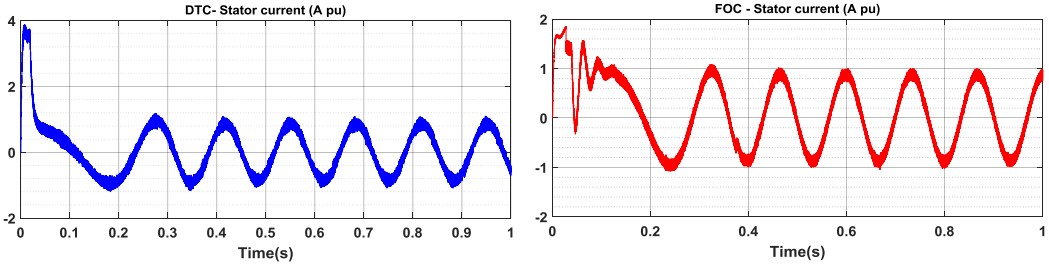

Figure 5.4: DTC & FOC Stator currents (steady-state analysis).

5.2.2 Dynamic performance comparison

Dynamic performance is tested by introducing steps in load torque, steps in stator/rotor flux and steps in speed command.

1. **Low speed dynamic operation**: By introducing a torque reversal step from 11 N.m (1pu) to -11N.m (-1pu) at very low speeds of around 0.5 RPM (0.00055pu) and constant nominal flux, the dynamic performance of advanced control schemes operation under very low speeds is compared. The load torque reversal is introduced at 1.5 seconds of simulation time, and the discussion is as follows;
   - As seen in Figure 5.5, DTC drive rotor speed takes 2.24 seconds to settle down after the torque reversal, whereas the FOC drive rotor speed takes 2 seconds to settle down. The speed overshoots between -0.0027pu to 0.00672pu during torque reversal in both the control schemes, which is within reasonable limits for a low speed operating condition. Again the advantage of FOC speed response is observed.

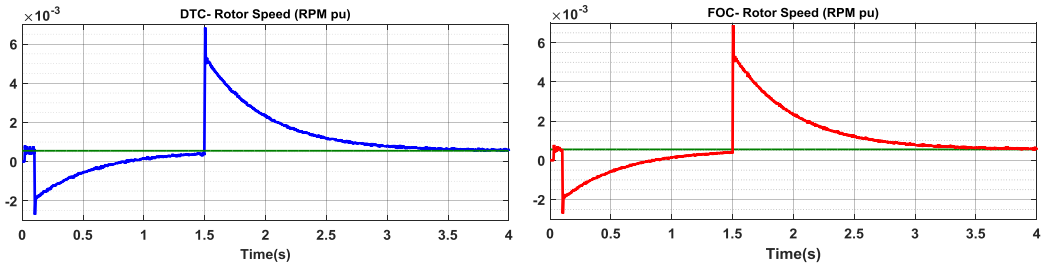

Figure 5.5: DTC & FOC Rotor speed (low speed dynamic response).

- As seen in Figure 5.6, torque settling down time in both the machine drives takes about 0.02 seconds after the reversal command. Showing similar torque dynamics at low speeds. However, it is worth noting that DTC scheme shows higher transient ripples due to torque hysteresis controllers.

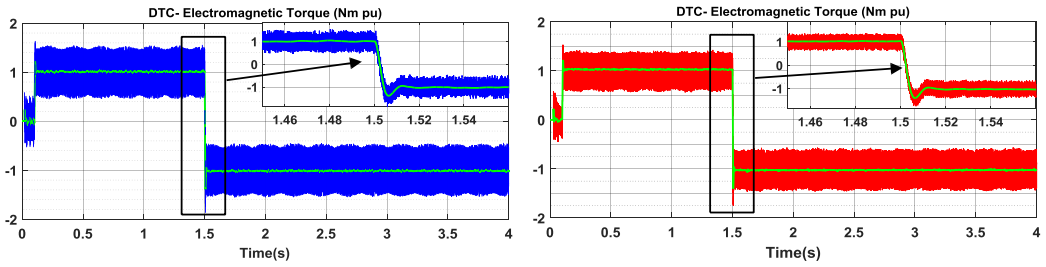

Figure 5.6: DTC & FOC Electromagnetic torque (low speed dynamic response).

- DTC scheme suffers from undesired flux weakening phenomena at low speeds. As seen in Figure 5.7, the stator and rotor fluxes have significant ripples during low speed operation when compared to FOC scheme. In this low speed region the DTC control system selects the zero voltage vectors several times.

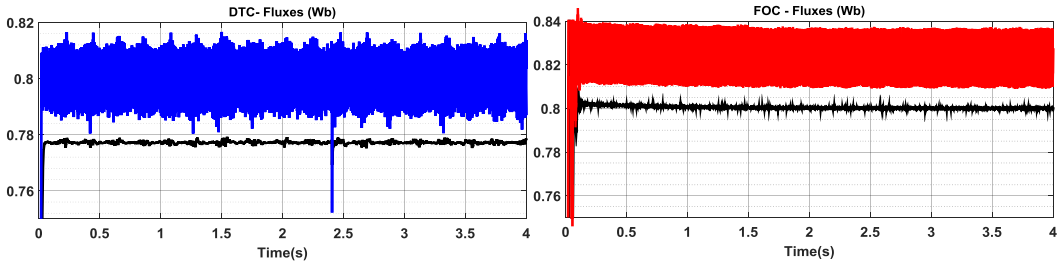

Figure 5.7: DTC & FOC Fluxes (low speed dynamic response).

- As seen in Figure 5.8, stator current ripples are observed at machine start up and also during torque reversal in both the schemes. DTC drive draws more currents when compared with FOC scheme during torque reversals, due to the absence of current regulators.

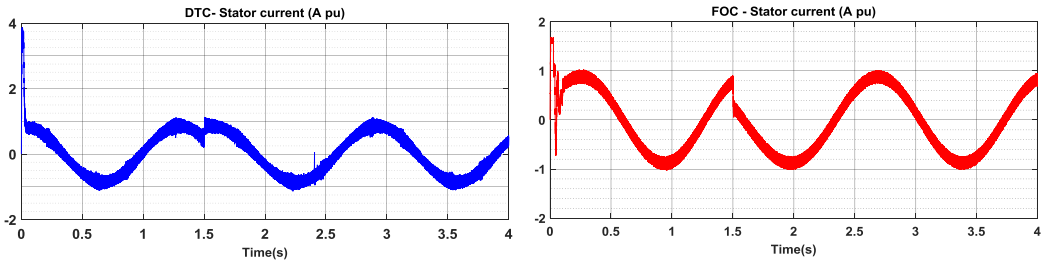

Figure 5.8: DTC & FOC Stator current (low speed dynamic response).

2. **High speed dynamic operation:** here again a torque reversal step similar to the first case is introduced at high speed of 900 RPM (1pu) and constant nominal flux, and the dynamic performance of the drives are compared. The torque reversal step change is introduced at 2 seconds of simulation time, and the discussion is as follows;

- As seen in Figure 5.9, speed settling times for both control drives schemes are comparable within 1.5 seconds of torque reversal step change. The rotor speed overshoot is also very small about 0.006pu. It is observed that there is some notable noise in DTC rotor speed; the transient ripples in electromagnetic torque have become evident in high rotor speeds.

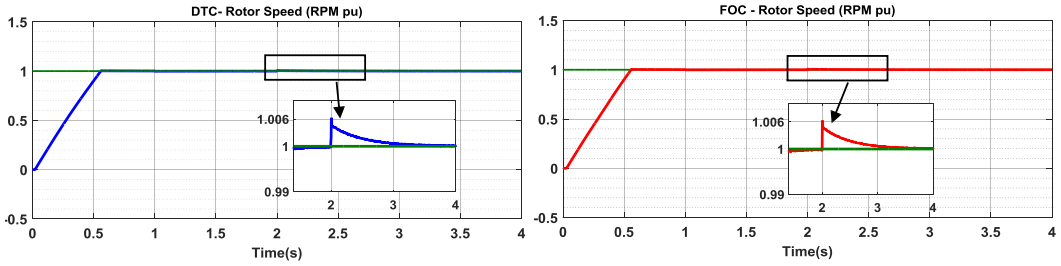

Figure 5.9:DTC & FOC Rotor speed (high speed dynamic response).

- As seen in Figure 5.10, DTC drive clearly shows better torque dynamic performance at high speeds. FOC drive has shown difference in torque dynamic behaviors at high and low speeds; this is due to the saturation of current controllers at high speeds in part of PWM cycle, because of higher counter EMF, the fundamental current loses track of the reference current in which case vector control becomes invalid.

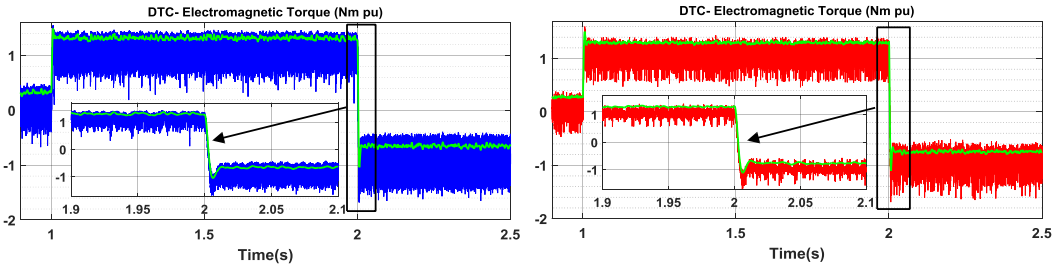

Figure 5.10: DTC & FOC Electromagnetic torque (high speed dynamic response).

- As seen in Figure 5.11, flux response of DTC drive is excellent at high speeds; the fluxes have no effect from torque reversal. FOC also has good flux response; there are some ripples in the stator and rotor flux at torque reversal point, but nothing significant. Both the control schemes show decoupled torque and flux operation.

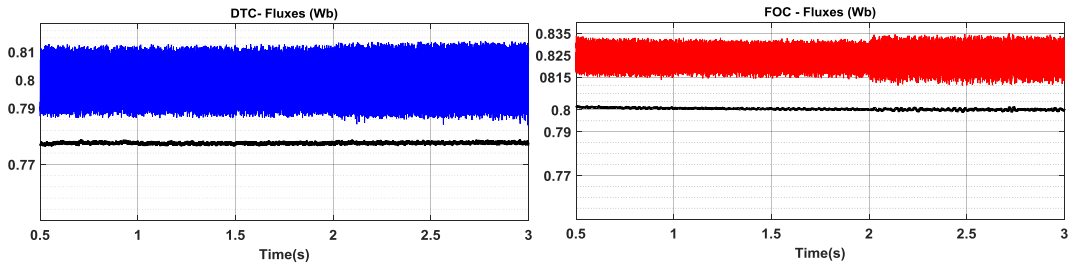

Figure 5.11: DTC & FOC Fluxes (high speed dynamic response).

- As seen in Figure 5.12, FOC drive has maintained machine's current limits even at high speeds when compared with DTC drive which draws more current at torque reversal point.

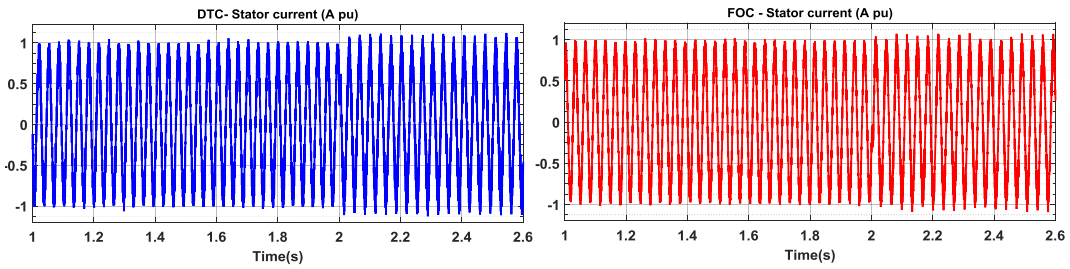

Figure 5.12: DTC & FOC Stator current (high speed dynamic response).

3. **Dynamic speed operation:** The machine's load torque has been fixed to 1 N.m (0.09pu) and flux is fixed to constant nominal flux of 0.8Wb, the rotor speed is varied between high and low speeds from 900 RPM (deceleration) to 100 RPM (0.11pu) and back to 900 RPM (acceleration), and the discussion is as follows;

- As seen in Figure 5.13, FOC drive has shown better speed response during acceleration and deceleration regions, with fewer transient ripples and quicker settling down time. On the other hand, DTC drive has more transient ripples during acceleration and deceleration regions, this is due to higher transient ripples observed in electromagnetic torque.

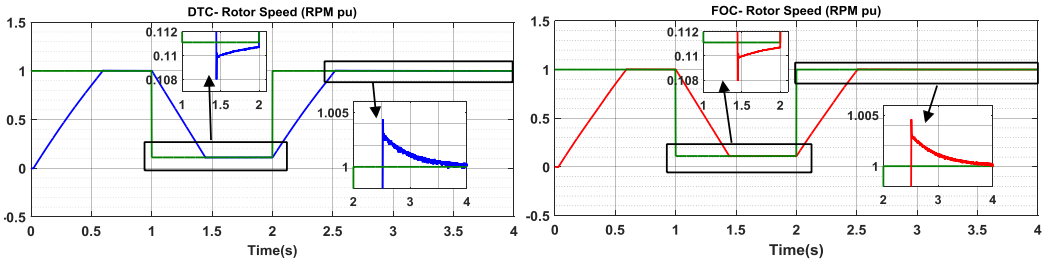

Figure 5.13: DTC & FOC Rotor speed (variable speed dynamic response)

- As seen in Figure 5.14, as the machine accelerates to increase the rotor speed the electromagnetic torque of the machine is increased to help with acceleration, and similarly when the machine decelerates to decrease the rotor speed, the electromagnetic torque is reduced. DTC drive has higher transient and overall torque ripples, when compared to FOC drive, but has better dynamic response time, showing advantage and drawback of three level torque hysteresis controller.

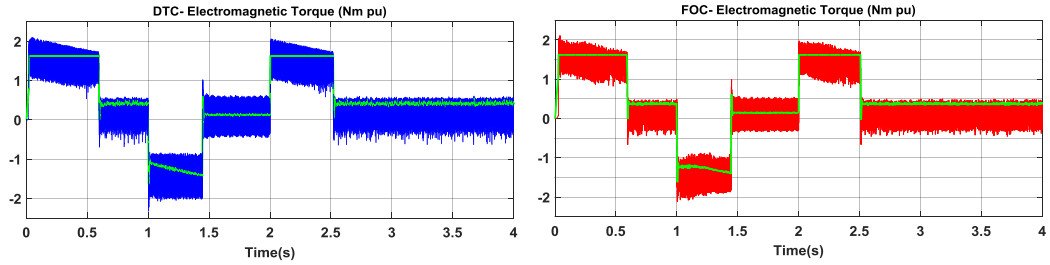

Figure 5.14: DTC & FOC Electromagnetic torque (variable speed dynamic response).

- As seen in Figure 5.15, both drives show no change in machine's stator and rotor fluxes during acceleration and deceleration of the motor, showing complete independent control.

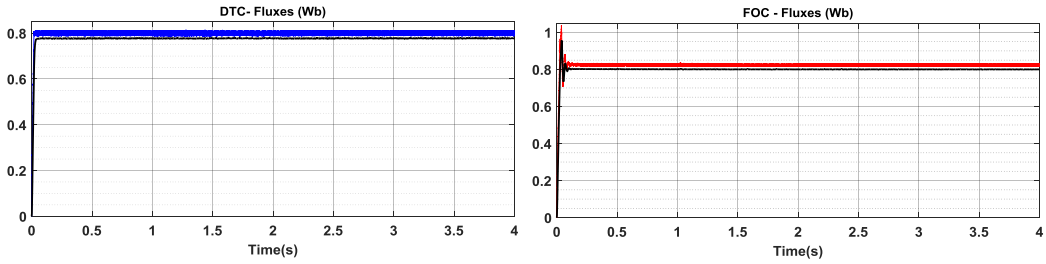

Figure 5.15: DTC & FOC Fluxes (variable speed dynamic response).

- As seen in Figure 5.16, DTC drive shows higher stator current ripples, as it draws more and more current during acceleration and deceleration regions. FOC drive has current controllers that limit the current drawn by the machine during accelerations and deceleration.

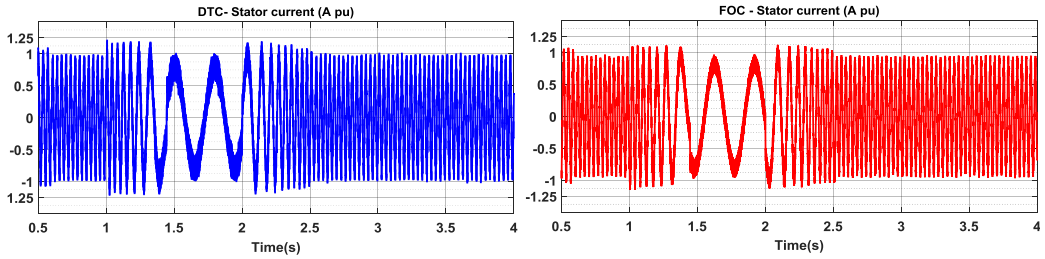

Figure 5.16: DTC & FOC Stator current (variable speed dynamic response).

4. **Dynamic flux operation:** The machine's rotor speed is kept constant at 900 RPM (1pu) with a constant load torque of 1 Nm, the machine's stator flux command is varied from nominal flux of 0.8Wb to 0.2Wb at 0.8 seconds and then to 0.5Wb at 1 second of simulation time. The results obtained are discussed as follows;

   - As seen in Figure 5.17, a change in stator flux reference command by a step is quickly followed by machine's stator flux for DTC drive, this quick dynamic response is obtained with the help of direct two level flux hysteresis controllers. The machine's rotor flux is delayed by the angle delta (δ) with a time constant of $\sigma \tau_r$ i.e. 0.04 seconds. In FOC drive there is no direct flux controller, and a step change in flux command will be delayed by the rotor time constant τ_r which is 0.14 seconds, for this small period of delay the torque and flux of the FOC drive will be coupled together, which will have its effects on machine's electromagnetic torque and rotor speed.

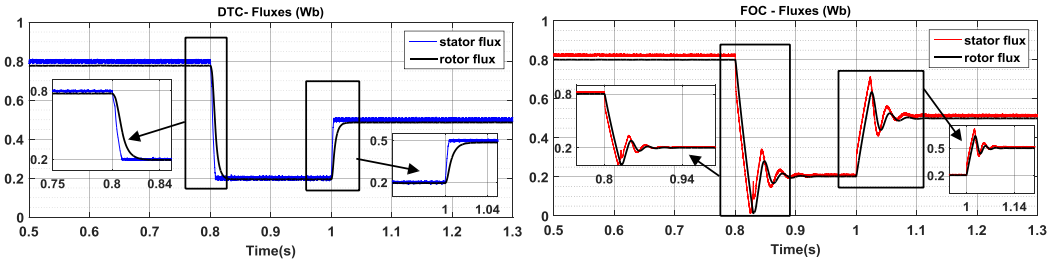

Figure 5.17: DTC & FOC Fluxes (dynamic flux response).

- As seen in Figure 5.18, DTC drive follows demand torque with some transient ripples when stator flux is changed; there is reduction in average torque ripples noticed with a decrease in value of stator flux. FOC drive has a significant transient ripple at 0.8 seconds which is quickly recovered within 0.14 seconds as soon as the rotor flux settles down.

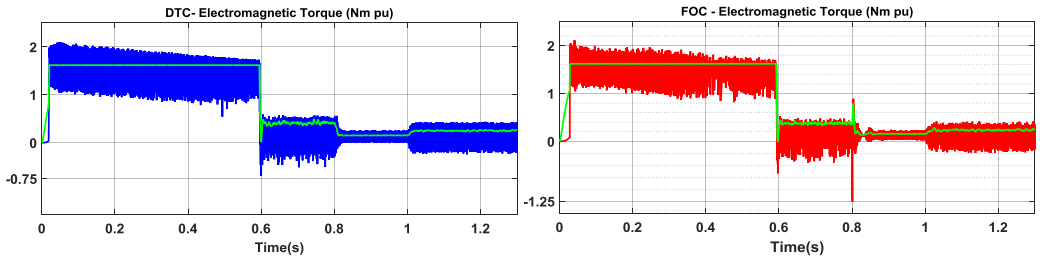

Figure 5.18: DTC & FOC Electromagnetic torque (dynamic flux response).

- As seen in Figure 5.19, a small change in stator flux will be accompanied by a large variation in stator currents, as there are no current limiters in DTC drive; the machine draws significantly larger amounts of currents for step changes in

stator flux. Similar observation is made on stator currents of the FOC drive, but due to current limiters, the variations in stator currents are not worse.

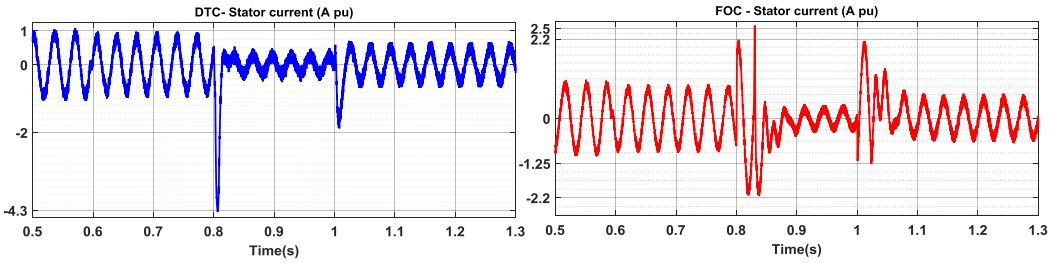

Figure 5.19: DTC & FOC Stator current (dynamic flux response).

- As seen in Figure 5.20, a slight drop in speed is noted in FOC drive at 0.8 seconds, which is recovered quickly within 0.14 seconds, when the rotor flux has settled down. On the other hand, DTC drive rotor speed is increased slightly at 0.8 seconds to compensate for stator flux step drop.

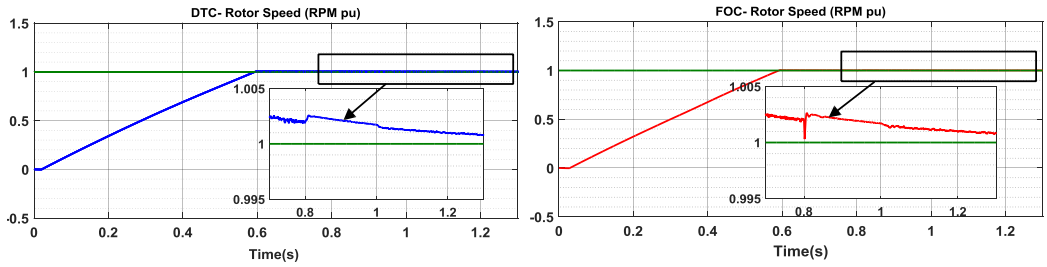

Figure 5.20: DTC & FOC Rotor speed (dynamic flux response).

5.2.3 Parameter Sensitivity

Since DTC and FOC drives are established on control scheme that is dependent on estimated values of variables, the accuracy of these calculations directly affects their performances. Many researchers have published papers on accurately estimating the induction machine parameters, and any number of methods can be used in practical implementation [69].Therefore, the behavior of both control drives is studied under a parameter sensitivity test to develop a fair comparitive study.

5.2.3.1 Parameter sensitivity of DTC drive

DTC drive operation is based upon calculated values of stator flux and electromagnetic torque. From equation 4.30; stator flux vector is calculated based on accurate estimation of stator resistor R_s, which varies as a function of temperature. Estimation of stator resistance at low speed and high speed operation of the machine can produce different outcomes. When the speed is lowered the difference in equation 4.30 is very small, making R_s accuracy significant, thus a small error in R_s estimation can result in inaccurate calculation of stator flux and reference torque values, resulting in performance degradation of the drive.

In order to study the effects of parameter variations in DTC drive, a step change is applied in the stator and torque calculator block of the controller to depict an estimation error in R_s. The machine drive is simulated in steady state at low speed of 0.056pu and at high speed of 0.89pu, with nominal load torque and reference flux of 0.8Wb. Step errors in R_s estimation is applied for 50% decrease (underestimation) and a 50% increase (overestimation). For low speed operation the step is applied after 0.5

seconds and for high speed operation the step is applied at 2 seconds of simulation time. The results are obtained for stator flux, rotor speed and electromagnetic torque and following observations are made;

- As seen in Figure 5.21, at low speed when R_s is underestimated, the stator flux value is also underestimated in the controller, and when R_s is overestimated the stator flux slowly becomes oscillatory with increasing amplitude. At high speed, when R_s is underestimated, the stator flux shows some oscillations that quickly recovers within 0.2 seconds because the estimation error is not significant enough to affect the system. However, when R_s is overestimated at high speed, stator flux shows high frequency oscillations with increasing amplitude making the system unstable.

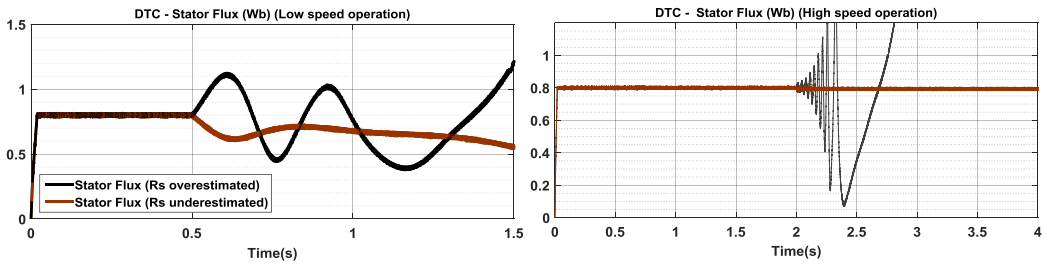

Figure 5.21: DTC Stator flux (parameter sensitivity response).

- It is observed in Figure 5.22, that at low speed when R_s is underestimated, the rotor speed starts to decline slowly and motor stalls after 1 second, and in case when R_s is overestimated, the rotor speed drops significantly and the motor stalls just in 0.7 seconds. At high speed operation, when R_s is underestimated, there is

no effect on the rotor speed because R_s has small significance at high speeds, but when R_s is overestimated, the rotor speed drops significantly and the motor stalls in 0.5 seconds.

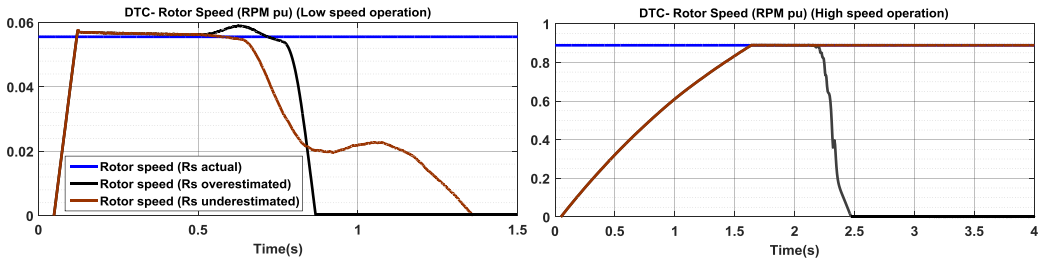

Figure 5.22: DTC Rotor speed (parameter sensitivity response).

- As seen in Figure 5.23, when R_s is underestimated at low speed operation, the calculated reference torque from the controller is slightly overestimated causing oscillations and ripples in the electromagnetic torque of the machine. Moreover, when R_s is overestimated at low speed, the calculated reference torque of the controller is underestimated resulting in severe oscillations in machine's electromagnetic torque. On the other hand, at high speed operation when R_s is underestimated, the calculated reference torque is not much off the course, causing some transient ripples in electromagnetic torque. However, when R_s is overestimated, machine's electromagnetic torque oscillates significantly with increasing amplitude, and the system becomes unstable.

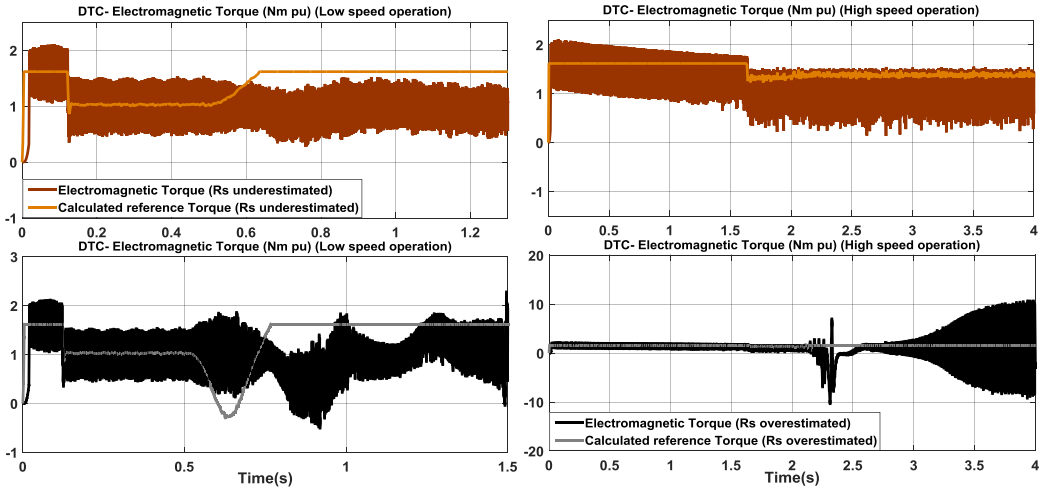

Figure 5.23: DTC Electromagnetic torque (parameter sensitivity response).

It is clearly seen that DTC drive has worse performance during low speed operation, if an estimation error is encountered in the stator resistance's value. The system becomes highly unstable and the control system deteriorates in case when R_s is overestimated, making DTC control scheme sensitive to stator resistance changes.

5.2.3.2 Parameter sensitivity of FOC drive

FOC drive controller operation is dependent upon the rotor time constant τ_r (L_r/R_r) which is essential for the calculation of slip frequency, as seen from equation 4.23. The rotor resistance varies as a function of temperature, and the rotor inductance varies with flux value, therefore and error in estimating τ_r will cause control system stability issues.

In order to evaluate the performance of FOC drive under parameter variations, a step change to depict an estimation error in the value of the rotor resistance is applied

to the control system. The machine is run in steady state with low speed of 0.056pu and high speed of 0.89pu with nominal load torque and reference flux of 0.8Wb. A step change of 50% decrease (underestimation) and 50% increase (overestimation) in the rotor resistor value is applied at 0.5 seconds and 2 seconds of simulation time for low speed and high speed operations respectively. The results of the simulations are discussed as follows;

- As seen in Figure 5.24, in both high and low speed operation of the drive, when R_r is underestimated, the rotor flux linkage is increased to 0.9Wb, and when R_r is overestimated the rotor flux linkage is dropped down to 0.75Wb.

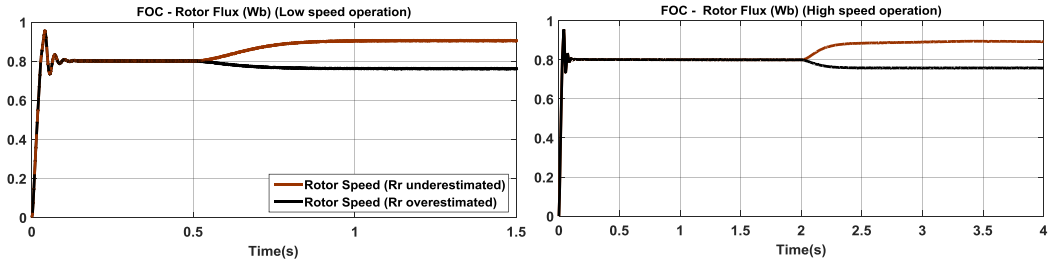

Figure 5.24: FOC Rotor flux (parameter sensitivity response).

- As seen in Figure 5.25, at low and high speed operations, when R_r is underestimated, the rotor speed drops down from its reference, but the drop is more significant during high speed operation, and the motor may stall afterwards. In case, when R_r is overestimated, there is no effect on the rotor speed in both operating conditions.

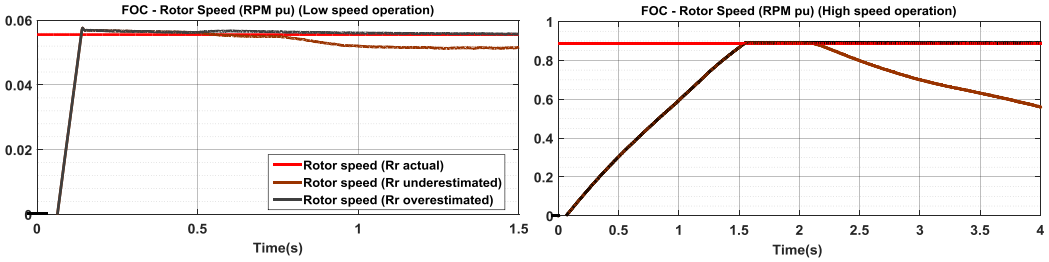

Figure 5.25: FOC Rotor speed (parameter sensitivity response).

- As seen in Figure 5.26, at low speed operating condition, when R_r is underestimated and overestimated, the calculated reference torque from the controller is overestimated and underestimated respectively, which results in electromagnetic torque transient ripples. On the other hand, during high speed operation, when R_r is underestimated and overestimated, similar to low speed operation the calculated reference torque from the controller is overestimated and underestimated respectively, which results in a drop of machine's electromagnetic torque and more severe transient ripples are observed.

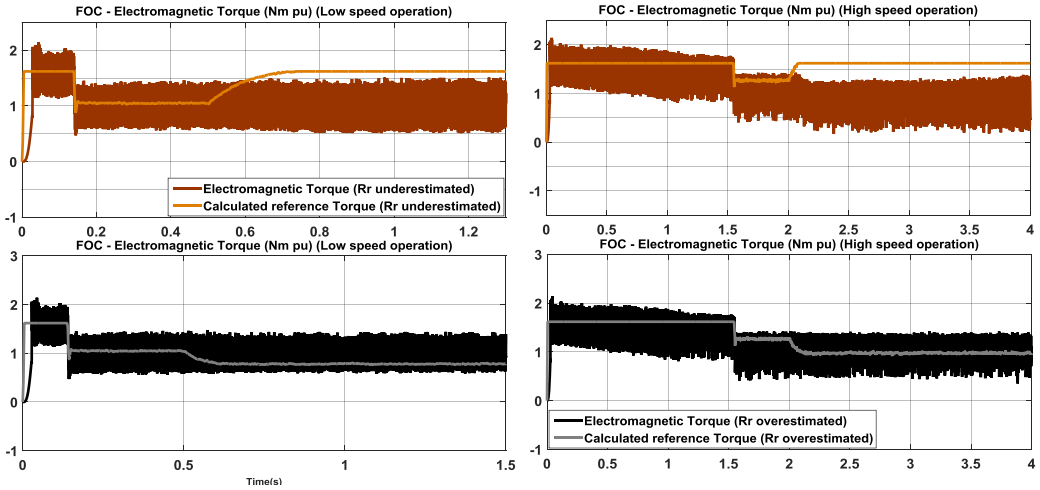

Figure 5.26: FOC Electromagnetic torque (parameter sensitivity response).

Finally it is summarized that FOC is affected by a change in rotor resistance of the machine, as it introduces an error in the rotor time constant calculation at the control level. However, when both the drive schemes are compared with respect to parameter sensitivity, DTC drive shows more severe control system performance degradation leading to system instability when stator resistor parameter has an estimation error. Therefore, it is seen that FOC drive is less sensitive to rotor resistor variations, but a more in-depth analysis maybe required that considers rotor leakage inductance. On the other hand, it is obvious that DTC is only affected by one parameter which is the stator resistance. In this section, the severity of system dependence only on stator resistance parameter variations has been studied.

5.3 Abnormal operating conditions

It is very crucial to test the performance of variable speed drive operated induction machine during abnormal conditions. Power system undergoes various

abnormalities such as voltage fluctuations, harmonic voltage/current distortions, interruptions etc. The effects of such power quality issues are studied on both the control schemes.

5.3.1 Voltage Sags and Interruptions

Voltage sag is a reduction in root mean square (RMS) voltage for a short duration of time. It could be caused by short circuits, start-up of high power motors and overloads. Voltage sag creates several types of problems in variable speed drive systems such as current peaks, torque distortions and speed losses, which can trigger motor protection system, these effects depends upon magnitude and duration of a voltage sag. Voltage sags are characterized as having loss of voltage magnitude between 10% to 90% for 3 to 30 cycle duration. The fault duration and magnitude depends on power system distribution distance from the fault originating site. The fault type could be three phase balanced, single phase to ground and phase to phase faults. Voltage sags experienced by a three phase load are classified into seven types A, B, C, D, E, F and G. Type A is three phase balanced sag, which is caused by three phase short circuit or overload, all three phasors drop in magnitude by the same amount [58];

$$\left.\begin{aligned} V_a &= hV \\ V_b &= -\frac{1}{2}hV - j\frac{\sqrt{3}}{2}hV \\ V &= -\frac{1}{2} + j\frac{\sqrt{3}}{2}hV_c \end{aligned}\right\} \tag{5.1}$$

Where, h is the sag magnitude between 0 and 1.

Type B is a single line to ground type fault, here magnitude of the faulted phase drops and not its angle, other two phases are unaffected, mostly sags are caused by single phase faults [58];

$$\left.\begin{aligned} V_a &= hV \\ V_b &= -\frac{1}{2}hV - j\frac{\sqrt{3}}{2}V \\ V_c &= -\frac{1}{2}V + j\frac{\sqrt{3}}{2}V \end{aligned}\right\} \tag{5.2}$$

Type C faults are either single line to ground or phase to phase faults, in this type of fault not only the magnitude of the phasors is dropped but also the angles of the phasors are affected.

$$\left.\begin{aligned} V_a &= V \\ V_b &= -\frac{1}{2}V - j\frac{\sqrt{3}}{2}hV \\ V_c &= -\frac{1}{2}V + j\frac{\sqrt{3}}{2}hV \end{aligned}\right\} \tag{5.3}$$

Table 9.2 in Appendix B shows the rest of the voltage sag types and their equations.

Interruptions are loss of voltage below 10% magnitude in any of the phases in a three phase load. Interruptions are divided into three main categories;

- Momentary interruptions between 0.5 cycles and 3 seconds.
- Sustained interruption longer than 3 seconds.
- Temporary interruption between 3 seconds and 1 minute. [59]

In this thesis three types of voltage sags are simulated; one balanced sag and two unbalanced sags; type A (balanced) which is a three phase balanced fault, type B

(unbalanced) which is a single line to ground fault and type C (unbalanced) which is a phase to phase fault. Momentary interruptions for each sag types is also simulated for both the control schemes with high load and high speed commands to compare the two advanced control schemes for worst case scenarios.

5.3.1.1 Voltage sag type B fault

The effects of unsymmetrical voltage sag type on variable speed drive for induction machine is simulated with a high load and high rotor speed. Sags of magnitude 20%, 50%, and 80% and a momentary interruption of 100% magnitude are simulated for durations of 20, 25 and 30 cycles. Fault introduced is phase A to ground with a fault and ground resistors connected to phase A as shown in Figure 5.27.

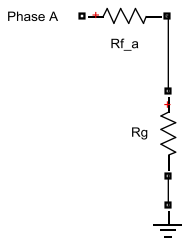

Figure 5.27: Phase A to ground fault circuit (in Simulink).

The two advanced induction machine drives under the faults will be studied in detail. Aspects of comparison will be the rotor speed deviation from the reference value, torque variations, stator current and DC link voltage which is the output of the diode rectifier and input to the VSI.

The simulation results are shown for 30 cycle duration only, as there is no effect of voltage sag fault type B for durations less than 30 cycles. AC line voltage sag for fault type B of magnitudes 20%, 50%, 80% and 100% occurs at 0.7s for 30 cycles (1.2s) are shown in Figure 5.28.

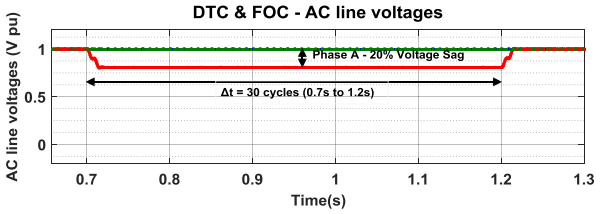

(a) Fault type B – Voltage sag of 20%

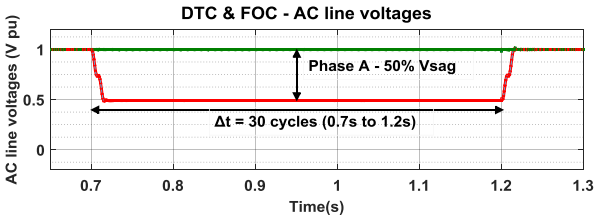

(b) Fault type B – Voltage sag of 50%

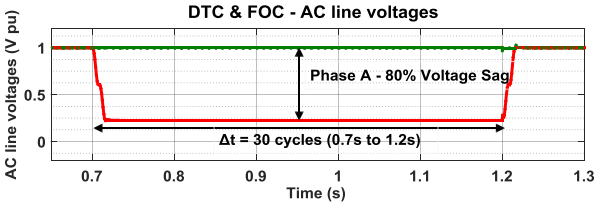

(c) Fault type B – Voltage sag of 80%

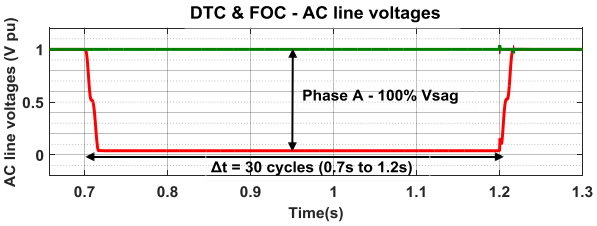

(d) Fault type B – Voltage sag of 100%

Figure 5.28 (a), (b), (c) & (d): AC line voltages for voltage sag fault type B (SLG).

Both the advanced drive schemes shows stability in speed, the rotor speed follows the speed command of 1pu (i.e. actual speed/nominal speed in RPM) very smoothly during the single line to ground fault which occurs after 0.7s to 1.2s. The rotor speed is also not affected by the voltage sag magnitude of 20%, 50%, 80% and interruption of 100% on phase A as shown in Figure 5.29.

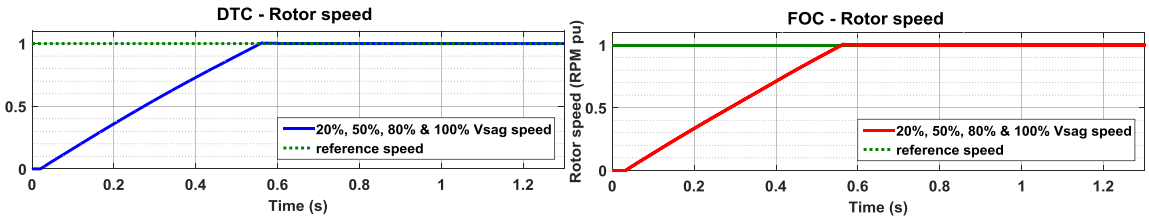

Figure 5.29: DTC & FOC Rotor speed (SLG fault type B).

Furthermore, the variations in electromagnetic torque are merely less than 0.25pu for voltage sags of 50% and 80% as shown in Figures 5.30(b) and (c), and no variations in 20% as shown in Figure 5.30(a). Whereas, in case of interruption fault the variation in the electromagnetic torque is 0.5pu in both the schemes under full load condition as shown in Figure 5.30(d).

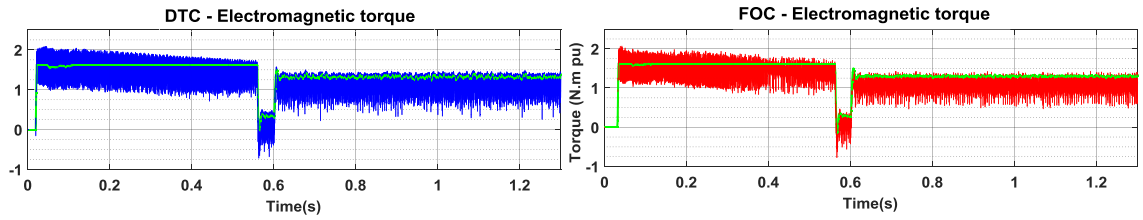

(a)Voltage sag of 20%

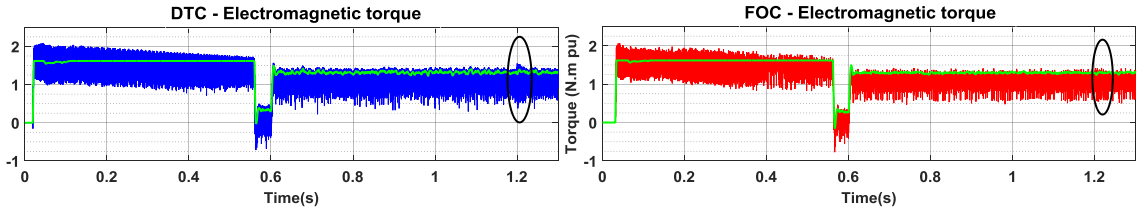

(a) Voltage sag of 50%

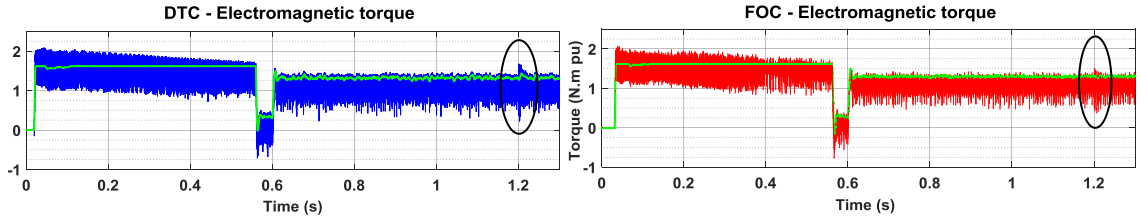

(b) Voltage sag of 80%

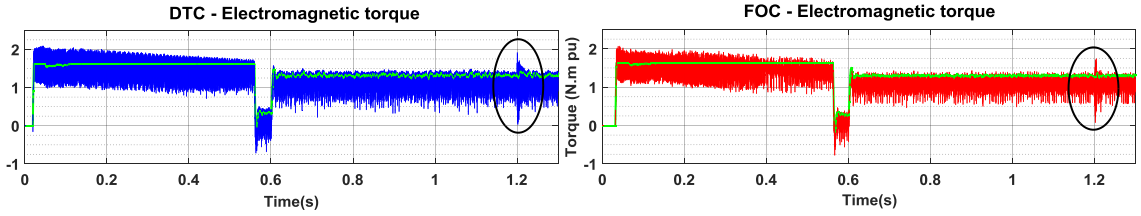

(c) Voltage sag of 100%

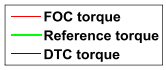

Figure 5.30 (a) & (b): DTC & FOC Electromagnetic torque (SLG fault type B).

As shown in Figure 5.31, the stator currents in the both schemes are within reasonable limits; there is a very small spike in the FOC drive after the fault is cleared at 1.2s for voltage sag of 100% as seen from Figure 5.31(d), but it is not significant.

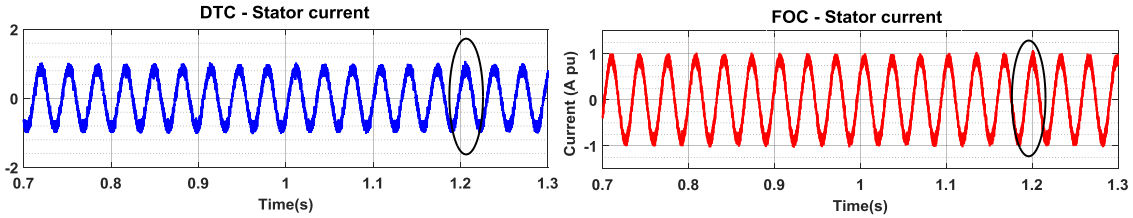

(a) Voltage sag of 20%

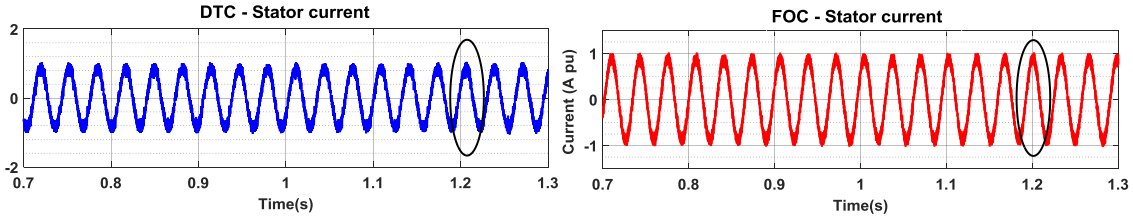

(b) Voltage sag of 50%

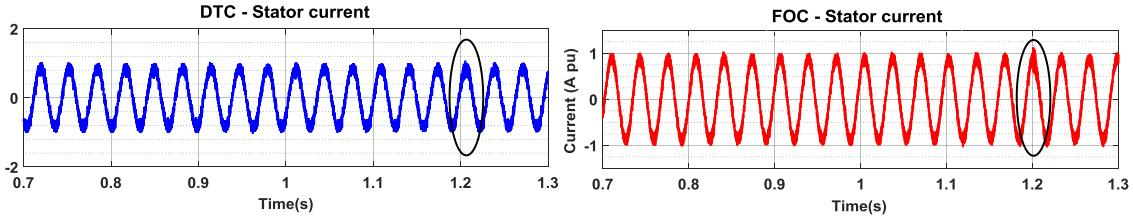

(c) Voltage sag of 80%

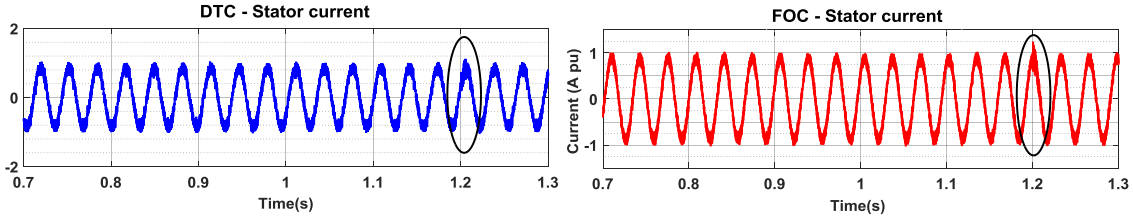

(d) Voltage sag of 100%

Figure 5.31(a), (b), (c), & (d): DTC & FOC Stator current (SLG fault type B).

The DC link voltage has ripples during the fault in both the drives, when the fault is cleared there is a spike in the DC link voltage, the deeper the voltage sag the higher the spike in the DC voltage as shown in Figure 5.32.

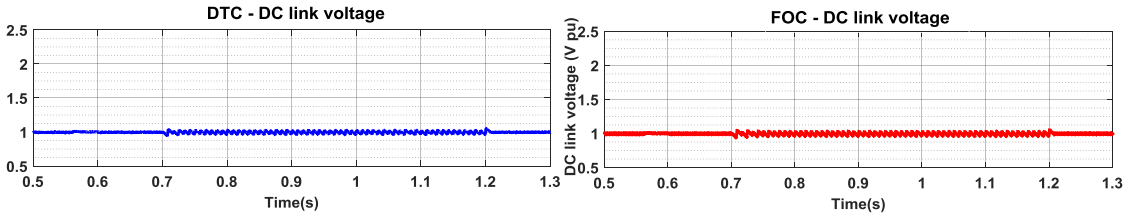

(a) Voltage sag of 20%

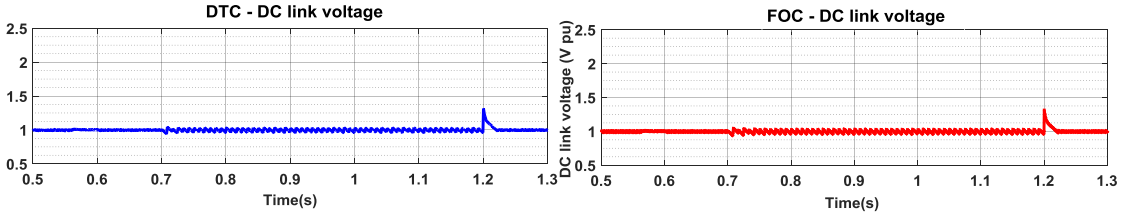

(b) Voltage sag of 50%

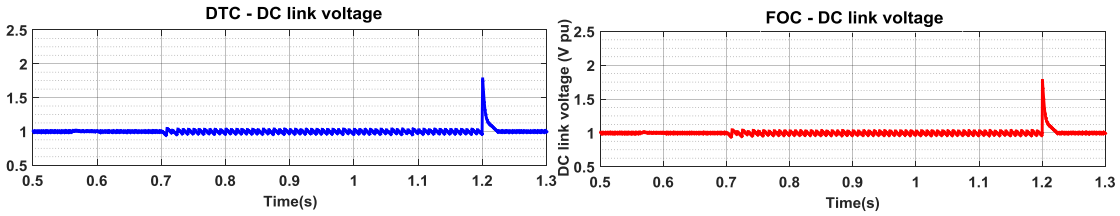

(c) Voltage sag of 80%

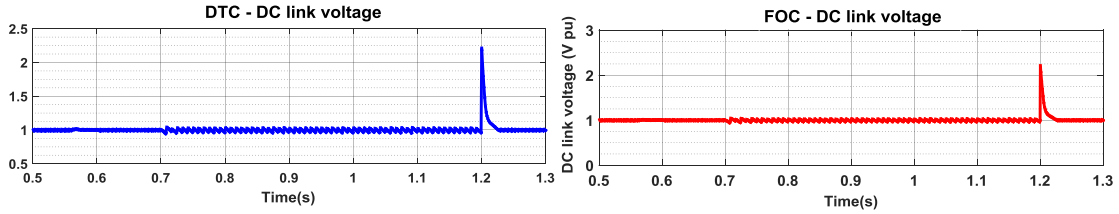

(d) Voltage sag of 100%

Figure 5.32(a), (b), (c) & (d): DTC & FOC DC link voltage (SLG fault type B).

To summarize, both the advanced drive schemes shows stability during type B faults which is a single line to ground fault; rotor speed, electromagnetic torque and

stator currents are almost unaffected. Summarized graphs showing variations due to type B voltage sag is shown in Figure 5.33.

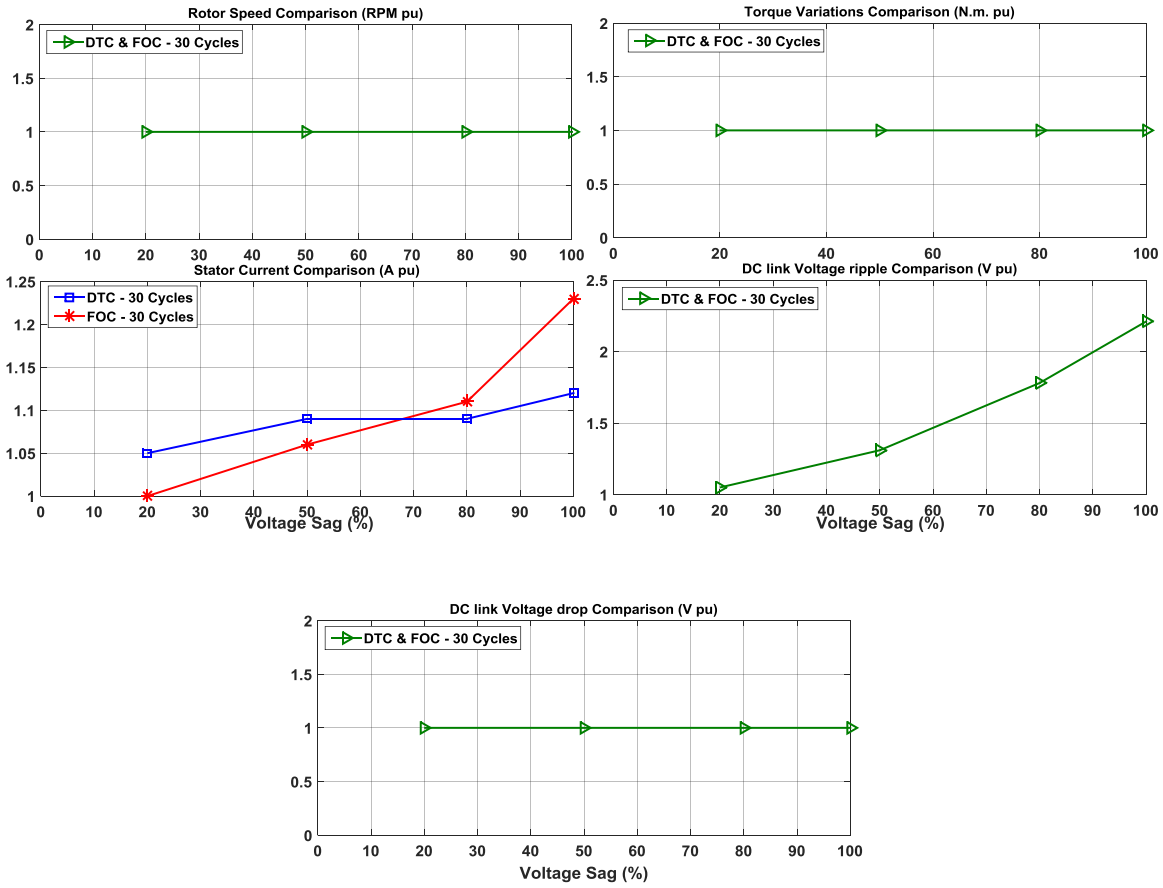

Figure 5.33: Fault type B voltage sag comparison graphs.

5.3.1.2 Voltage sag type C fault

Voltage sag type C is a phase to phase type fault, where the two phases drop in magnitude and also their phase angles change, but there is little or no effect on the third phase. The faulted phases are A & B, and the Simulink circuit is shown in Figure 5.34.

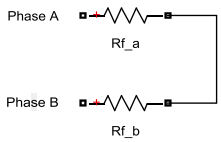

Figure 5.34: Phase A & B fault circuit (in Simulink).

The machine is loaded with similar conditions of full load and high speed and is simulated under type C faults of voltage magnitude 20%, 50%, 80% and an interruption of 100% magnitude for 30 cycles, the fault is introduced at 0.7s until 1.2s, the AC line voltages are shown in Figure 5.35, and its effect on machine rotor speed, electromagnetic torque, stator currents and DC link voltage are observe

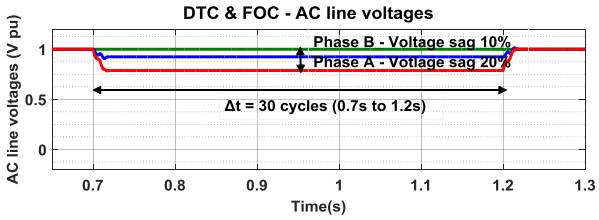

(a) Fault type C – Voltage sag of 20%

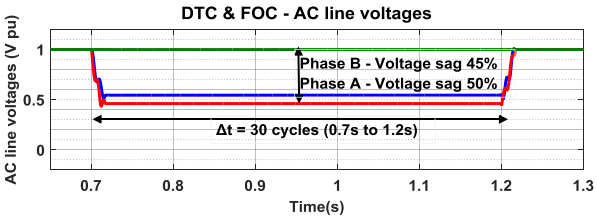

(b) Fault type C – Voltage sag of 50%

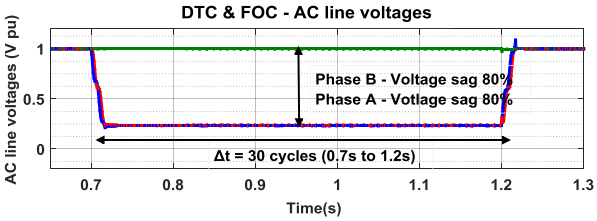

(c) Fault type C – Voltage sag of 80%

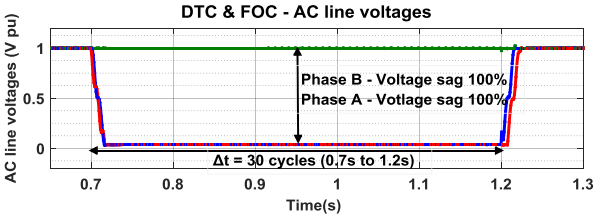

(d) Fault type C – Voltage sag of 100%

Figure 5.35: AC line voltages for voltage sag fault type C (two phase fault).

As shown in Figure 5.36, the rotor speed remains unaffected by sags of magnitude 20% to 50%, and the rotor speed starts to drop by 0.2pu when the sag is of 80% magnitude and drops down by 0.4pu during a momentary interruption in both the control schemes, the recovery is much quicker in FOC control scheme as soon as the fault is cleared within 0.5s (80% voltage sag) to 0.8s (100% voltage sag) when compared

with the DTC control scheme which takes about 0.1s longer to recover; showing the advantage of FOC control scheme over DTC control in terms of speed dynamics.

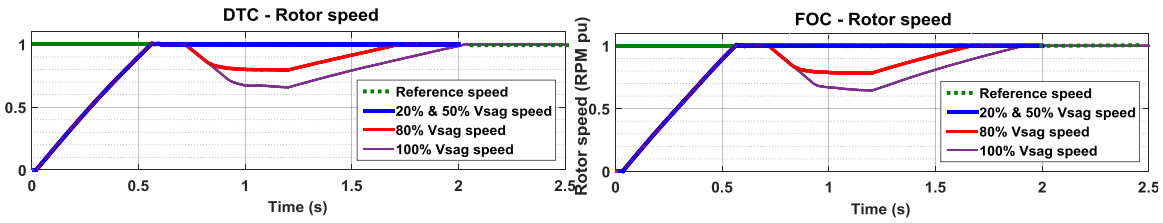

Figure 5.36: DTC & FOC Rotor speed (two phase fault type C).

As shown in Figure 5.37, the electromagnetic torque has no significant variations for sag magnitudes of 20% and 50%, but when the sag magnitude increases to 80% and above the torque varies by 2.25pu during the fault and recovers as soon as the fault is cleared. DTC scheme shows higher torque ripples when compared with FOC scheme, owing to the fact that the torque is controlled by the hysteresis controller in DTC scheme.

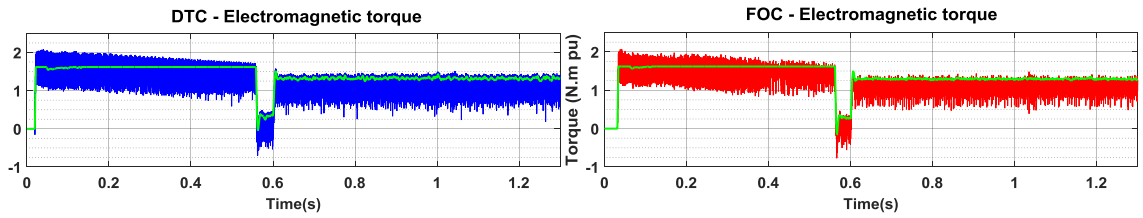

(a) Voltage sag of 20%

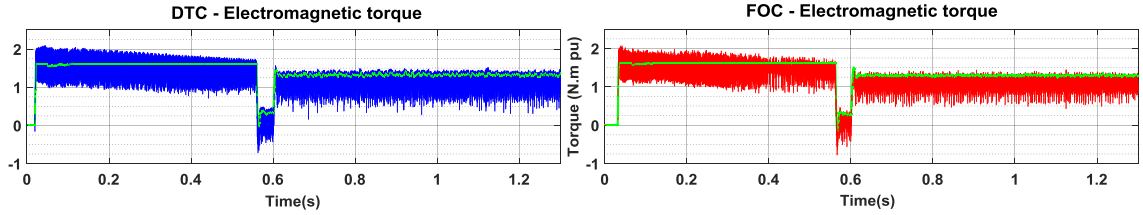

(b) Voltage sag of 50%

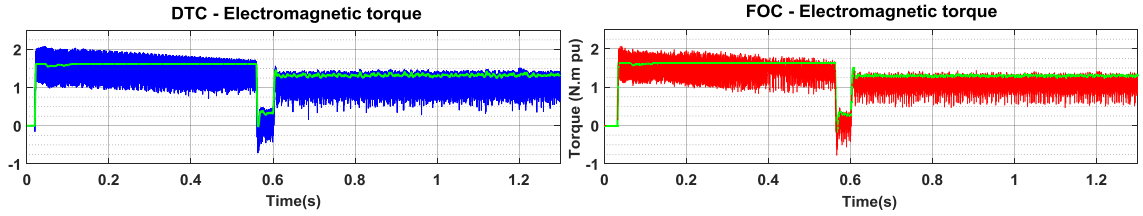

(c) Voltage sag of 80%

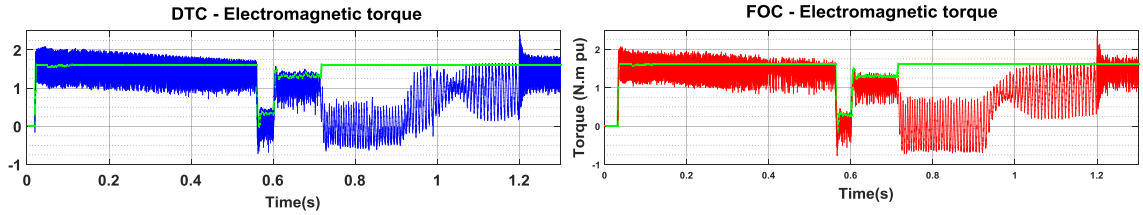

(d) Voltage sag of 100%

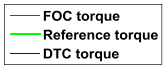

Figure 5.37: DTC & FOC Electromagnetic torque (two phase faulty type C).

As shown in Figure 5.38, stator currents for both the control drives are within reasonable limits under all sag magnitudes and shows some spikes when the voltage sag magnitude is of 80% and above. It worth noting that DTC drive shows more current distortions and spikes as compared with FOC drive during phase to phase faults.

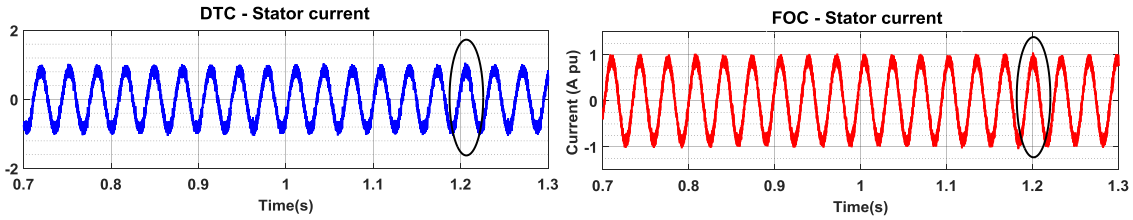

(a) Voltage sag of 20%

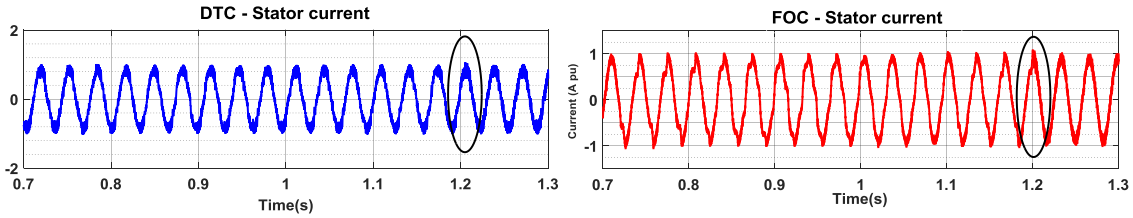

(b) Voltage sag of 50%

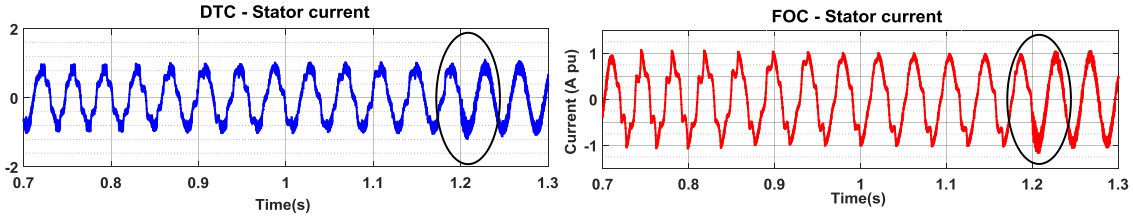

(c) Voltage sag of 80%

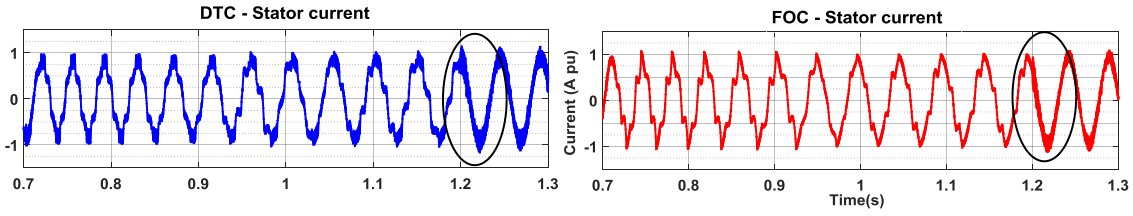

(d) Voltage sag of 100%

Figure 5.38: DTC & FOC Stator current (two phase fault type C).

Similar to type B faults, the DC link voltage has some ripples during 20% voltage sag and voltage overshoots when the fault is cleared. When the voltage sag of magnitude 50% and above is introduced there is a voltage drop during the fault followed by a spike when the fault is cleared. The deeper the sag, the higher the voltage drop and the voltage overshoot as shown in Figure 5.39. It is worth noting that the DC link voltage overshoot after the fault is cleared is 50% more in FOC driven than DTC drive.

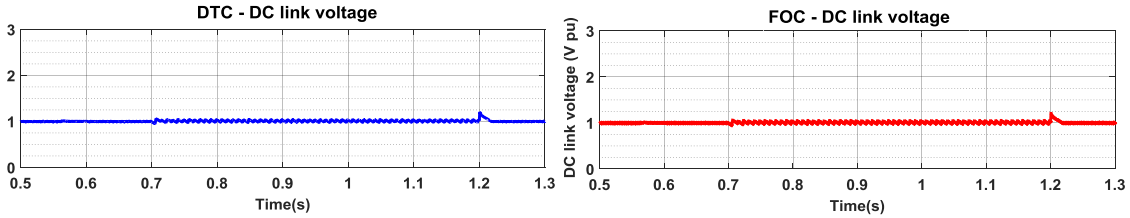

(a) Voltage sag of 20%

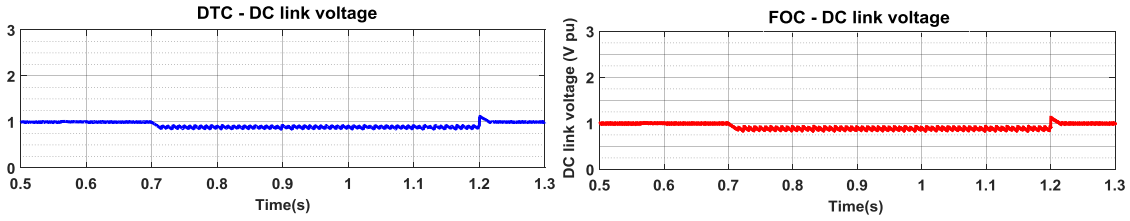

(b) Voltage sag of 50%

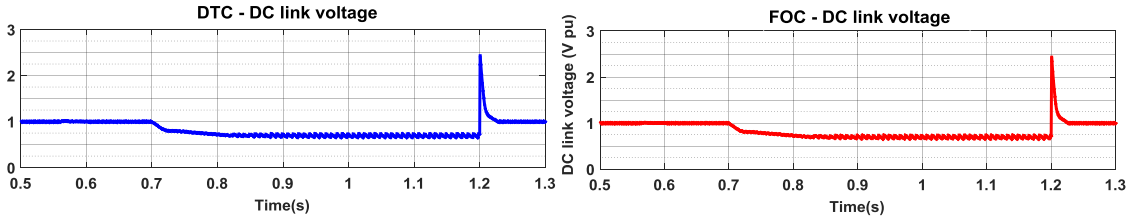

(c) Voltage sag of 80%

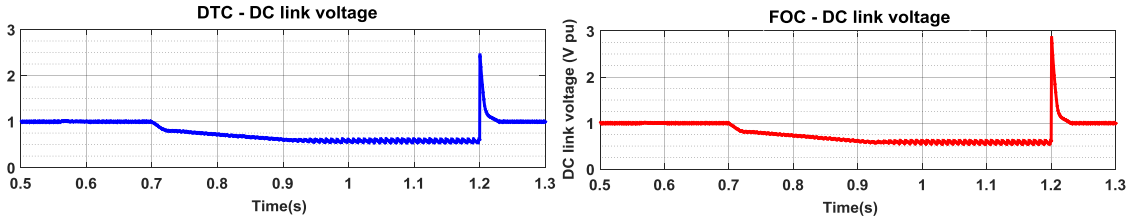

(d) Voltage sag of 100%

Figure 5.39: DTC & FOC DC link voltage (two phase fault type C).

To summarize, both drives show excellent responses during type C fault which is a phase to phase fault with drop in magnitudes and change in phase angles. Both the schemes have comparable performance during this type of fault. The results are summarized in Figure 5.40.

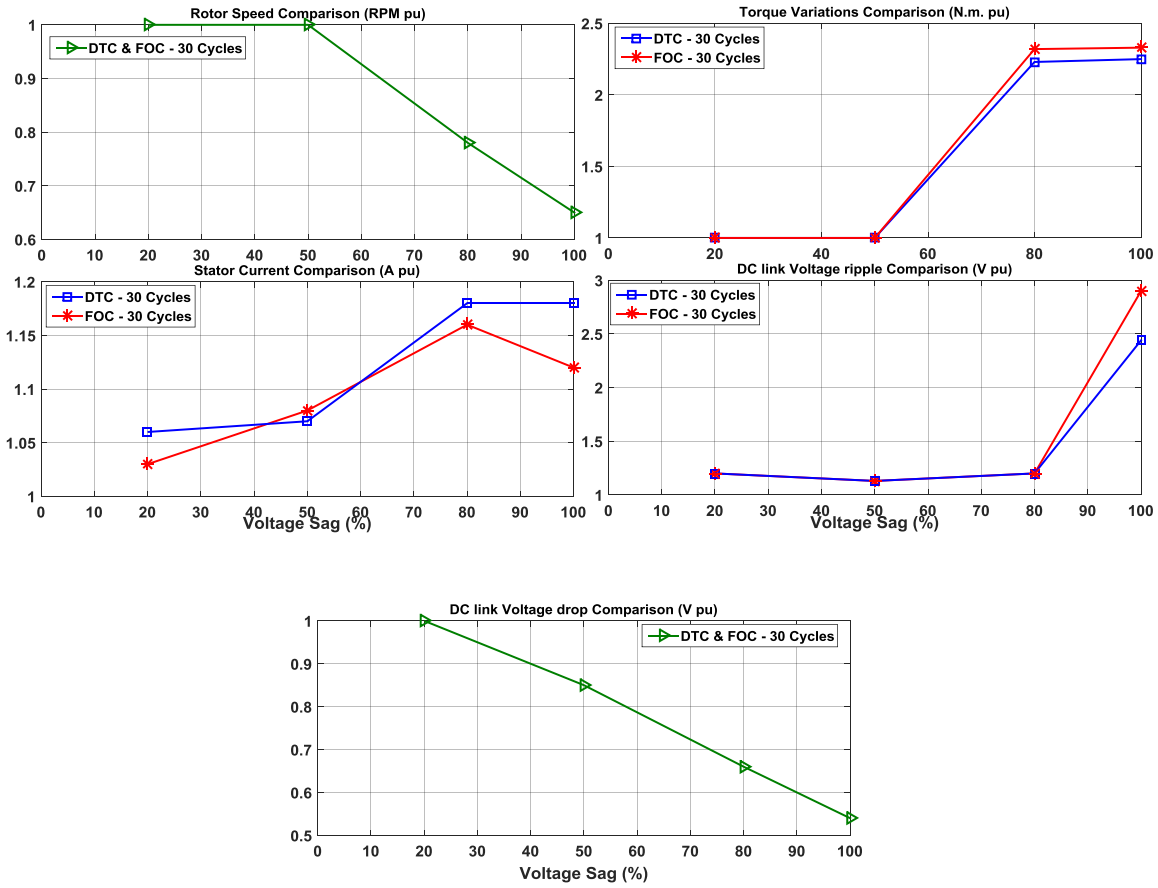

Figure 5.40: Fault type C voltage sag comparison graphs.

5.3.1.3 Voltage sag type A fault

The effects of symmetrical voltage sag type A on variable speed drives for induction machine is simulated with full load torque and a high rotor speed (identical to previous settings). The three phases to ground fault circuit developed in Simulink is shown in Figure 5.41.

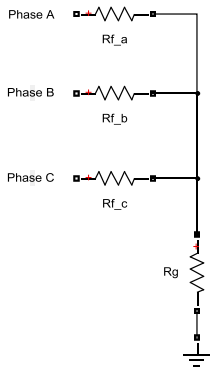

Figure 5.41: Three phase to ground fault circuit (in Simulink).

Sag of magnitudes 20%, 50%, and 80% and an interruption of 100% magnitude are simulated for durations of 20, 25 and 30 cycles. The effects of type A voltage sag on DTC and FOC drive for induction machine is studied for speed deviation, torque variations, stator current ripples and DC link voltage drop. Type A is the worst case scenario where all the three phases drop in voltages, thus the simulation is run for various cycles as mentioned above. DTC and FOC schemes have proven to be very rugged during single line to ground and phase to phase faults as shown in previous sections. The AC line voltages for fault type A that are simulated for various durations are shown in Figure 5.42.

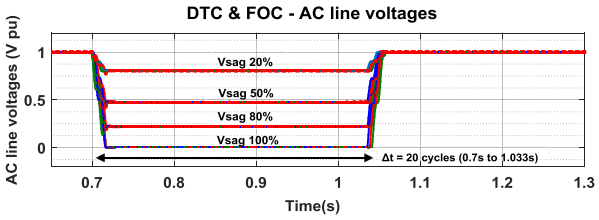

(a)Fault type A for duration of 20 cycles

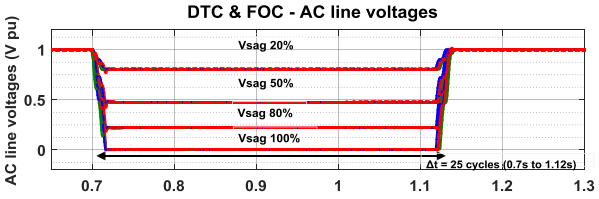

(b) Fault type A for duration of 25 cycles

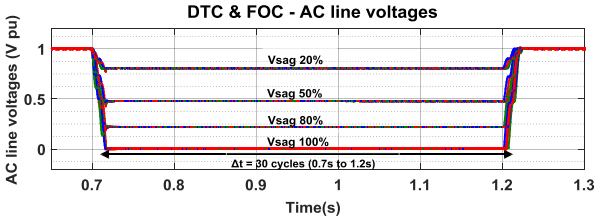

(c) Fault type A for duration of 30 cycles

Figure 5.42 (a), (b) & (c): AC line voltages for voltage sag fault type A (TLG).

A 20% voltage dip for 20, 25 and 30 cycles has very minor speed drops in both the control schemes. However, the rotor speed starts to drop significantly from 50% voltage sag for 20, 25 and 30 cycles as shown in Figure 5.43; The rotor speed drops down to about 0.55pu for a voltage sag of 50% for all three cycle durations in both the control schemes. Moreover, the rotor speed doesn't dip below 0.55pu for voltage sags

between 50% to 100% for 20 cycles duration as shown in Figure 5.43(a). Showing stability of both the advanced control schemes for a voltage sag of short duration (20 cycles in this case). However, rotor speed reduces down by 0.1pu and 0.2pu from 0.55pu for voltage sags between 80% to 100% during 25 and 30 cycles respectively as shown in Figures 5.43(b) and (c). It is noted that the rotor speed drop is slightly more in the case of FOC when compared to DTC. However, in FOC drive the recovery of the rotor speed to its nominal value takes shorter time, showing the advantage of FOC over DTC.

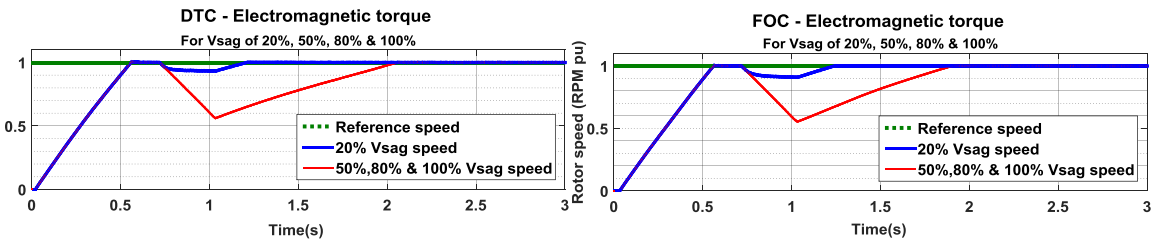

(a) Duration 20 cycles.

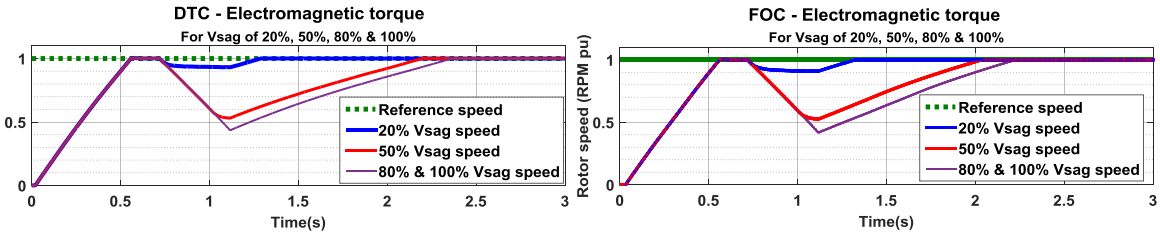

(b) Duration 25 cycles.

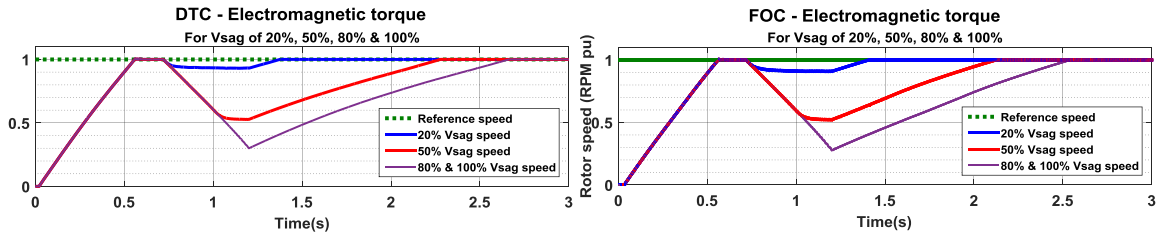

(c) Duration 30 cycles

Figure 5.43 (a), (b) & (c): DTC & FOC Rotor speed (TLG type A fault).

The electromagnetic torque is controlled through a bang-bang hysteresis controller in DTC control scheme as explained in previous sections. On the other hand, torque is not controlled directly, but indirectly through the quadrature current component i_q in FOC scheme. Keeping this in mind it is observed that there are higher torque deviations from its reference values in FOC control scheme compared to that of DTC, and this variation in toque is higher as the voltage sag is deeper and the fault

duration is longer as shown in Figure 5.44. The hysteresis torque controllers in DTC scheme ensures that torque stays within its bandwidth limits during faults. However, DTC electromagnetic torque has higher ripple content, the disadvantage of not having a fixed switching frequency due to hysteresis band controllers for torque and flux. It is also worth noting, that the torque overshoot after the fault is cleared is more for voltage sag of 80% than voltage sag of 100% in both drives.

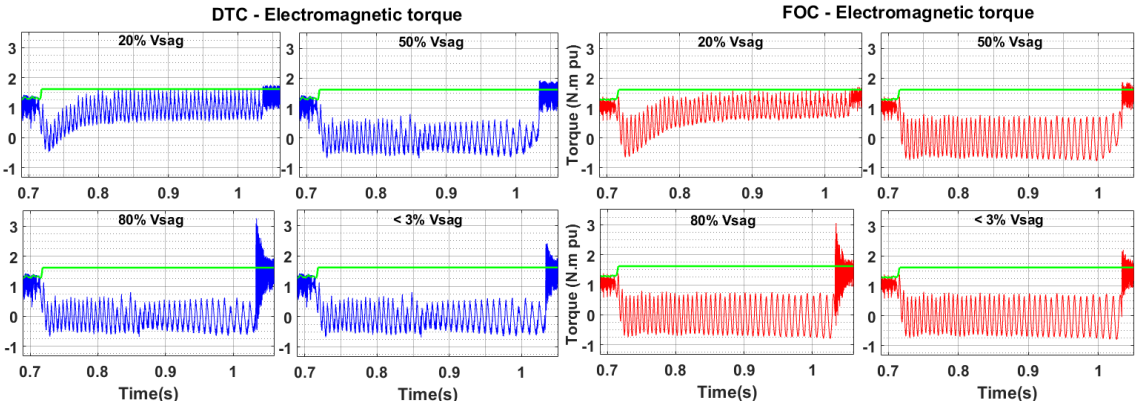

(a) Duration 20 cycles

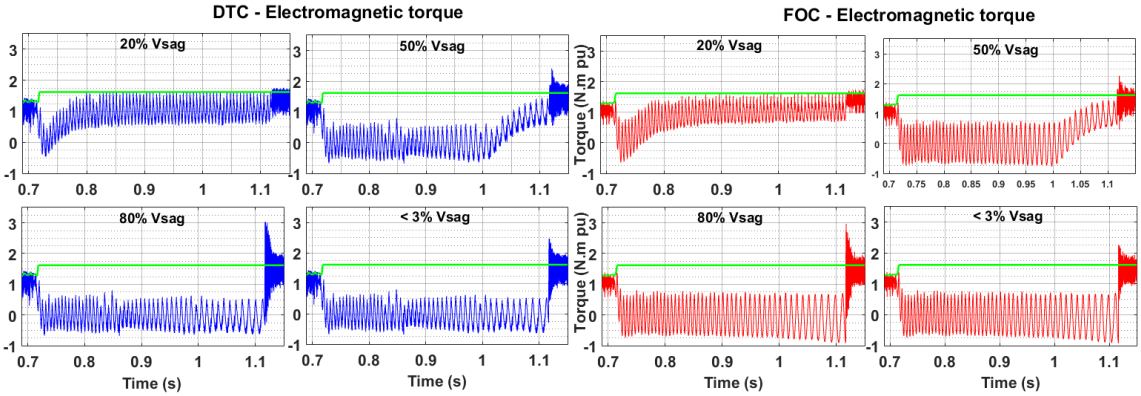

(b) Duration 25 cycles

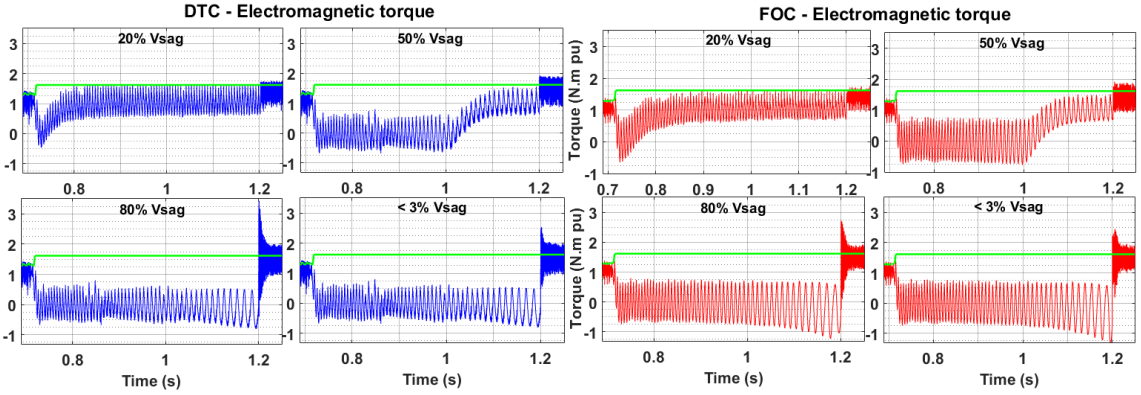

(c) Duration 30 cycles

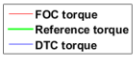

Figure 5.44 (a), (b) & (c): DTC & FOC Electromagnetic torque (TLG fault type A).

Stator currents are very crucial during the faults, as the motor can easily draw high currents, which could lead to overheating, decrease in machine's life, and damage to internal circuitry. In both the control schemes, the stator currents are well within limits for voltage sag duration less than 20 cycles. As shown in Figure 5.45, stator current ripples are observed just when the fault is removed, in DTC control scheme there are no current regulators, and as mentioned before the switching frequency of the VSI is also not constant, leading to higher current ripples. In FOC control scheme, the machine draws higher currents as soon as the fault is removed, this could be due to several reasons;

1. The torque demand is more when the fault is cleared, thus the machine demands for higher currents to maintain reference torque values.
2. Due to the absence of voltage modulation techniques such as space vector or sinusoidal PWM, the hysteresis current controllers have variable switching frequency.
3. The speed drop in FOC scheme is slightly more when compared to DTC, which demands more electromagnetic torque to maintain nominal rotor speed, overloading the machine and drawing higher currents.

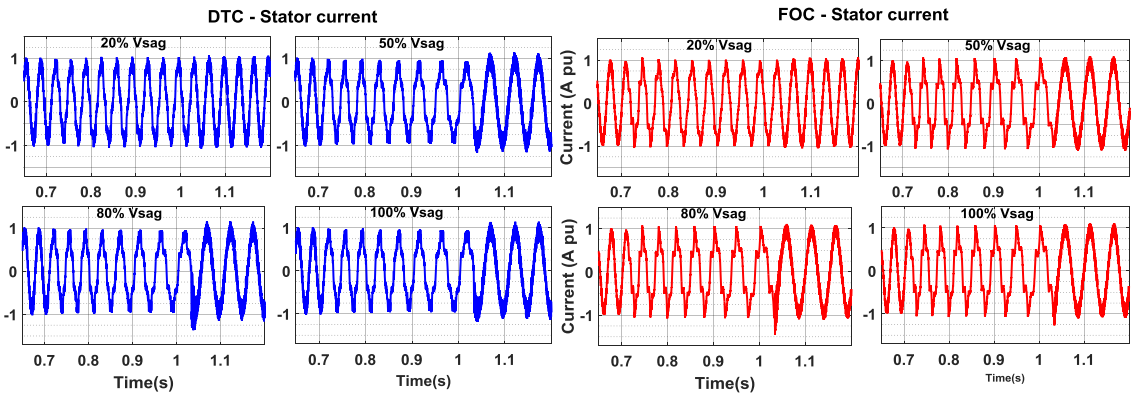

(a) Duration 20 cycles

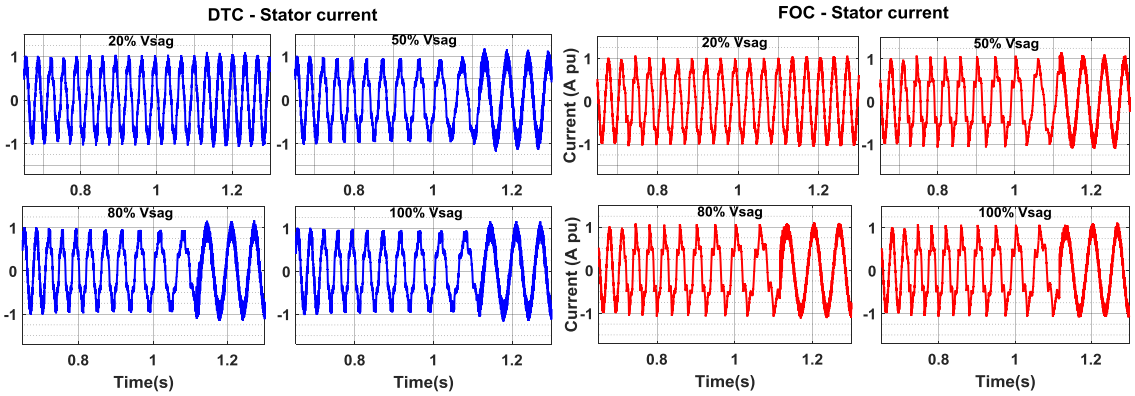

(b) Duration 25 cycles

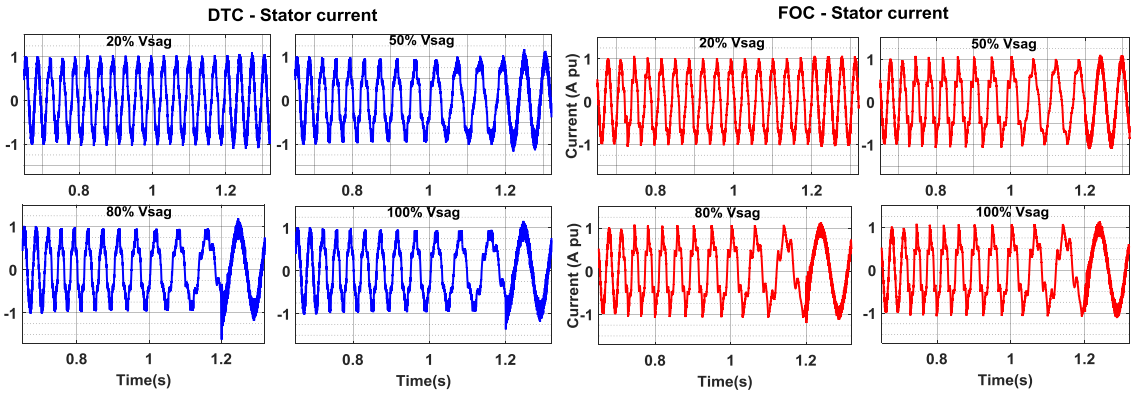

(c) Duration 30 cycles

Figure 5.45 (a), (b) & (c): DTC & FOC Stator current (TLG fault type A).

As seen in Figure 5.46, DC link voltage drops in both the control schemes when a three phase fault is introduced, and as soon as the fault is cleared there is a voltage overshoot, before it goes back to its rated value. The voltage overshoot in both the schemes is same during voltage sags of 20%, 50%, 80% and 100% with an overshoot of about 0%, 25%, 425% and 225% respectively for durations of 20 and 25 cycles as observed from Figures 5.46(a) and (b). Whereas, there is a slightly higher voltage ripple observed in FOC drive for 30 cycles voltage sags duration as seen in Figure 5.46(c), which is obviously due to a higher torque and current demand after the fault is removed. For the same reasons, the DC link voltage drop in FOC drive is observed to be more when compared with DTC drive.

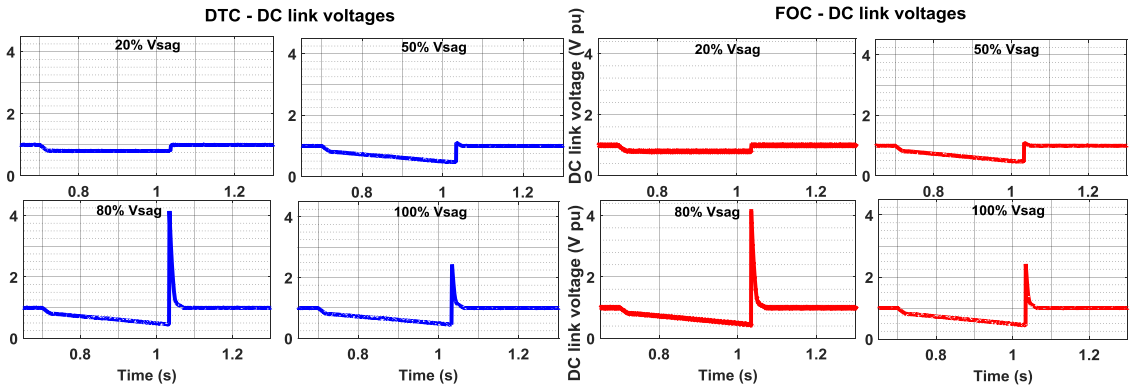

(a) Duration 20 cycles

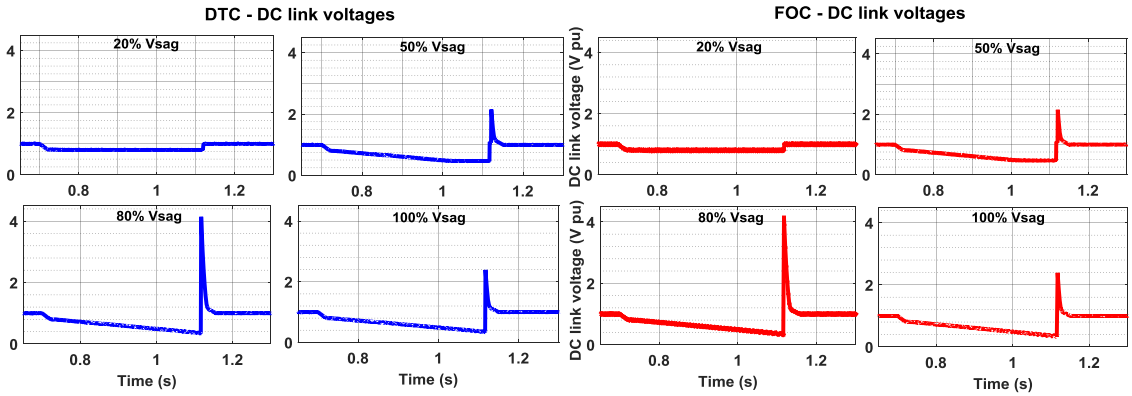

(b) Duration 25 cycles

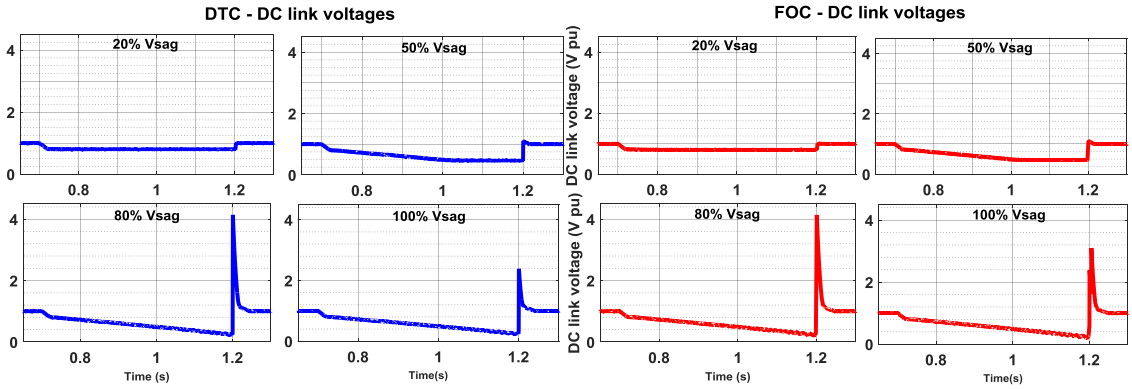

(c) Duration 30 cycles

Figure 5.46(a), (b) &(c): DTC & FOC DC link voltage (TLG fault type A).

The summarized results are shown in Figure 5.47, showing performances of both the advanced control schemes during type A faults for various magnitudes and duration. It is observed that FOC has better performances in terms of rotor speed recovery time during type A faults taking about 100ms to 150ms quicker compared to DTC control scheme. On the other hand, FOC has degraded performance in terms of electromagnetic torque deviation, but has less electromagnetic torque overall ripples. DTC control scheme shows higher torque ripples and stator current ripples, but reasonable deviations in its torque. Both schemes have high DC link voltage overshoot, but it gets cleared within couple of milliseconds.

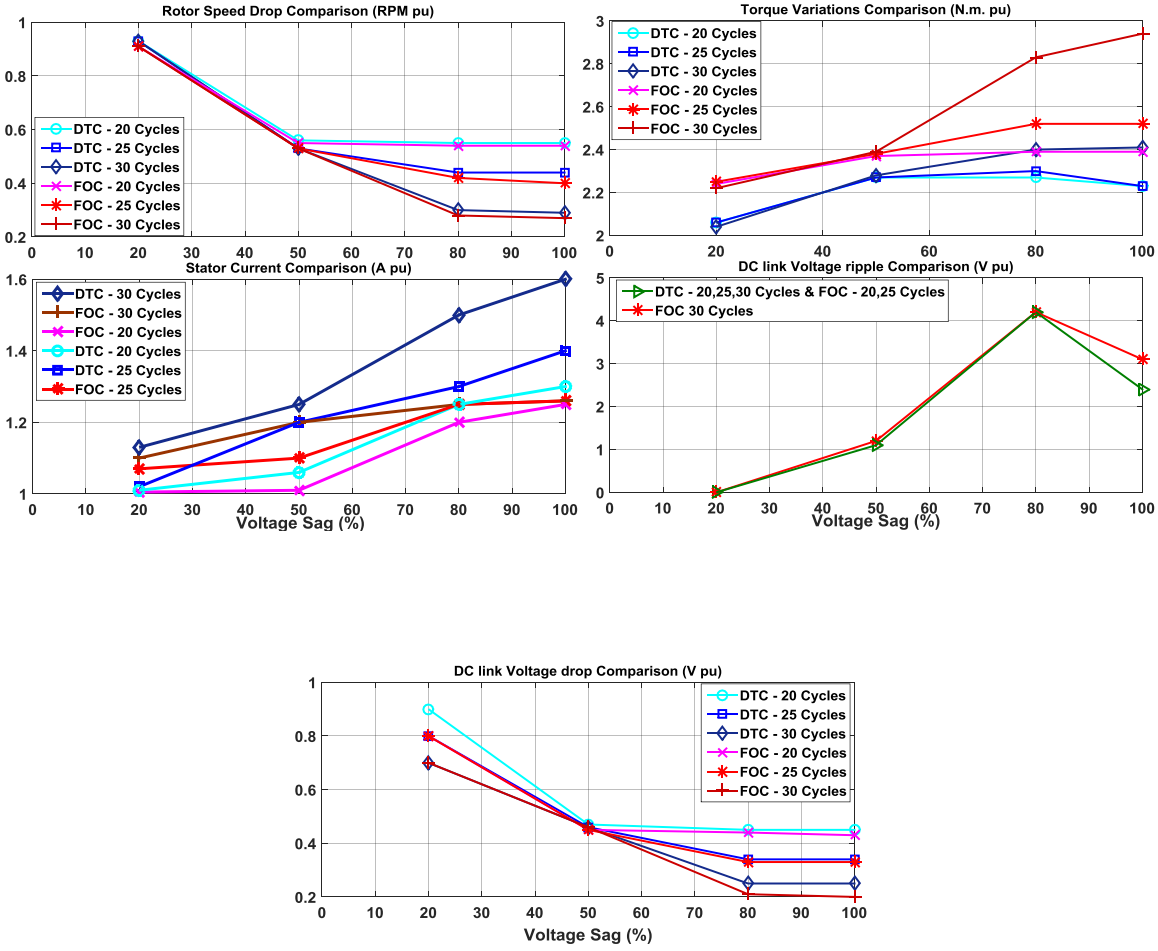

Figure 5.47: Fault type A voltage sag comparison graphs.

5.3.2 Harmonic Voltage distortion

There are three contributors to the harmonic voltage distortions;

1. Voltage generation by synchronous machine
2. HVDC lines, due to power electronic converters
3. Main contributors to harmonic voltage distortions are non-linear loads that draw non-sinusoidal currents.
4. Faults and inrush currents in transformers.

Voltage harmonic distortions cause induction machine iron and copper losses in magnetic frame of the machine, hysteresis and eddy current losses are part of iron losses in the motor that are produced in the core due to alternating magnetic field, leading to high temperatures. Stator and rotor resistances increase linearly with increase in temperature, which leads to parameter variations [1]. The presence of harmonics in the stator excitation creates torque pulsations. At low frequencies it can cause a significant speed fluctuation and shaft fatigue [2].

In this thesis, 5^{th} and 7^{th} order harmonics are introduced to the supply voltage for about 1 second. The magnitudes of the harmonics are set to 30% of the fundamental component; the control schemes are simulated with full load torque of 1pu and high speed of 1pu, i.e. the worst case scenario.

The 5^{th} harmonic voltage component has a negative phase sequence and 7^{th} harmonic voltage component has a positive phase sequence. The 5^{th} harmonic voltage component will create an air gap flux which will rotate in the opposite direction or backward direction as the fundamental component, whereas, the 7^{th} harmonic voltage

component will create an air gap flux which will rotate in the same direction or forward direction as the fundamental component. The slip for 5^{th} harmonic will range from 1.2 to 1.0 and slip for 7^{th} harmonic will range from 0.857 to 1.0. As seen in the simulation results in Figure 5.48; When 7^{th} harmonic is introduced in the supply voltage, the electromagnetic torque has increased, as it increases the torque production by rotating in the same direction as the fundamental component. On the other hand, when 5^{th} harmonic voltage is introduced the torque has pulsating ripples in the downward direction, as the 5^{th} harmonic component opposes the torque production by rotating in the opposite direction of the fundamental. DTC drive shows worse torque pulsations and ripples due to the introduction of harmonics in the supply voltage; because of the three level torque hysteresis controllers used in the control system. FOC drive shows fewer spikes in comparison to DTC drive.

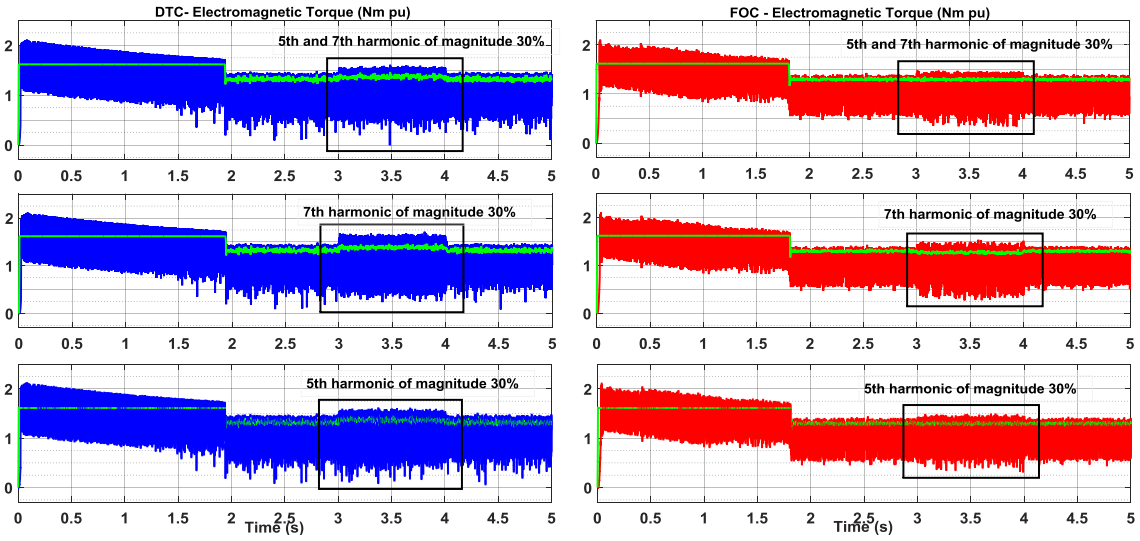

Figure 5.48: DTC & FOC Electromagnetic torque (harmonic pulsations)

5.4 Performance Comparison

Table 5.1: Performance Characteristics Comparison between IFOC and DTC Schemes for Induction machine.

Comparison Aspects	Indirect Field Oriented Control	Direct Torque Control
Flux	No Direct Control Dependence on rotor time constant Fast dynamic response (0.14s)	Direct control through hysteresis controllers Very fast dynamic response (0.04s)
Speed	No speed drops during fault type B Good stability during other fault type C and A. Speed recovery time is quicker (0.36s)	Speed deteriorates in flux weakening regions No speed drops during fault type B Good stability during other fault type C and A. Speed recovery time is quick (0.38s)
Electromagnetic torque	Fast dynamic response (0.03s) Reasonable torque ripples	Very fast dynamic response (0.02s) Suffers from high torque ripples Harmonics causes bad torque pulsations
Machine stator currents	Direct current controllers Reasonable current ripples (2pu)	No direct current controllers High current ripples (4pu).
Implementation complexity	Complex due to trigonometric functions.	Easier to implement No complex functions.
Parameter Sensitivity	Dependent upon rotor resistor and inductance, due to the use of rotor time constant	Only dependent upon stator resistor Fails badly at low speed operation due to parameter variations.

6 Conclusions & Future Work

6.1 Conclusions

This thesis focuses on two popular advanced control techniques for induction machine drives. In-depth case studies have been carried out to highlight the differences in performance characteristics of the two schemes under power quality issues. These case studies highlights the differences in performance and system stability issues of the two drives during power line faults such as voltage sags and interruptions. Profiles of the torque, speed and current are examined to compare the two schemes during these abnormal operating conditions.

The major contributions of this thesis are as follows;

- Detailed control system models of indirect field oriented control (IFOC) and direct torque control (DTC) schemes have been realized using Matlab-Simulink power system package. The design of the entire power electronics system includes a 3-phase diode rectifier, braking chopper module, 3-phase VSI and induction machine.
- Comparisons of the simulation results with the two advanced control schemes, under dynamic operation and power line faults have led to the following conclusions:

- **Speed response:** IFOC has shown excellent speed tracking response during acceleration and deceleration regions. DTC rotor speed drop is greater in field weakening regions (very low speeds). Induction machine speed is not affected by voltage sag fault type B; this is due to PI controllers that regulate the reference torque when one phase develops a fault. Fault type C shows a similar response as to fault type B up until a voltage sag of 50%. But after that, the motor is unable to meet the reference command torque from the controllers and causes the speed to drop as the fault magnitude increases. However, for fault type A, the rotor speed drops by a maximum of 75% in both schemes even during a 100% voltage reduction in all three phases. The speed recovery time after fault removal is faster in IFOC, confirming that IFOC scheme has better speed response than DTC scheme during three phase balanced faults, even though speed drops slightly lower in IFOC than DTC.
- **Electromagnetic torque response:** DTC shows faster torque dynamics, but has higher transient ripples, because of the absence of current regulators. Furthermore, torque performance degrades due to parameter sensitivity, but the average torque does not exceed the reference torque during dynamic variations owing to three-level torque hysteresis comparators. While IFOC has slow torque response time, it has low transient ripples owing to the presence of current regulators. In both control schemes, torque is not affected by voltage sag fault type B. However, variations are observed during fault type A and C in IFOC because of absence of direct torque controllers,

unlike DTC. Under harmonic analysis, DTC shows higher torque pulsations and ripples compared to IFOC. This confirms that DTC scheme has better torque response time than IFOC scheme, but it also has higher torque ripples than IFOC scheme, even during power quality issues.

- **Machine stator currents:** DTC suffers from higher currents drawn during machine start-up, transients and faults because of absence of current controllers, in turn affecting speed and torque responses. There are large variations in stator currents, for even a small change in stator flux. IFOC has stator currents which are well maintained because of three-level current regulators. During fault type B, both schemes have reasonable current spikes after the fault is cleared. During fault type C, DTC shows higher current spikes after the fault is cleared. During fault type A, IFOC and DTC both draw high currents due to heavy load; therefore overcurrent protection is necessary for both the schemes when the machine is fully loaded. Overall, IFOC has reasonable current spikes during faults.
- **Implementation complexity:** For IFOC drive controller, calculations are done in rotating reference frame that require trigonometric functions, increasing processing time and therefore leading to slower performance. On the other hand, DTC drive controller calculations are carried out in stationary reference frame that uses space vector modulations, making it easier to implement and requiring less hardware, thus it is more cost effective.

- DC link voltage drop during fault analysis in both the control schemes can be improved by a larger size of DC bus capacitor.
- DTC shows sensitivity only to stator resistance, whereas IFOC is less sensitive to variations in rotor resistance. Due to the use of rotor time constant calculations, IFOC has dependency on rotor leakage inductance parameter variations.

DTC offers clear advantages in terms of torque and flux response times, but IFOC shows quick speed recovery response and lower current ripples. DTC based variable-speed drives can be used for all types of pumps, such as centrifugal, constant torque, and screw pumps. DTC technology allows drive to self-adjust to varying application requirements; for instance in screw pumps, VSD employing DTC control will be able to adjust for sufficient starting torque to ensure startup. Furthermore, power loss ride through will improve pumping availability during shorter power failures. The inherent torque control availability of DTC based VSD allows the torque to be limited, in order to avoid mechanical stress on pumps and pipelines [66]. On the other hand, IFOC allows wider range of speed operation, making it a better choice for applications where precise speed control is crucial and torque is available at zero speeds (field weakening region), in sensitive industrial process control environments. For applications such as aerators and conveyors both DTC and IFOC based variable-speed drives are feasible.

6.2 Future work

Based on this thesis, following future research work is suggested;

- A technique to improve DTC switching frequency to a fixed value to improve overall performance of the system.
- Real time simulations for a complete fault profile and other power quality issues.
- Development of a protection system to limit overcurrent issues during machine start-up and line faults.
- Replacing voltage vector look-up tables for DTC to improve processing times further, and reducing hardware requirements thus making it more cost effective.
- Experimental verification of the research work presented in this thesis, to further validate behavior of the two advanced control schemes under power line faults.
- Studying the effects of DC faults and size of the DC link capacitor on the two advanced control schemes for induction machine drive.
- Replacing the diode rectifier with controlled rectifier that employs IGBT switches instead, to eliminate the need of a braking chopper (DC/DC buck converter).

7 References

[1] B. K. Bose, *Modern Power Electronics and AC Drives*.: Prentic Hall, 2002.

[2] T.M. Undeland, W.P. Robins, N. Mohan, *Power Electronics Converters, Applications and Design Third Ed.*: John Wiley & Sons, 2003.

[3] R. Krishnan, F. Blaabjerg M.P. Kazmierkowski, *Control in Power Electronics Selected*. Academic Press, 2002.

[4] R. Krishnan, *Electric Motor Drives - Modeling, Analysis, And Control*. Prentice Hall, 2001.

[5] D. Capararo, G. Tomasso, C. Attaianese, "A low cost digital SVM modulatorwith dead tine compensation ," in *IEEE International Symposium on Industrial Electronics*, 2001.

[6] X. Xue, T.G. Habetler, D.M. Divan, Y. Xue, "A low cost Stator Flux Oriented Voltage Source Variable Speed Drive," *Industry Applications Society Annual Meeting, 1990., Conference Record of the 1990 IEEE*, vol. 1, pp. 410-415, 1990.

[7] K. Hasse, "Drehzahlregelverfahren fur schnelle Umkehrantriebe mit stromrichtergespeisten," *Regelungstechnik*, vol. 20, pp. 60-66, 1972.

[8] F. Blaschke, "The principle of field-orientation as applied to the Transvector closed-loop control system for rotatin-field machines," *Siemens Reviev*, vol. 34, pp. 217-220, 1972.

[9] Dr. Noaman, M. Noaman, "Robust Sliding Mode Control Based On IFOC Induction Machine with speed estimator," *IJCCCE*, vol. 7, no. 1, 2007.

[10] J. Chiasson, R. Novotnak, M. Bodson, "High performance induction motor control via input-output linearization," *IEEE Contr. Syst. Mag*, vol. 14, pp. 25-33, 1994.

[11] M. Pietrzak-David, B. de Fornel Fornel, "Non-Linear control with adaptive observer for sensorless induction motor speed drives," *ESPE J.*, vol. 11, no. 4, pp. 7-13, 2001.

[12] D. G. Taylor, "Nonlinear control of electric machies: An overview," *IEEE Contr. Syst. Mag*, vol. 14, pp. 41-51, 1994.

[13] M. P. Kazmierkowski and D. L.Sobczuk, "Sliding mode feedback linearized control of PWM intverter-fed induction motor," *Proc. IEEE IECON'96*, pp. 244-249, 1996.

[14] R. Krishnan, F. Blaabjerg, Eds., M. P. Kazmierkowski, *Control in Power Electronics*. San Diego, CA: Academic, 2002.

[15] R. Marino, "Output feedback control of current-fed induction motors with unknown rotor resistance," *IEEE Trans. Contr. Syst. Technol.*, vol. 4, pp. 336-347, 1996.

[16] S. Peresada, P. Valigi, R. Marino, "Adaptive partial feedback linearization of induction motors," *Proc. of the 29th Conference on Decision and Control*, pp. 3313-3318, 1990.

[17] Z. Krzeminski, "Nonlinear control of induction motors," *Proc. 10th IFAC World Congr.*, pp. 349-354, 1987.

[18] A. Loria, P. J. Nicklasson, H. Sira-Ramirez, R. Ortega, *Passivity-based Control of Euler-Lagrange Systems*. London: Springer Verlag, 1998.

[19] T. Noguchi, I. Takahashi, "A new quick-response and high efficiency control strategy of an induction machine," *IEEE Trans. on Industrial Applications*, vol. 1A-22, no. 5, pp. 820-827, 1986.

[20] M. Depenbrock, G. Gierse, U. Baader, "Direct Self Control (DSC) of Inverter-Fed-Induction Machine - A Basis for Speed Control Without Speed Measurement," *IEEE Trans. of Industry Applications*, vol. 28, no. 3, pp. 581-588, 1992.

[21] M. Depenbrock, "Direct Self Control of Inverter-Fed Induction Machines," *IEEE Trans. on Power Electronics*, vol. PE-3, no. 4, pp. 420-429, 1988.

[22] M. Depenbrock, "Direct self-control of the flux and rotary moment of a rotary-field machine," 4,678,248.

[23] J. N. Nash, "Direct Torque Control, Induction Motor Vector Control Without an Encoder," *IEEE Transaction*

on Industry Applications, vol. 33, no. 2, pp. 333-341, 1997.

[24] P. Pohjalainen, C. Stulz, "Method and Apparatus for Direct Torque Control of a Three-Phase Machine," 5,734,249, March 1998.

[25] S. Heikkila, "Direct Torque Control Inverter Arrangement," 6,094,364, July 2000.

[26] F. Profumo, A. Tani, D. Casadei, "FOC and DTC: Two Viable Schemes for Induction Motors Control," *IEEE Transactions on Power Electronics*, vol. 17, no. 5, pp. 779-787, 2002.

[27] I. Boldea, S. A. Nasar, "Torque vector control (TVC)–A class of fast and robust torque speed and position digital controller for electric drives," *Proc. EMPS'88 Conf.*, vol. 15, pp. 135-148, 1988.

[28] F. Profumo, G. Serra, A. Tani, D. Casadei, "FOC and DTC: Two Viable Schemes for Induction motors torque control," *IEEE Trans. on Power electronics*, vol. 17, no. 5, pp. 779-787, 2002.

[29] G. Grandi, G. Serra, A. Tani, D. Casadei, "Effects of flux and torque hysteresis band amplitude in direct torque control of induction machines," in *IECON'94*, Bologna, Italy, 1994.

[30] P. Pohkalainen, J. Lalu, P. Tiitinen, "The next generation motor control method: Direct torque control (DTC)," *EPE* , vol. 5, no. 1, pp. 14-18, 1995.

[31] G. Serra, A. Tani, D. Casadei, "Improvement of direct torque control performance by using a discrete SWM technique," in *PESC'98*, Fukuoka, Japan, 1998.

[32] J. N. Nash, "Direct torque control, induction motor vector control without an encoder," *IEEE trans. on Industry applications*, vol. 33, pp. 333-341, 1997.

[33] T.G. Habetler, "Direct Torque Control of Induction machine using space vector modulation," *IEEE trans. on industry applications*, vol. 28, no. 5, pp. 1045-1053, 1992.

[34] F. Profumo, M. Pastorelli, T. G. Habetler, "Direct Torque control of induction machines over a wide speed range," in *IEEE-IAS'92*, Houston, 1992.

[35] F. Profumo, G. Griva, T. Habetler, T. Abe, "Evaluation of a high performance motor drive using direct torque control," in *PCC'93*, Yokohama, Japan, 1993.

[36] T. Habetler, M. Pastorelli, F. Profumo G. Griva, "Performance evaluation of a direct torque controlled drive in the continuous PWM-square wave transition region," *IEEE Trans. on Power Electronics*, vol. 10, pp. 464-471, 1995.

[37] H.M. Suryawanshi, M.M. Renge, U.V. Patil, "Performance Comparison of DTC and FOC Induction Motor Drive in Five Level Diode Clamped Inverter," in *IEEE International conference on ICAESM*, 2012.

[38] N. Pappa , S. Kumar, K. Hemavathy, "Comparison of Indirect Vector Control and Direct Torque Control Applied to Induction Motor Drive," in *IEEE International conference on ICACCCT*, 2014.

[39] B.Sebti, K.Mebarka, B.Tayeb, N.Farid, "Performance Analysis of Field-Oriented Control and Direct Torque Control for Sensorless induction motor drives," in *Mediterranean conference on control and automation*, Athens, Greece, 2007.

[40] P. Mahajan, N. Gupta, H. Saroa, R. Garg, "A Comparative Study between Field Oriented Control and Direct Torque Control of AC Traction motor," in *IEEE International conference on ICRAIE*, Jaipur, India, 2014.

[41] H. Le-Huy, "Comparison of Field-Oriented Control and Direct Torque Control for induction motor drives," in *IEEE Industry Applications Conference*, Phoenix, AZ, 1999, pp. 1245-1252.

[42] S. Toliyat, H.A. Nandi, "Condition monitoring and fault diagnosis of electrical machines - a review," *35th IEEE IAS Annual Meeting*, vol. 1, no. 35, pp. 197-204, 1999.

[43] B.K. Bose, D. Kastha, "Investigation of Fault Modes of Voltage-Fed Inverter Systems for Induction Motor Drives," *IEEE Transaction of Industry Applications*, vol. 30, no. 4, pp. 1028-1038, 1994.

[44] R. Peuget, S. Courtine, J.P. Rognon, "Fault Detection and Isolation of PWM Inverter by Knowledge-Based Model," *IEEE Transaction on Industry Applications*, vol. 34, no. 6, pp. 1318-1325, 1998.

[45] Y. Yang, W. Liu, X. Wang, "Simulation of vector controlled adjustable speed System of induction motor based on Simulink," in *IEEE conference on CSSS*, Nanjing, 2011, pp. 2563-2566.

[46] V. Blasko, "Analysis of a hybrid PWM based on modified space-vector and triangle-comparison mehtods," *IEEE Transactions on Industry Applications*, vol. 33, no. 3, pp. 756-764, 1997.

[47] Y. Lai, C. Liu, T. Chen, "A new space vector modulation technique for inverter control," in *Power Electronics*

Specialists Conference, vol. 2, 1999, pp. 777-782.

[48] J. Kim, S. Sul, D. Chung, "Unified voltage modulation technique for real-time three-phase power conversion," *IEEE Transactions on Industry Applications*, vol. 34, no. 2, pp. 374-380, 1998.

[49] K. Suzuki, S. Fukuda, ""Using harmonic distortion determining factor for harmonic evaluation of carrier-based PWM methods," in *Industry Applications Conference, Thirty-Second IAS Annual meeting*, 1997.

[50] R.J. Kerkman, T.A. Lipo, A.M. Hava, "A high performance generalized discontinuous PWM algorithm," in *Applied Power Electronics Conference and Exposition, APEC*, 1997.

[51] R.J. Kerkman, T.A. Lipo, A.M. Hava, "Simple analytical and graphical tools for carrier based PWM methods," in *Power Electronics Specialists Conference, PESC '97 Record, 28th Annual IEEE*, 1997.

[52] D.G. Holmes, "The significance of zero space vector placement for carrier-based PWM schemes," *IEEE Transactions on Industry Applications*, vol. 32, no. 5, pp. 1122-1129, 1996.

[53] J. Holtz, "Pulsewidth modulation for electronic power conversion," *Proceedings of the IEEE*, vol. 82, no. 8, pp. 1194-1214, 1994.

[54] S. Legowski, A.M. Trzynadlowski, "Minimum-loss vector PWM strategy for three-phase inverters," *IEEE Transactions on Power Electronics*, vol. 9, no. 1, pp. 26-34, 1994.

[55] B. Wu, *High-Power Converters and AC-Drives*.: IEEE Press, 2006.

[56] P. Vas, *Sensorless Vector and Direct Torque Control*. New York: Oxford University Press, 1998.

[57] A.Iqbal, J,Guzinski H.Abu-Rub, *High Performance Control of AC Drives*. West Sussex: Wiley & Sons Ltd., 2012.

[58] F. Corcoles, J. Pedra, L. Guasch, "Effects of Unsymmetrical Voltage Sag types E, F and G on Induction Motors," in *9th International Conference* , vol. 3, 2000, pp. 796-803.

[59] H. J Bollen, *understanding power quality problems: voltage sags and interruptions*.: IEEE Press, 2000.

[60] F.Corcoles, J.Pedra, L. Guasch, "Effects of Unsymmetrical Voltage Sag types E,F and G on Induction Motors," *IEEE*, pp. 796-803, 2000.

[61] G. Grandi, G. Serra, D. Casadei, "Study and implementation of a simplified and efficient digital vector controller for induction motors," *conf. Rec. EMD'93, Oxford, UK*, pp. 196-201, 1993.

[62] O. Wasynczuk, S. D. Sudhoff, P. C. Krause, *Analysis of Electric Machines and Drive Systems*. New York: Wiley-IEEE Press, 2002.

[63] L. Harnefors, "Control of Variable-Speed Drives," Sweden, 2002.

[64] EDVARD. Construction of 3-Phase AC induction motors. [Online]. http://electrical-engineering-portal.com/construction-of-3-phase-ac-induction-motors

[65] J.I Leon, S.Kouro, L.G. Franquelo, J. Rodrigues, B. Wu, "The Essential Role and the Continuous Evolution of Modulation Techniques for Voltage Source Inverters in Past, Present and Future Power Electronics," in *IEEE Transaction on Industrial Electronics*, vol.PP, 2016.

[66] S. Kouro, J. Rodriguez, B. Wu, S. Bernet, M. Perez, “Powering the future of industry: High-power adjustable speed drive topologies,” *IEEE Industry Applications Magazine*, vol. 18, no. 4, pp. 26–39, July 2012.

[67] Y. Kumsuwan, S. Premrudeepreechacharn, V. Kinnares, “A carrierbased unbalanced pwm method for four-leg voltage source inverter fed unsymmetrical two-phase induction motor,” *IEEE Transactions on Industrial Electronics*, vol. 60, no. 5, pp. 2031–2041, May 2013.

[68] J. Hudgins, “Power electronic devices in the future,” *IEEE Journal of Emerging and Selected Topics in Power Electronics*,, vol. 1, no. 1, pp. 11–17, March 2013.

[69] F.Barrero, "Recent Advances in the Design, Modeling, and Control of Multiphase Machines-Part I," *IEEE Transaction on Industria Electronics,* vol. 63, no. 1, pp. 449-458, January 2016.

8 Appendix A

8.1 Matlab-Simulink models and blocks

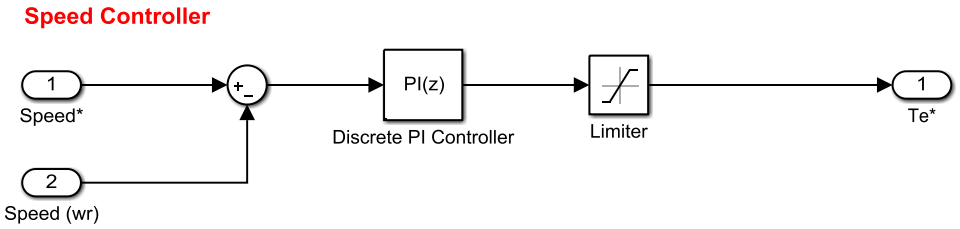

Figure 8.1: Speed controller block (in Simulink).

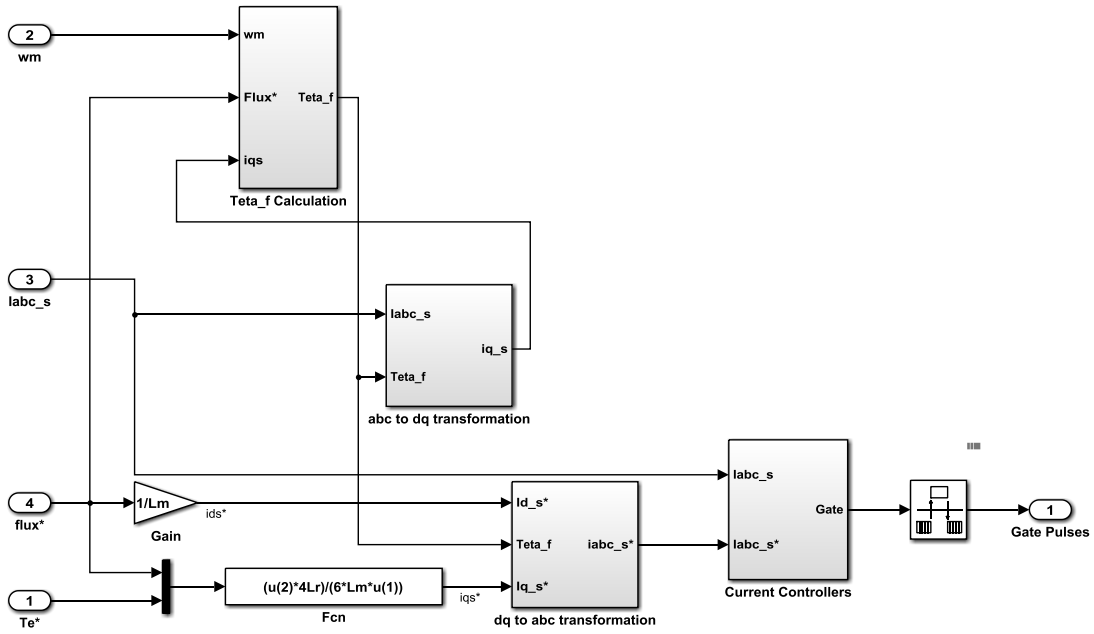

Figure 8.2: Indirect Field Oriented Controller block (in Simulink).

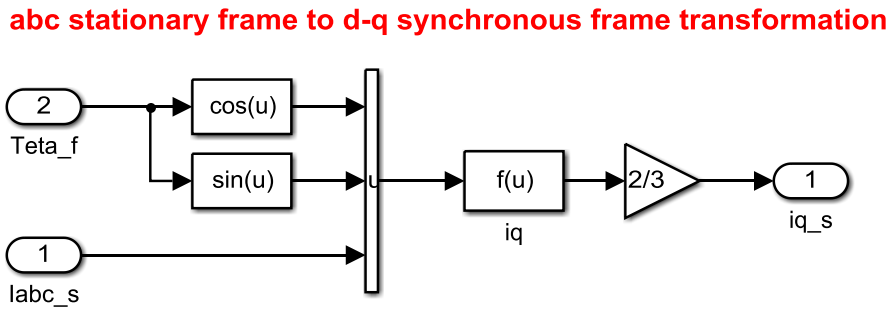

Figure 8.3: abc to d-q synchronous frame transformation block (in Simulink).

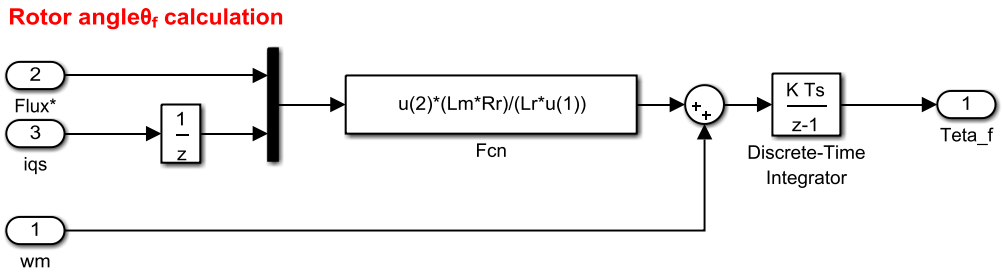

Figure 8.4: Calculation of θ_e block (in Simulink).

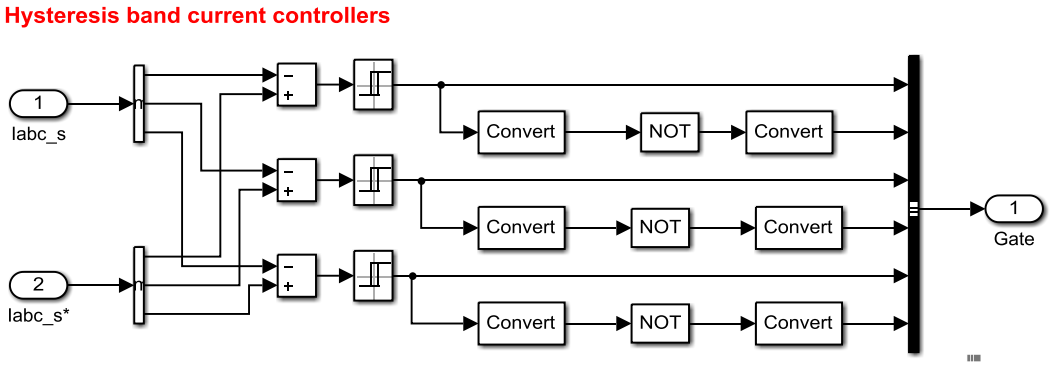

Figure 8.5: Three level hysteresis current controllers (in Simulink).

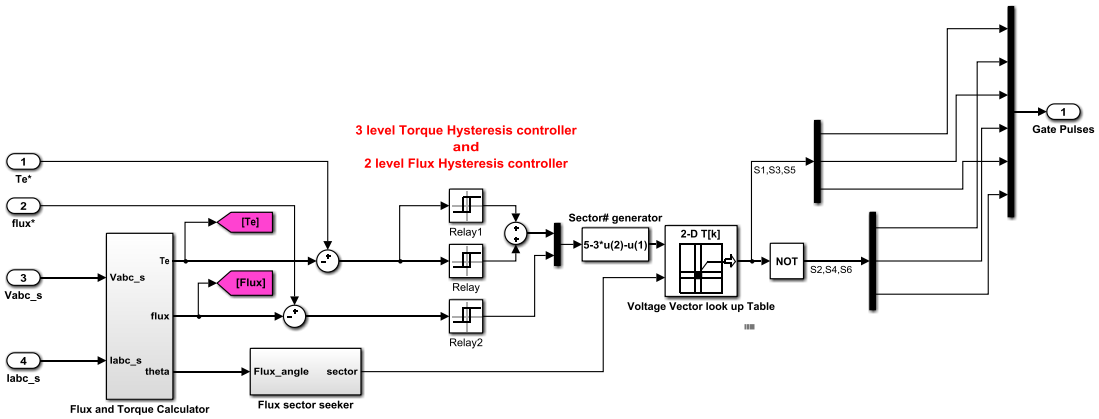

Figure 8.6: Torque and Flux hysteresis controllers (in Simulink).

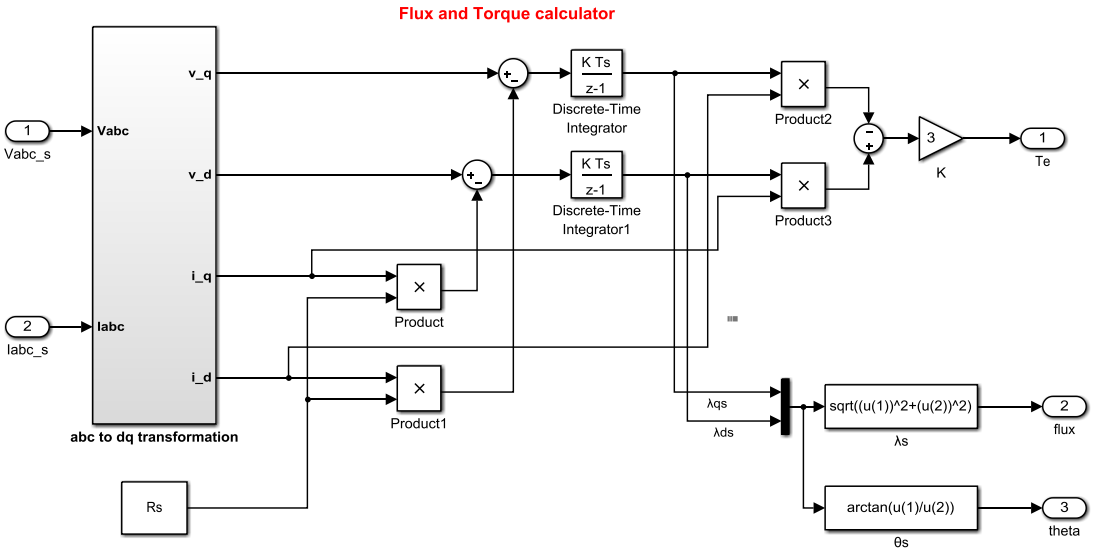

Figure 8.7: DTC Flux and Torque calculation block (in Simulink).

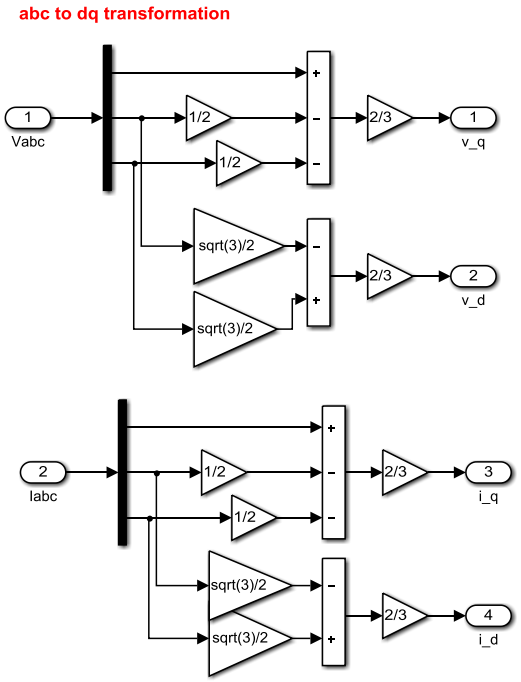

Figure 8.8: abc to d-q transformation blocks (in Simulink).

8.2 Braking Chopper

DC chopper module acts as a voltage regulator for maintaining DC link bus voltage, as shown in Figure 8.9. The chopper hysteresis controller checks for DC bus voltage levels between 320V and 340V as the nominal DC link voltage is 300V. During regeneration when DC bus voltage rises above 340V, the IGBT is turned ON, allowing current to flow in the braking resistor, which dissipates regenerative heat energy, making DC bus voltage to drop. Once, the DC bus voltage drops below 320V, the IGBT is turned OFF, resuming back to motoring mode. The turn ON and turn OFF voltages sets the threshold levels for the chopper hysteresis voltage controller between 340V to 320V

that generates duty cycle pulses for the switching device. The ramp generator in the chopper hysteresis controller is set to switching frequency of 4 kHz.

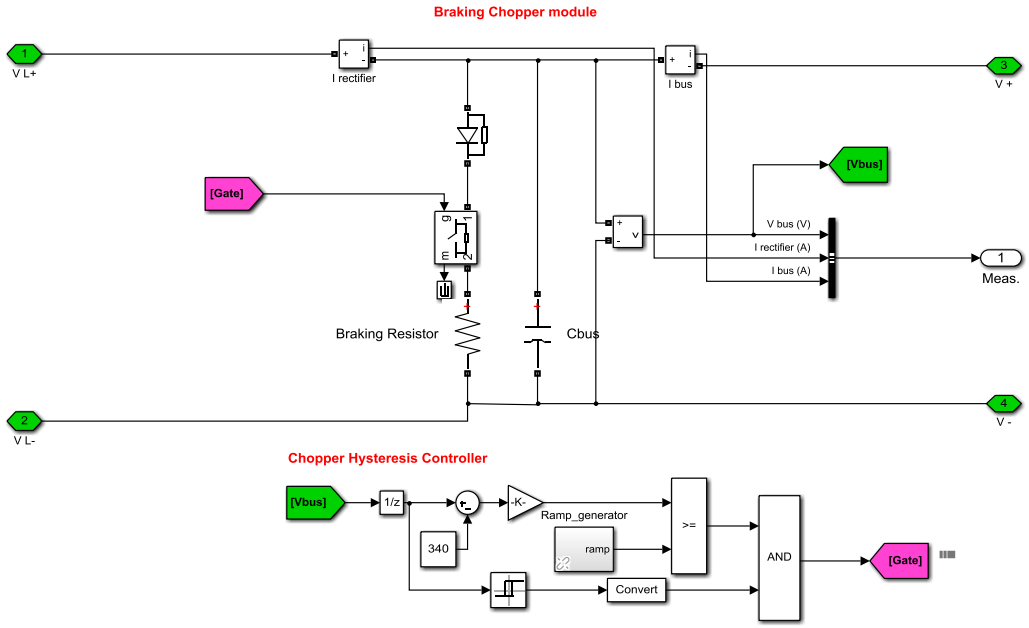

Figure 8.9: Braking chopper module circuit (in Simulink).

9 Appendix B

Table 9.1: System Parameters

Induction machine parameters	
Power rating	3 HP (2.2kW)
Voltage rating	220 V
Current rating	14.2 A
Frequency	60 Hz
Number of machine poles	2
Nominal Speed	900 RPM
Nominal Torque	11 N.m
Limit Torque	17.8 N.m
Stator leakage inductance L_s	2 mH
Stator resistance R_s	0.435 Ω
Rotor leakage inductance L_r	2 mH
Stator resistance R_r	0.816 Ω
Magnetizing inductance L_m	69.31 mH
Inertia	0.089 kgm^2
Friction	0.005 Nms
Initial machine flux (nom. Flux)	0.8 Wb
DC bus rating	
DC link voltage	300 V
DC capacitor	1500 uF
DTC Controller rating	
Torque hysteresis bandwidth	0.5 N.m
Flux hysteresis bandwidth	0.01 Wb
FOC Controller rating	
Current regulator hysteresis bandwidth	0.1 A
Simulation	
Time step	2 us

Table 9.2: Equations for sag types D, E, F and G [60].

Type D	**Type E**
$V_a = hV$ $V_b = -\frac{1}{2}hV - j\frac{\sqrt{3}}{2}V$ $V_c = -\frac{1}{2}hV + j\frac{\sqrt{3}}{2}V$	$V_a = V$ $V_b = -\frac{1}{2}hV - j\frac{\sqrt{3}}{2}hV$ $V_c = -\frac{1}{2}hV + j\frac{\sqrt{3}}{2}hV$
Type F	**Type G**
$V_a = hV$ $V_b = -\frac{1}{2}hV - j\frac{1}{\sqrt{12}}(2+h)V$ $V_c = -\frac{1}{2}hV + j\frac{1}{\sqrt{12}}(2+h)V$	$V_a = \frac{1}{3}(2+h)V$ $V_b = -\frac{1}{6}(2+h)V - j\frac{\sqrt{3}}{2}hV$ $V_c = -\frac{1}{6}(2+h)V + j\frac{\sqrt{3}}{2}hV$